

Imbibition in Disordered Media

Mikko Alava

*Helsinki University of Techn., Lab. of Physics, P.O.Box 1100, 02015 HUT, Finland and
SMC-INFN, Dipartimento di Fisica, Università "La Sapienza", P.le A. Moro 2 00185 Roma, Italy*

Martin Dubé

CIPP, Université du Québec à Trois-Rivières, C.P. 500, Trois-Rivières, Québec, G9A 5H7 Canada

Martin Rost

Abteilung Theoretische Biologie, IZMB, Universität Bonn, Kirschallee 1, 53115 Bonn, Germany

The physics of liquids in porous media gives rise to many interesting phenomena, including imbibition where a viscous fluid displaces a less viscous one. Here we discuss the theoretical and experimental progress made in recent years in this field. The emphasis is on an interfacial description, akin to the focus of a statistical physics approach. Coarse-grained equations of motion have been recently presented in the literature. These contain terms that take into account the pertinent features of imbibition: non-locality and the quenched noise that arises from the random environment, fluctuations of the fluid flow and capillary forces. The theoretical progress has highlighted the presence of intrinsic length-scales that invalidate scale invariance often assumed to be present in kinetic roughening processes such as that of a two-phase boundary in liquid penetration. Another important fact is that the macroscopic fluid flow, the kinetic roughening properties, and the effective noise in the problem are all coupled. Many possible deviations from simple scaling behaviour exist, and we outline the experimental evidence. Finally, prospects for further work, both theoretical and experimental, are discussed.

PACS numbers: 74.60.Ge, 05.40.-a, 74.62.Dh

I. INTRODUCTION

It is easy to do qualitative observations on the physics of fluid penetration in inhomogeneous media: a drop of coffee on a napkin or a sugar cube held partly in the same coffee cup are enough to demonstrate two fundamental facts. A moving interface is formed between the wet and non-wet regions of the medium. It becomes apparent that the disordered pore structure and uneven surface of the paper or the structure of the sugar cube both influence its behaviour: the interface is clearly rough. Furthermore, the dynamics of the phenomenon slows down with time, meaning that the wetted area of the napkin or volume of coffee absorbed by the cube increases more and more slowly. In fact, the average position of the interface H of the wet front usually increases in time as $H(t) \sim t^{1/2}$. The coffee drop shows an example of spontaneous imbibition, and it obeys what is known as Washburn's law [339]. The force driving the liquid from the liquid reservoir to the front between the wet region and the air in the medium has a weaker and weaker effect on the total flow as the distance between these two gets larger. Such a naive first glance at an imbibition experiment can be seen in Figure 1.

There are many similar examples of situations in which a liquid invades a porous medium and pushes aside another viscous liquid or gas. They are often of importance for technological applications or as ingredients in another field than the physics of fluids. In Table I we list some scenarios in which imbibition plays a role — they range from oil recovery (using water to displace it out of rock)

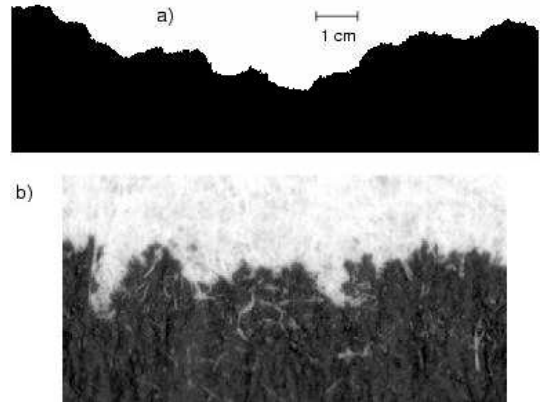


FIG. 1: Front of black ink sucked into a paper towel. a) digital photograph, ca. 1200 pixels horizontal resolution, dark and light grey values were enhanced to black and white. b) high resolution scan (1000 dots per cm) of a small part (ca. 0.8 cm wide) in grey-scale. The structure of the medium, as the fibres on the paper top surface, and its effect on the fluid front becomes visible.

to biology (water in living organisms) and manufacturing processes. The flow of liquids through porous media thus forms a very vast field which combines the porous structure of the medium with the surface chemistry and physics of the liquids and/or gases involved and is characterised by several parameters such as the viscosity contrast of the fluids, their wettability and surface tension as well as the displacement rate. The simplest realisation of imbibition involves two immiscible fluids, one being

displaced by the other, both liquids being characterised by their viscosity η and the surface tension σ of their interface.

The solid matrix interacts with the fluids through their wetting properties, as described by the Young-Dupré equation for a drop a liquid in contact with a solid surface, shown schematically on Fig. 2:

$$\sigma_{s2} - \sigma_{s1} = \sigma \cos \theta \quad (1)$$

where σ_{s1} and σ_{s2} are the surface tensions of the solid with fluids 1 and 2 respectively. The contact angle θ determines whether liquid 1 is wetting ($\theta < \pi/2$) or non-wetting ($\theta > \pi/2$).

Imbibition means that a wetting fluid displaces the non-wetting one, while the opposite case is called drainage. Spontaneous imbibition takes place when the invading fluid does so under the sole influence of capillary forces, with no external pressure. Forced imbibition involves a combination of capillary phenomena and an externally enforced flow rate or pressure difference.

TABLE I: Practical and experimental realisations of imbibition

Oil recovery	Displacement of a liquid by another, possibly in presence of a third phase [2, 61, 77, 241, 310, 349]
Printing processes	Ink penetration in paper [285]; Coating of paper [266, 280]; Absorbing materials [301]
Food industry	Cooking [265]; Wine filtering [333]
Biological sciences	Fluid transport in plants or imbibition of water into seeds (see Section IV C); Water penetration into soils [33]; Medical applications [204]
Surface chemistry	Contact angle measurements [58, 59, 171, 215]; Droplets on surfaces [62]
Composite materials	Invasion of voids by a resin or a metal in filler or metal-metal composites. [8, 9, 80, 92, 230, 231, 232]
Textiles	Behaviour of garments in the presence of liquids [57, 133, 134, 152, 272]
Construction	Water penetration into concrete or cement pastes [50, 195]

Although empirical relations for the flow of liquids through a porous medium existed for a long time, an effort, in part inspired by statistical mechanics, to quantitatively understand and predict the flow led to the study of *pattern formation* or the geometry of the regions occupied by the invading/receding fluids. At this level, the physics is dependent on the combination of viscous and

capillary forces at the boundary between invaded and “dry” regions. The viscous part arises due to the fluid flow in the (partly) saturated pore space, and the relative importance of viscous and capillary effects is described by the *capillary number* :

$$C_a = \frac{\eta v}{\sigma} \quad (2)$$

where η is the viscosity of the fluid, v its average velocity and σ the interfacial surface tension.

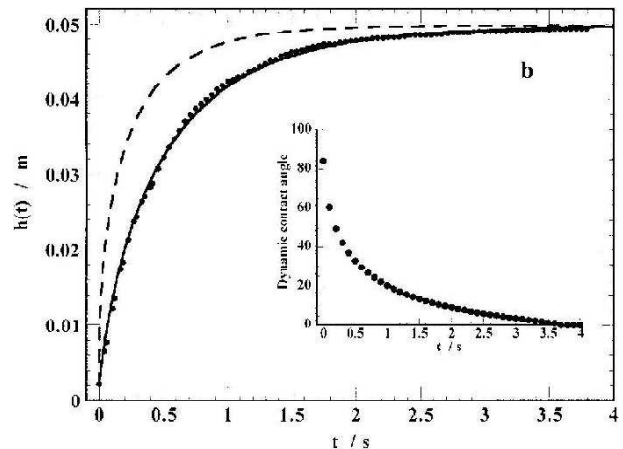


FIG. 2: Liquid drop in contact with a solid surface. The contact between the surface and liquids 1 and 2 is characterised by surface tensions σ_{s1} and σ_{s2} respectively while the interface between the two fluids has surface tension σ . If the contact angle $\theta < \pi/2$, fluid 1 wets the solid.

The stability and existence of an interface was experimentally investigated through the injection of liquid into various specially designed porous networks by Lenormand [187] (see also [185, 186, 338]) who qualitatively summarised it as a phase diagram with three possible outcomes, illustrated on Fig 3: (i) discontinuous formation of wetted domains due to *surface flow* in pores, (ii) formation of non-compact branched structures due to weak surface tension, and finally (iii) compact domains with well defined interfaces.

A phase diagram in terms of both the capillary number and the viscosity ratio of the two liquids (or liquid/gas) involved can then be established, illustrating the competition of viscous and capillary forces. The former stabilises the interface while the latter, if dominating, leads to situations like (ii) above.

If imbibition dynamics are dominated by capillary forces and pore-level invasion mechanisms like film flow, the effective surface tension of an interface can vanish. Then percolation-like phenomena can ensue, which means that the medium is apparently penetrated in disjoint clusters of the imbibing liquid. On the pore scale, one thus has to deal with either piston-like displacement or such gradual processes, leading finally to “snap-off”, as narrow pore throats become completely filled by the invading liquid [239, 284].

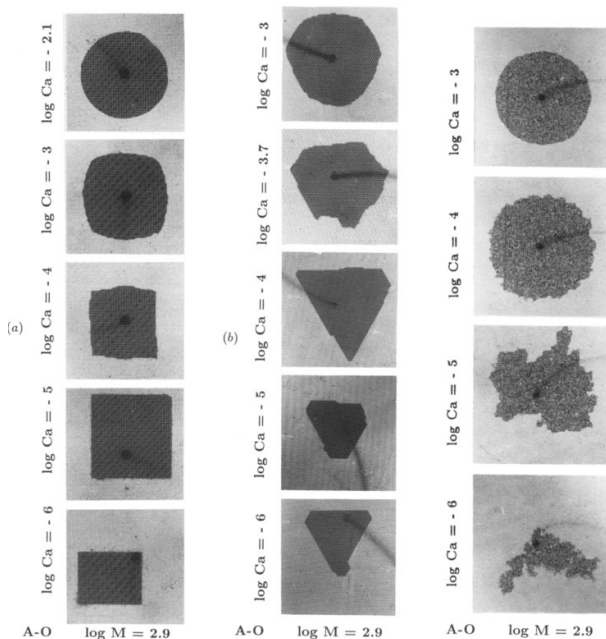


FIG. 3: Various cases of a fluid (oil) displacing air in a network, with varying pore size distributions. From left to right: a square network geometry, a triangular one, and finally a square one with very wide pore sizes. As the Capillary number C_a is varied, the effective surface tension of the cluster of invaded pores changes. Note the results for $\log C_a = -6$ in particular (after Lenormand, [187]).

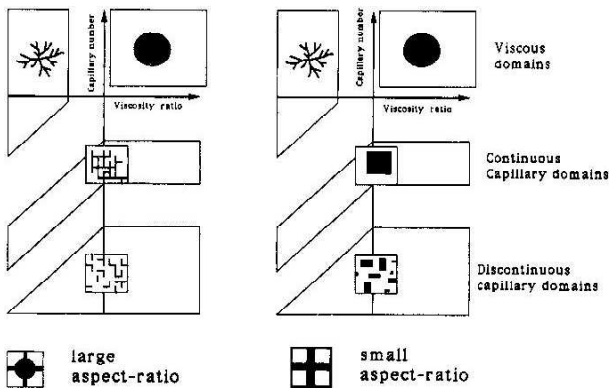


FIG. 4: A phase diagram for the geometry of imbibition as proposed by Lenormand [187], with the capillary number C_a and the viscosity ν being varied on one hand, and the pore-level geometry on the other hand. Notice the possibilities of apparently non-local (discontinuous) invasion, and of vanishing surface tension.

If the imbibing fluid is sufficiently more viscous than the defending one the invasion front is compact. Typically, as in the example of the sugar cube or the paper napkin, it is not flat but presents a random rough structure. This additionally complicates any effective theory or equation of motion for the invading fluid.

The main issues to be discussed in this review article are related to the rough *interface* between the two

phases involved in a compact imbibition invasion. This is accomplished by *coarse-graining* from the level of individual pores to the average position of the interface, meaning that the micro-structure of the medium is averaged out when possible. This is particularly complex in the case of spontaneous imbibition and can fail, due to the slowing down of the fluid penetration and/or due to the presence of competing mechanisms in the pore scale invasion dynamics.

This focus is also of fundamental interest to any imbibition process since a correct interfacial description requires the knowledge of the time- and length-scales that control the entire process. For many practical applications like soil mechanics or oil recovery it is of importance to understand this kind of “upscaling” [29, 241, 336] in order to estimate remaining non-wetting fluid saturations or relative permeabilities from laboratory scale measurements or from microscopic simulations. Future advances can also be expected in more complicated scenarios, as in the case of non-Newtonian fluids, in the presence of chemical reactions between the fluids involved, as well as in the rapidly developing field of microfluidics.

The process of imbibition is affected by *noise*, part of which stems from ever-present thermal fluctuations, while the rest is due to the quenched, frozen-in structure of the porous medium. The quenched nature of the noise becomes particularly important if the phase interface moves slowly in avalanche-like behaviour. Then the dynamics consists of localised bursts whose description directly couples the noise and the dynamical fluctuations of the interface.

An interesting theoretical question is then the universality of these phenomena, i.e., whether the statistical description of the interface is similar to the roughness observed in fire fronts, cracks and rupture lines, domain walls in ferromagnets. The same question arise with respect to the description of burst and avalanches in connection to the concept of Self-Organised Criticality. These questions are far from academic. In one part, the description of roughening in non-equilibrium phenomena has received lots of attention from the theoretical side (witness the large number of publications devoted to the Kardar-Parisi-Zhang (KPZ) equation [147]), but it is only recently that experimentalists were able to convincingly demonstrate the link between the proposed theoretical models and the observed phenomena (see [229] and references therein for KPZ behaviour in fire fronts). The same is true for roughening in imbibition.

Although it was examined in the early 1990’s [7, 45] in connection with percolation theory and deviations from KPZ behaviour, recent work [82, 99] pointing to the importance of fluid conservation, has led to a flurry of new experimental results [101, 122, 311, 312, 313] supported by further theoretical work [178, 261]. Even though many details remain obscure, we feel that the general theoretical picture of *roughening in imbibition* is now well established. The goal of this review is thus to highlight, from a statistical physics point of view, the central aspects of

imbibition that are understood, to relate them to existing experimental results and to point to remaining gray zones that deserve further studies. At the same time, we want to contrast this with the array of experimental evidence and numerical simulation models used for applied purposes and in connection to multi-phase flows. New theoretical results on the dynamics of avalanches and on interface roughening at constant flow and for columnar disorder are also presented and related to the recent experiments [122, 311, 312, 313] in Sections III G 3, III G 5 and III G 6.

The experimental situation is reviewed after that, with a brief remainder of possible complicating effects and comments on non-Washburn-like scaling in various setups. Next follows an account of various experiments on front roughening, ranging from Hele-Shaw cells to paper imbibition, divided between the forced fluid flow and the spontaneous cases. In contrast to the recently focussed theoretical progress, the experimental picture is much more delicate and we discuss it in the light of the theoretical sections. It turns out so that there are many confusing results, some of which can be related to the theoretical ones, and some of which clearly call for further work.

It is now clear that the physics of imbibition in disordered media couples *randomness*, *kinetic roughening properties*, and *interface velocity* in a complex fashion. This is illustrated schematically in Figure 5. The

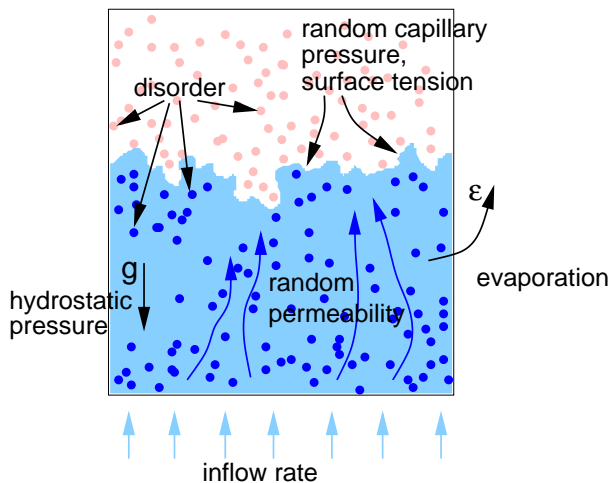


FIG. 5: Schematic representation of elementary processes involved in quasi-two-dimensional imbibition.

randomness acts as an effective noise that roughens the interface, but the same randomness also influences the fluid flow in the bulk, and thus the interface velocity and the net volume flow in the imbibition process. Therefore, we must conclude that all these aspects are intimately coupled and cannot be discussed separately. This creates intriguing experimental and theoretical questions and brings engineering and technological interests, surprisingly, close to those of fundamental statistical mechanics.

At the basis of models and experiments dealing with imbibition interface roughening lies the understanding of bulk fluid transport and saturation in the invaded medium. In the section to follow next, an overview is given from basic hydrodynamics in the medium to special effects related to non-Newtonian fluids.

II. PHYSICS OF IMBIBITION

A. Fluid flow in porous media

The detailed description of liquid flow through a porous medium is greatly complicated by the many time and length scales that are involved. The flow takes place at the level of the pores (say $1 \mu\text{m}$ or less) but the quantity of interest is the flow averaged over the whole macroscopic sample.

Similarly, a pore may be invaded vary rapidly or may remain blocked for the whole invasion time, which may be several hours or even days in spontaneous imbibition. A description of the flow makes sense only over a “representative volume element”, loosely defined as the minimal volume that can be defined such that the properties of the flow (and of the porous medium itself) within it remain statistically similar no matter where it is placed in the bulk of the medium (see [227, 348] for some recent advances using tomographic techniques).

At this level, it was already empirically found long ago by Darcy that the flow is essentially proportional to the pressure gradient across the medium, a result which can intuitively be explained by considering the flow of a liquid through a capillary tube. A consequence of this result is that the height H of a fluid column invading spontaneously a porous medium from a reservoir increases in time as $H(t) \sim t^{1/2}$, due to a combination of fluid conservation law (since any amount of invading fluid must be transported from the reservoir) and capillary forces. Before going further into the concepts of interface roughening, it is interesting to see how this result arises, and under which conditions it can be expected to be valid.

1. The Lucas-Washburn description

The simplest way to illustrate imbibition is the capillary rise. It translates easily to the basic phenomenological description of flow in porous media and it represents an important microscopic mode of flow propagation. As illustrated in Fig. 6, we consider a capillary tube of length L and radius R_0 , immersed into a reservoir at ambient atmospheric pressure P_0 .

The two fluids are immiscible with an interface, of surface tension σ , located at a height $z = H$ above the reservoir and we assume that the fluid in the region $z < H$ wets the solid walls. A meniscus is formed at the interface, characterised at equilibrium by the contact angle θ

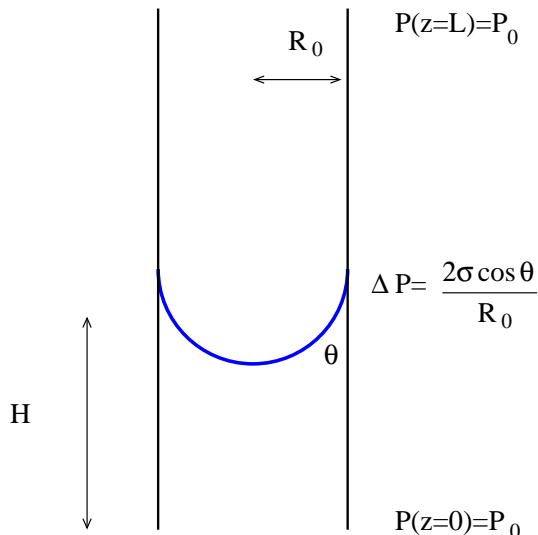


FIG. 6: Illustration of capillary rise, the fluid at $z = 0$ is in contact with a reservoir at atmospheric pressure P_0 and the top of the tube is either closed or open. The fluid from the reservoir wets the walls of the tube, which means that a curved interface, to which corresponds a capillary pressure difference p_c exists across the interface.

obtained from Eq. (1). The combination of the curved interface with the surface tension creates a pressure difference or capillary pressure $p_c \equiv \Delta P = 2\sigma \cos \theta / R_0$. This Gibbs-Thomson or Laplace effect gives rise to a thermodynamical force that will move the fluids. It also applies in more general imbibition problems directly at the level of individual pores.

In its full generality the solution of the flow dynamics for this problem needs to take into account the detailed flow right at the contact line between the fluids and the solid [70, 143] as well as inertial effects at the entrance of the tube [319]. For now, these effects are neglected, but are discussed in greater detail below. Neglecting the structure of the meniscus means that the pressure field changes only along the length of the tube, $P = P(z)$, with the interface described mathematically by the height H . Likewise, neglecting inertia means that the fluids are only described in terms of their viscosity η using Stokes' Equation [179].

$$\eta \nabla^2 \mathbf{v} = \nabla P \quad (3)$$

Three different cases can be then be easily examined:

(i) *Two incompressible Fluids*: The two fluids are described by Stokes' equation, with a longitudinal velocity field depending only on the radial coordinate $\mathbf{v} = \hat{\mathbf{z}} v_z(r)$:

$$\eta_i \frac{1}{r} \frac{d}{dr} \left(r \frac{dv_{zi}(r)}{dr} \right) = \frac{dP(z)}{dz} \quad (4)$$

where $i = w$ or n denotes respectively the wetting ($z < H$) and non-wetting ($z > H$) fluids. The tube is open at the top, to allow the second fluid to leak out. The

incompressibility condition leads to a Laplace equation $\nabla^2 P = 0$ for the pressure field, where the instantaneous position of the interface appears only as a boundary condition

$$\begin{aligned} P(z=0) &= P_0 \\ P(H^+) - P(H^-) &= p_c \\ P(z=L) &= P_0. \end{aligned} \quad (5)$$

The Laplace equation for the pressure means that the pressure gradient is constant, so that each fluid has a Poiseuille velocity field

$$v_{zi} = \frac{1}{4\eta_i} (r^2 - R_0^2) \frac{dP}{dz} \quad (6)$$

and the velocity of the interface is associated with the average flow velocity

$$\pi R_0^2 \frac{dH}{dt} = \int d\mathbf{a} v_{zw}(r) = \int d\mathbf{a} v_{zn}(r) \quad (7)$$

where $d\mathbf{a}$ is the area element of the tube, which leads to a pressure

$$P(z < H) = -\frac{\eta_w}{\eta_w H + \eta_n(L-H)} p_c z + P_0 \quad (8)$$

$$P(z > H) = -\frac{\eta_n}{\eta_w H + \eta_n(L-H)} p_c (z - L) + P_0$$

and to an interfacial velocity

$$\frac{dH}{dt} = \frac{R_0^2}{8} \frac{p_c}{\eta_w H + \eta_n(L-H)} \quad (9)$$

The wetting fluids thus continuously displaces the non-wetting fluid until it occupies the whole length of the tube. Notice that at the beginning, it does so as $dH/dt \sim p_c/H$, which implies an initial motion of the interface $H(t) \sim t^{1/2}$.

(ii) *Second fluid is compressible*: If the second fluid is a very compressible liquid or a gas, it simply adjusts itself to the pressure of the wetting fluid and does not support any pressure gradient. In the case of an open tube, the second fluid is the ambient gas, and its pressure is constantly at the atmospheric pressure P_0 , such that

$$P(z < H) = -p_c \frac{z}{H} + P_0 \quad (10)$$

$$P(z > H) = P_0$$

In this case, the classic result of Washburn [339] and Rideal [278] is obtained: the interface position is described in time as

$$H^2(t) - H^2(t_0) = \frac{R_0^2 p_c}{8 \eta_w} (t - t_0) \quad (11)$$

where $H(t_0)$ is the initial height. This result is also obtained for two incompressible fluids (Eq. (9)), as long as $\eta_w H \gg \eta_n L$.

If the tube is closed at the top, so that the gas cannot escape, the pressure of the gas phase increases as the fluid occupies more and more volume. If the gas was initially filling the whole tube with pressure P_0 , then the pressure if the interface is at height H ,

$$P(z > H) = P_0 \left(\frac{L}{L - H} \right)^\gamma \quad (12)$$

where $\gamma = C_p/C_v$, the ratio of the heat capacities at constant pressure and volume respectively. The flow field of the wetting fluid is not modified, and the resulting interface equation

$$\frac{dH}{dt} = \frac{R_0^2}{8} \frac{1}{\eta_w} \frac{P(H) - P_0 - p_c}{H}. \quad (13)$$

Again, as long as $P(H)$ is not too far from the atmospheric pressure, the Washburn-Rideal result is obtained. However, in real porous media, trapping of gas by the invading fluid may occur, in which case the propagation of the menisci, given by Eq. (13) may be markedly different from Washburn behaviour Eq. (11).

(iii) *Capillary rise and gravity*: gravity acts on the fluids through their density ρ as

$$\eta_i \nabla^2 v_{zi} = \frac{dP(z)}{dz} - \rho_i g \quad (14)$$

where g is the gravitational constant. Assuming that the second fluid is the ambient gas, with an open tube, the interfacial rise is

$$\frac{dH}{dt} = \frac{\kappa}{\eta} \rho g \left(\frac{H_{\text{eq}}}{H(t)} - 1 \right), \quad (15)$$

where we define the permeability $\kappa = R_0^2/8$, and the equilibrium height $H_{\text{eq}} = p_c/(\rho g)$, at which the hydrostatic and capillary pressures are balanced. The relevant parameter is the equilibration time $\tau_{\text{eq}} \equiv H_{\text{eq}}\eta/\kappa g(\rho)^2$. For times $t \ll \tau_{\text{eq}}$ (which corresponds to $H \ll H_{\text{eq}}$) or in absence of gravity (“horizontal imbibition”) the time-dependence follows the square-root law, Eq. (11) seen earlier. At later times, $t \gg \tau_{\text{eq}}$, the finite equilibrium height H_{eq} (if it exists) is approached exponentially

$$H(t) \sim H_{\text{eq}} (1 - e^{-t/\tau_{\text{eq}}}), \quad (16)$$

in a way that is simply related to the equilibrium quantities H_{eq} and τ_{eq} . This simple law is interesting in many aspects since the relevant parameters (contact angle, surface tension) are easy to determine and the resulting easy-to-grasp predictions make it attractive and suitable in interpreting experiments.

However, these results may be invalid for a number of reasons. For example, in a liquid-liquid system Mumley et al. [242], comparing dry and prewetted tubes, have

shown that viscous dissipation at the contact line and precursor film dynamics [70, 143] may lead to both Washburnian or slower (in terms of the rise exponent) behaviour depending on the contact angle and the condition of the capillary rise.

Inertial effects as Bosanquet-flow [36] may also be important in the early stage of pore invasion, before the dynamics is described by Eq. (11) [319]. Dimensionally, it is easy to see that the characteristic time scale over which inertial effects will be important $\tau_i \sim \rho R_0^2/\eta$, after which the usual Washburn dynamics follows. Before this time the fluid enters the capillary as

$$H(t) \sim \left(\frac{\sigma}{\rho R_0} \right)^{e/2} t. \quad (17)$$

Although the time τ_i can be very small, the $R_0^{-1/2}$ dependence of the rise on the radius of the capillary must be compared to the $R_0^{1/2}$ of Eq. (15). Although the effect of inertia lasts for a very short time in small pores, the capillary rise can nevertheless be quite rapid. Experimentally inertial effects can give rise to effective initial height and time, H_0 and t_0 in Eq. (15) that must be taken into account in fitting measured data [173, 174].

2. Macroscopic description of flow in porous media

Equation (15) is also often used in more general terms for porous media. Already at the level of Stokes' equation, a simple dimensional analysis implies that $\mathbf{v} \sim (\kappa/\eta)\nabla P$ where κ must have units of $(\text{length})^2$. In fact, a common description of single-phase fluid flow in porous media is Darcy's equation [292, 295],

$$\langle \mathbf{q} \rangle = -\frac{\kappa}{\eta} (\nabla P - \rho \mathbf{g}), \quad (18)$$

where $\langle \mathbf{q} \rangle$ is the average volume of fluid transported per unit time per unit cross-section of the porous medium, and κ and η are the *average* permeability and viscosity respectively. This equation is obtained by coarse-graining the structure of the porous medium, ignoring all fluctuation and pore scale effects, using a line of reasoning based on “representative volume elements” [22, 295].

The extension to two-phase or multi-phase flow is in principle straightforward, the dimensionless saturations of wetting and non-wetting fluids s_w and s_n are defined as the ratio of fluid present with respect to void space in a given representative volume element. Alternatively, the concentrations are defined as $c_i = \mathcal{P} s_i$ where \mathcal{P} is the porosity. The dynamics of the concentration is then obtained through continuity equations to reflect the conservation of liquid. If the fluid densities and the porosity are constant,

$$\begin{aligned} \mathcal{P} \frac{\partial s_w}{\partial t} + \nabla \cdot \mathbf{q}_w &= 0 \\ \mathcal{P} \frac{\partial s_n}{\partial t} + \nabla \cdot \mathbf{q}_n &= 0 \end{aligned} \quad (19)$$

together with the constraint $s_w + s_n = 1$. The flux \mathbf{q}_i of each fluid obeys Eq. (18) and a *coarse-grained* capillary pressure is included as a closure relation between the pressure in the two fluids $P_w - P_n = p_c$. Since the permeability is only a geometric factor, both fluids should have the identical values of κ and the pressure gradient, $\nabla P \sim \hat{\mathbf{z}} p_c/H(t)$ then follows immediately.

If the imbibition front remains compact, the volume-flow per unit area is nothing but the velocity of the interface, which leads to $\langle q \rangle = dH/dt$ and to the results described in Eq. (9), and Eq. (11) if the second fluid cannot sustain a pressure gradient. This however assumes that the fluid pushed away has an easy escape, a situation denoted in the petrophysics community as “co-current flow”.

What kind of dynamical behaviour can now be expected in realistic porous media? Simplistic analysis predicted by the above Washburn law, Eq. (11), can be invalidated by many factors. For example, evaporation (to be examined in more details in Section III G) may slow down imbibition when the quantity or volume of liquid needed to follow the typical Washburn scaling is not available. Similar effects arise if the solid phase matrix is permeable and acts as a sink. Likewise, for three-phase flows, often important in industrial problems, the separation of the two liquids may cause the introduction of new time-scales. In general, simply having several length-scales to describe the structure of the porous medium can lead to complications that obfuscate the Washburn scaling. In the following, we briefly discuss when this scaling may fail, or what could be expected in various kind of porous media.

Despite all these possible complications Washburn behaviour *is* often observed experimentally. It is therefore an useful approach to study roughening first under well controlled situations that lead to the $t^{1/2}$ progression of the average interface, and then to look at possible deviations. We will therefore devote the major part of this Review to Washburnian imbibition. The expected roughening behaviour when $H(t) \sim t^\delta$ with $\delta \neq 1/2$ is commented on at special occasions, in particular in the concluding Section.

3. Pore geometry and inertia

At the microscopic level, it is clear that any simple picture of a porous medium as a collection of capillary tubes with effective permeability κ is wrong, the pore geometry can be extremely important, in particular when sharp corners or edges are present.

It is already established that a compact (albeit rough) imbibition front is formed if the viscosity of the invading fluid is sufficiently greater than the viscosity of the defending fluid, as indicated on the phase diagram proposed by Lenormand [187], reproduced in Fig. 4. Thus, although containing interesting physics at the level of pattern formation, the question of disconnected inva-

sion clusters is trivially not relevant in the context of interface roughening (see e.g. refs. [24, 126] for percolation approaches). The main exception to this rule is the possibility of a “dynamic” transition between well-defined interfaces and fingering instabilities in spontaneous imbibition due to the slowing down of the interface [120, 328]. A second possibility is the role of prewetting layers, whose presence may again render an interfacial description meaningless [201, 202, 203], since the essential dynamics are ruled by the prewetting.

In most cases it cannot be decided a priori whether the expected macroscopic Washburn-Darcy behaviour is valid or not. The early studies of Lenormand, later augmented by the studies of Bernadiner, Knackstedt et al. and others, have managed to shed further light into the question of relevance or irrelevance of pore-scale physics [25, 302]. Three basic invasion processes were observed. A cylindrical pore may be invaded either as in the basic capillary rise (piston flow) or by surface flow, followed by collapse (snap-off) of the film, as shown in Fig. 7. At the crossing of several cylindrical pores, there is a drastic change in the shape of the meniscus, followed by a rapid pinch-off leading to the invasion of the pore (Fig. 8). Each of these modes of invasion are characterised by different length scales, which can lead to a dynamical behaviour that is very different from the one predicted by Eq. (11). Blunt et al. [30] argue that the width of a film flow zone in networks (under forced imbibition) should scale as $w_{ff} \sim C_a^{-1} (w_t/R_0)$ where w_t/R_0 is a rough estimate of the ratio of tube wall roughness to its diameter. Percolation-style arguments for snap-off region sizes indicate that the associated length-scale increases much more weakly with $1/C_a$ [30].

One question related to the pore-level description is whether *correlations* matter. In various types of rocks the local permeability may be correlated over considerable length-scales due to geological processes. The evidence from numerical modelling based on microscopically faithful descriptions of pore-networks seems to indicate, that multi-phase flow phenomena as imbibition in particular are much more prone for correlation-induced effects than, e.g., simple one-phase permeability [10, 42, 66, 94, 141, 153, 212, 257, 258, 308, 326, 334]. Typical quantities where this would be visible are relative permeabilities for given saturations, and remaining saturations of the non-wetting fluid. Note that there are no studies of the front dynamics in imbibition in the presence of “typical” correlations of pore structure, as arising in empirical contexts.

In addition, inertial effects [281, 299] may be important in the early stage of pore invasion, where they can lead to a preferential invasion of small pores (see Eq. (17)) [281, 299]. But inertia can also be important at all stages of the capillary invasion, whenever a sudden change in the flow occurs, as in film snap-off, or pinch-off at a corner. In these cases, the front position could advance as t^k with $k \leq 1$ [270, 271]. On short time scales (smaller than a few seconds), the front penetration may also proceed in

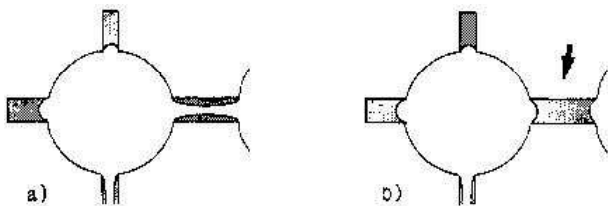


FIG. 7: In large pores or channels, the fluid can first cover the surfaces and then collapse to fill the whole void [187].

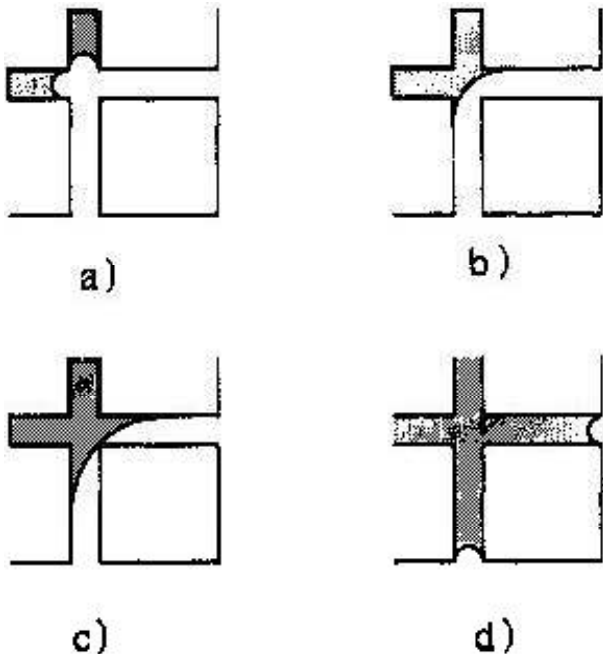


FIG. 8: Examples of pore invasion mechanisms [187]: the progress is gradual from a) to b) as the meniscus radius increases, and leading, at c), to a situation when the fluid suddenly invades the channels.

pores first with the establishment of a prewetting layer through *diffusion* [90, 114] or (precursor) film flow [63].

4. Dynamical Saturation

In general capillary flow occurs simultaneously with film flow and can lead to a gradient in the concentration of the invading fluid: complete saturation is established only over a certain distance. In addition, *trapping* of the defending fluid in certain regions modifies the flow of the imbibing fluid and may block some paths of progression, leading to a reduced permeability for the invading fluid (e.g., Eq. (13) for the simplest case). It is also often possible that the imbibing liquid interacts directly with the porous matrix, changing directly the spatial structure of the porous medium and leading to a slow change in the permeability (as observed in concrete with water [197], or in ordinary paper [54]).

These phenomena can, to some extent be taken into account by introducing different permeabilities for each fluid in Eq. (19): $\mathbf{q}_i = \kappa_i(\nabla P_i - \rho_i g \mathbf{z})/\eta_i$ with $i = w, n$. In addition, the permeabilities and capillary pressure will often be function of the saturation of the medium, $\kappa_i = \kappa_i(s_i)$ and $p_c = p_c(s_w)$.

However, even this basic set of equations has to be augmented to account properly for surface tension and surface areas [123, 124]. In fact, the two-fluid interfacial area is one of the fundamental quantities — it also partly defines the driving thermodynamic force in the case of spontaneous imbibition. Many authors have addressed this question by network models and experiments on one hand or by thermodynamical considerations [106, 108, 255, 276, 294]. Again the physics at pore level is complicated by the presence of precursor films and the question of how entrapped volumes of the non-wetting fluid behave.

If both permeabilities are equal and independent of saturations, and likewise for the capillary pressure, then the ideal case of two incompressible fluids in a capillary, Eq. (9), is recovered. As mentioned above, this implies that the non-wetting fluid can easily be pushed away by the wetting liquid. This corresponds to “co-current flow” and $\mathbf{q}_w = \mathbf{q}_n$. The opposite case is “counter-current flow”, the mass-flow of the expelled liquid takes place in the exactly opposite direction from the invading one: $\mathbf{q}_w = -\mathbf{q}_n$ [196]. In both cases, if the geometric setup allows for a one-dimensional equation we arrive at the effective diffusion equation

$$\mathcal{P} \frac{\partial s_w}{\partial t} + \frac{\partial}{\partial x} \left(M_w \frac{\partial s_w}{\partial x} \right) = 0 \quad (20)$$

where $M_w(k_{rw}, k_{rn}, \partial p_c / \partial s_w)$ is an effective mobility and the subscript r refers to relative permeabilities. This has naturally a scaling solution with x/\sqrt{t} as a scaling parameter. Notice that this is also related to the piston-like fronts in the Buckley-Leverett theory [43, 87], and that the implied scaling properties are of practical interest, as well [206, 347]. If the non-wetting fluid cannot support a pressure gradient (and we assume that it is free to escape), then $P_n = P_0$ and Richard’s Equation [277] appears as a special case of Eq. (20).

When dynamical saturation is present, the concept of an interface can easily become ill-defined if there is no sharp jump in concentration between the wet and dry parts of the medium. In many cases the permeability is a rapidly increasing function of the saturation (e.g., $\kappa(s_w) \sim \exp(\beta(s_w - s_0))$ [100, 236]) so that a sharp division exists between the invaded and non-invaded part of the medium, which also leads to the basic scaling $H(t) \sim t^{1/2}$ for spontaneous imbibition.

Hysteresis is also an omnipresent feature [23]. Partly it occurs between what commonly is called “primary” and “secondary” imbibition. Such history effects arise if there is already a presence (residual saturation) of the wetting fluid.

Saturation can be studied dynamically since the gradual increase in the local fluid volume fraction can be followed by Nuclear Magnetic Resonance (NMR) and by X-ray Computer Tomography (CT) techniques. These have reached already accuracy levels in which individual pores can be monitored as filled or not, and perhaps in the near future the interfacial features will become accessible as well (see [341] for a hydrology example) to allow studies of interface dynamics in detail [28, 320]). One of the important practical questions is the dynamics of entrapped fluid. Though percolation-based descriptions of such residual clusters have existed for quite some time [342], the physics of such “ganglions” is still quite open, often accessible only via numerical models.

Imaging techniques are sufficient to demonstrate phenomena like *swelling* of the solid volume fraction [320] in the case of disordered fibre networks (see also [113, 132, 251, 337]). Swelling, coupled to the fact that the porosity undergoes a simultaneous decrease, leads to reduced fluid flow towards the interface and possibly to deviations from Washburn behaviour. The problem of deformable porous media is difficult to understand in general terms, and involves from the theoretical viewpoint the solution of coupled elastic and fluid mechanics problems (see e.g. [268, 309]). Other NMR studies have been recently performed in situations that are of relevance for construction engineering (water imbibition into cement pastes [50, 195]) and the oil industry [2, 274, 349]. In the latter case, the displacement of oil by water is an important practical question, as is the achieved level of saturation. NMR imaging has now developed to a level, where one can consider the saturation vs. pore sizes — and distinguish between co- and counter-flow due to the importance of film flow in the latter one [55].

By simply comparing the mass intake and the optical appearance of a paper sample, it has been noted that the saturation and the actual visual front may both display similar temporal scalings (Washburn-like). This would define a widening “saturation front” as the partially saturated volume behind the interface that drives the imbibition process [27]. The principal question is whether the saturation takes place in the wake of a “front” or whether the process as a whole obeys diffusion into, e.g., small pores first [114]. The first limit corresponds to piston-like advance (a term using a one-dimensional analogy), and the second to a flat saturation profile (which changes by the time-scale contained in the scaling variable).

Recent imaging data [18, 227, 228] show convincingly the capabilities of both CT and NMR approaches in demonstrating both limits, and the cross-over in-between. Figure 12 exhibits a clear example of an experimental front with only partial saturation [349]. In the close future one would expect that such techniques yield much more empirical evidence [79, 87, 296] by looking at saturation profiles and concomitantly capillary pressure curves as the saturation is varied.

The transport of liquid into the less-saturated regimes can further be complicated by the presence of an initial

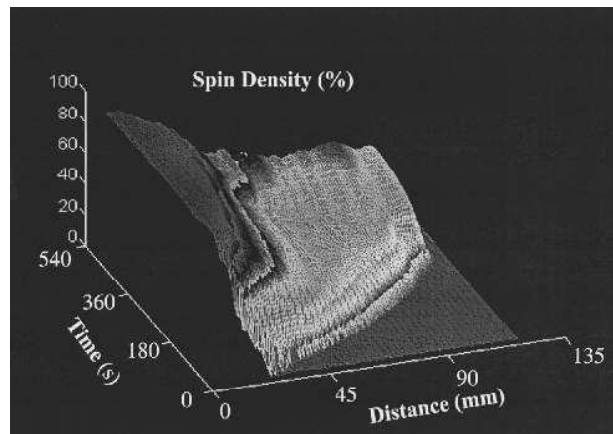


FIG. 9: Saturation profile of the liquid in a fibre assembly (plug) [320], as a function of time and distance from the liquid reservoir.

(residual) saturation [141]. Figure 13 shows an example of how the presence of wetting fluids is supposed to influence the *front* geometry [136]. The width of the front can spread in time and exhibit what is called “hyperdiffusivity” via the dependence of the $\kappa(s_w)$ on the local wetting fluid saturation. This is in fact related to the question of diffusive hydrodynamic spreading of tracers, and has been debated in the literature [14, 67, 69]. Recent imaging experiments indicate that the hyper-dispersion can be related in a power-law fashion to s_w [227, 228]. This would result from saturation dynamics following film behaviour in the pores.

Further such complications become evident if the description by Richard’s equation is modified by, e.g., a time-dependent porosity [197], or if anomalous diffusion is invoked [169], both resulting presumably from liquid-porous matrix interactions. The usual saturation dynamics, contained in simulation models [283, 324], would indicate diffusive intake — which then would exhibit similar scaling as the spontaneous imbibition front position [168]. The saturation dynamics can thus complicate the dynamics at the front due to the conservation of the liquid that a sample intakes per unit time [305], an issue that has not been studied systematically to our knowledge in spite of some “snapshots” in the literature, as Figure 13.

5. Surfactants, additives and other non-Newtonian effects

Finally, additives to a carrier fluid, such as dye, give rise to phenomena that can cause a deviation from Washburn-like behaviour. The dye particles diffuse as usual Brownian particles but are also carried by the imbibing fluid, which gives rise to hydrodynamic dispersion [292]. The dynamics of dispersion is of fundamental interest in the imbibition context for two main reasons: In some cases, the dye front is (maybe somewhat dangerously) identified with the “elastic interface” for which

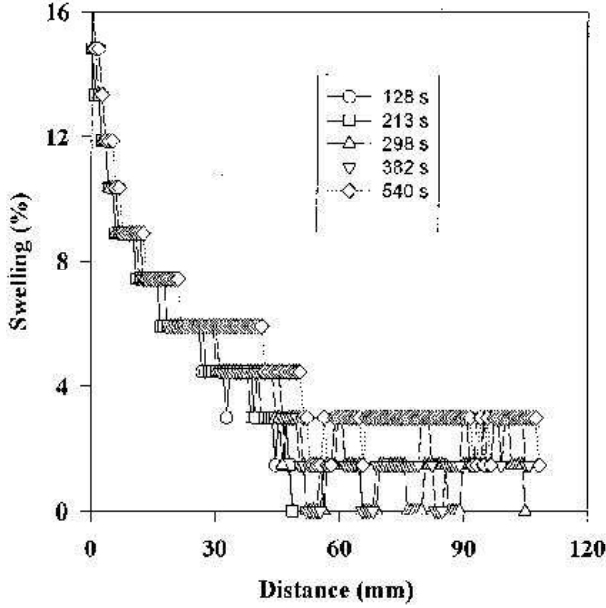


FIG. 10: The swelling of fibres, as a function of time and distance, in a plug ([320]). A concomitant change in local permeability, and thus fluid flow, is expected.

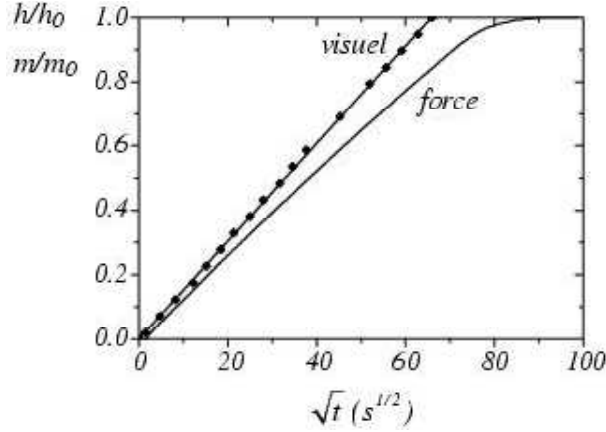


FIG. 11: The front and the mass (of the silicone fluid) in a paper sample vs. time (Washburn-scaling, $\sim t^{1/2}$), according to Ref. [27]. The implication is that the saturation is incomplete behind the front.

theoretical models are built. The dynamical contact angle at the advancing front is generally dependent on the local dye concentration. This may act as a surfactant, with a time-dependent concentration. Similar behaviour can be observed for various mixtures of liquids: time-dependent changes to the composition vary the viscosity and affect the time-scales [72]. Alternatively the absorption can be slow on the time-scale of the dynamics [325]. We do not want to deal extensively with the effects that these complications may have on the reformulation of the interfacial theories for imbibition, but list below only some possible effects that one should keep in mind.

If the surfactant transport is diffusive, one gets ac-

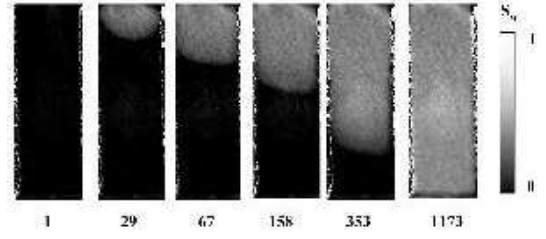


FIG. 12: X-ray computer tomography of spontaneous counter-current imbibition of water into *n*-decane in diatomite [349]. Notice the slowing-down of the sharp interface between dark and light (the latter denoting water-saturated regions).

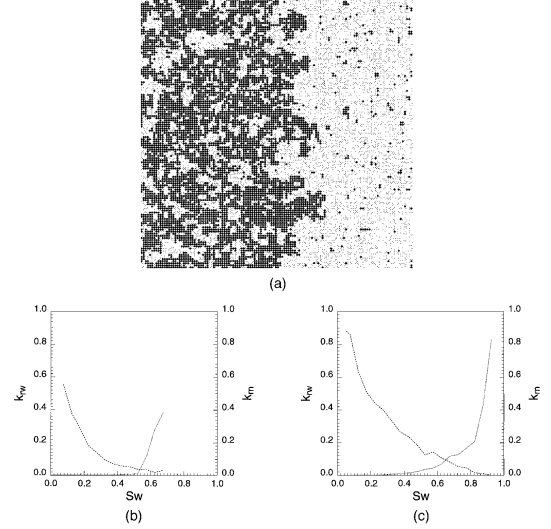


FIG. 13: Dynamic simulations of imbibition, showing how a front can exist even in conditions of “secondary imbibition” or initial wetting phase saturation. [136]. The capillary number is $C_a = 10^{-7}$, and the wetting saturation 0.4. In the top panel, a snapshot, while the two lower ones show the relative permeabilities for two and three dimensional systems (128^2 and 20^3 , the contact angle $\theta = 50$ degrees. Initial wetting phase saturation was chosen as 0.063.

identally Washburn-like dynamics but anomalous diffusion can clearly change this and lead to almost arbitrary temporal scalings. At the very least, the expected length and time scales will change, sometimes drastically [56, 127]. The effect of the surfactant (or time-dependent composition) (e.g. [205, 273]) can be understood based on, e.g., viscous dissipation at the contact line, which changes the dynamical contact angle. This is a research field in its own, related to the physics of thin films and droplet spreading (see [68, 217, 315, 316] among others).

Generally, deviations from Washburn behaviour can easily exist. This is particularly so at early times, due to the dissipation-induced changes [270]. The fast movement of menisci, coming from microscopic geometric considerations, coupled to the viscosity of the fluids involved, leads to dissipation at the front (viscous stresses) and should persist in all regimes and at all times in sponta-

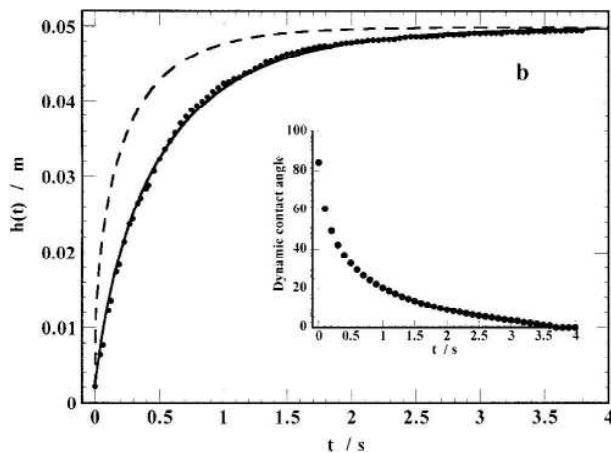


FIG. 14: The rise of a column of water (and the effective dynamic contact angle) vs. time in a capillary rise example. Notice the changing angle and the deviations from Washburn’s law (best fit with the dashed line) [118].

neous imbibition [328, 329]. Some progress in accommodating dynamical phenomena can be made by modifying directly the contact angle in Washburn-like effective equations [117], see Fig. 14.

It should not be forgotten that the porosity can be also be changed in a time-dependent way by the deposition of any particles carried by the invading liquid [97, 98, 340], which again may lead to some erratic behaviour for the front. We note that the same conclusions can coincidentally be obtained in the case of non-Newtonian fluids [60, 262, 343]. Only recently there have been some experimental developments on the scale of network model systems [327]. Similarl to three-phase systems [76, 96] such work highlights the upscaling problems when the pore-level behaviour varies widely. For shear-thinning fluids the local fluid response inside a single pore depends on the flow rate, i.e., on both the global front dynamics (due to fluid conservation) and on pore details such as size or connectivity. A possibly general trend is a less distinct front due to microscopic flows. Similarly, it should be noticed that ink, often used in imbibition experiments behaves rheologically as a non-Newtonian fluid [13]

The treatment of microscale dynamics, such as inertia and film flow at the pore-level, is very delicate at the level of hydrodynamic equations and initial conditions [159, 193]. However, the central point is that these details enter the hydrodynamical description in a coarse-grained way. This leads to a macroscopic front velocity which has either a Washburn-like behaviour, but with effective permeability and capillary pressure, or to a completely different scaling behaviour [302]. Microscopic simulations of capillary imbibition imply that modified Washburn-type equations ensue [219]. Nevertheless, on a macroscopic scale, averaged over a history of penetration and a representative volume, the situation is of course open.

B. Non-equilibrium processes and roughening of fronts

The front between the wet and dry regions roughens as it propagates. This is the main emphasis in our review. The spatial and temporal statistics of the interfaces is easily observed by the naked eye, as in Fig. 1, and they remind, in general terms, of other “rough” objects such as fractures in inhomogeneous media, fronts in slow combustion, flux lines in disordered superconductors, and Brownian paths in diffusion [20, 116, 148, 224]. The existence of so many analogies poses the fundamental question of universality. If the roughness is *scale-invariant*, it can be described by fluctuations and correlations that possess power-law behaviour, reflected in typical quantities such as the spatial and temporal two-point correlation functions, $G_2(r)$ and $C_2(t)$ respectively (see Eqs. (47) and (49)). These functions exhibit dynamical scaling that establishes *critical exponents*, understood in the usual sense of statistical mechanics. The exponents — like those of the celebrated Kardar-Parisi-Zhang (KPZ) equation [147] — are related to a particular *universality class* with its symmetries embedded in a Langevin-like equation for the interface. In Sections III C 1 to III C 5 we review the appropriate parts of the theory of kinetic roughening.

In the late 1980’s much effort was put into the physics of fluid fronts (e.g., in disordered Hele-Shaw cells) to produce clear power-laws with well-established exponents related to a particular universality class. The hope in the imbibition context was that the non-local nature of the problem could be neglected in favour of a local description, partially for simplicity but also because the complications involved would otherwise seem unsurmountable [157]. In reality, the experimental picture turned out to be much more complicated and often not directly related to any of the expected universality classes and the question of an effective theory for imbibition front remains.

The main problems that a theoretical description must solve are the nature of the noise acting on the interface and the effect of non-locality induced by fluid conservation. At the simplest level the fluid pushing the interface flows according to Darcy’s law, which already implies that the advances of sections of the fluid front are coupled. Often a length scale ξ_\times along the interface emerges, which is related to the average motion of the interface and sets the maximum extent of “local fluctuations”.

This is intuitively clear for spontaneous imbibition since fluctuations have a larger instantaneous velocity when behind the front compared to when that are ahead of it. Consider an effective surface tension γ^* , representing the macroscopic energy cost of a curved interface. The curvature arising from fluctuations changes the pressure by $\Delta P = \gamma^*W/\xi_\times^2$ (the Laplace pressure or Gibbs-Thomson effect) where W is the vertical and ξ_\times the lateral scale of the fluctuation. This pressure change slows down advanced parts of the interface. Comparing it to the overall pressure drop across the same vertical

distance, $\Delta P = p_c W/H$, yields a lateral length scale

$$\xi_x^2 \sim \gamma^* H/p_c. \quad (21)$$

This indicates that fluctuations on a scale larger than ξ_x are suppressed by the pressure field gradient p_c/H . For an interface slowing down in spontaneous imbibition it follows directly from Eq. (11) that $\xi_x \sim H^{1/2} \sim t^{1/4}$ and for the transversal width of interface fluctuations $W \sim t^\beta$ with $\beta = \chi/4$ where χ is the roughness exponent of the interface (see Section III G for a more detailed discussion of χ and the criticality of imbibition fronts).

Since the velocity of the interface $v = (\kappa p_c)/(\eta h)$, the length scale ξ_x can be rewritten in term of the capillary number $\xi_x = (\kappa/C_a)^{1/2}$, which highlights the importance of low capillary number experiments. Theoretical analysis, to be presented in Section III also shows that ξ_x is present in forced flow experiments, where it separates two different spatial scaling regimes.

The fluctuations of the interface have three sources: variations in the permeability $\delta\kappa$ (the fluid has to flow to the interface but does not do so uniformly), capillary forces δp_c and volume (the advancing fluid has various pores to fill, thus Δh depends on such fluctuations). It will be shown in Section III that disorder coming from saturation disorder can usually be neglected and that capillary and ‘‘mobility’’ (arising from the random permeability) noise act on different length scales, characterised by $\xi_{\text{mob}} \sim \kappa^2 \delta p_c / v \eta \delta \kappa$. On lengths $l \ll \xi_{\text{mob}}$, capillary noise is dominant, while mobility disorder is relevant on length $l \gg \xi_{\text{mob}}$. Of course, the permeability can also be influenced by an interaction between the fluid and the medium and complicate this picture.

It is also possible that for small interfacial velocities the physics changes. Instead of the liquid front propagation via jumps or advancement of the menisci, pores in contact may be partially wetted by film flow. From a fundamental viewpoint this is the regime that, if described by local interface equations, would exhibit *avalanche behaviour*: most of the interface stays quiescent while only parts advance. The description for such dynamics in usual kinetic roughening involves geometrical ideas that draw parallels to directed percolation and its cousins in various branching processes [216, 314].

III. THEORETICAL APPROACHES TO IMBIBITION

The usual models, to analyse imbibition, can be divided into two main groups. There are ones built in close connection to experimental studies, whose goal is to further develop any details important for applications. Roughly speaking these are related to the microscopic or small scale properties of the imbibition systems. We shall also present some of these aspects in Chapter IV when reviewing experiments. Such models are particularly useful when the microscopic physics at the front include prewetting layers, film flow or when the saturation properties

of the whole medium, as a function of time, need to be addressed. In the latter case one often needs to include detailed considerations about the behaviour of residual pockets of the gas/liquid left behind the imbibition front.

On the other hand the models presented in this Chapter are more concerned with questions of universality in the morphology of the wetted region. Generally they include microscopic details on a more abstract ground, incorporated, e.g., in the noise terms included. They are meant to highlight the connection between the essential mechanisms, as ingredients into the model, and the outcome in macroscopic morphology.

A. Morphological phases in imbibition

The stability of the interface between the invading and the defending liquid was one of the first issues to be studied [317]. A relation between the capillary number of the fluid invasion process and the size of fingering structures in the interface has been found. In the limit of very thin fingers the invading fluid forms a self-similar fractal cluster which belongs to the universality class of invasion percolation [154]. In fact, there is a transition between compact and fractal morphology of the invading fluid cluster [142, 154, 187]. The capillary number C_a in Eq. (2) relating viscous and capillary forces is a control parameter, e.g., in an experimentally obtained phase diagram and examples of morphologies from [187] are shown in Figures 3 and 4. If the porous medium is easily wetted the cluster tends to be compact. The wetting properties, measured in terms of the static contact angle θ , are related to the fingering width of the interface. With increasing wetting tendency it increases and finally diverges at a critical contact angle θ_c , below which the invading fluid cluster remains compact and forms a well defined albeit rough front [154].

Compact invasion clusters with self-affine rough fronts have already been reported earlier [288]. At the same time theoretical description and modelling as well as experimental studies of roughening interfaces were intensively studied and have thus created a lot of interest in imbibition. The central objective of this Review are rough fronts in imbibition, and in this Chapter we present different model approaches to them and their theoretical evaluation. Before that we give a phenomenological introduction to the elementary processes in imbibition (Section III B), as well as a brief recall on kinetic roughening in Section III C.

B. Phenomenological approach to imbibition with rough fronts

The interest on front roughening in imbibition was first and foremost motivated by the assumed connection to the KPZ equation [147] and its underlying theoretical relation to experimental systems. Such spatially local

equations were considered after the “full” problem was proven to be very complicated and they hope to capture the essential features by focusing on the interface only. This description is valuable, perhaps, for (nearly) pinned interfaces, although also here interesting physical complications arise near the pinning transition which are the subject of Section III D.

It was however quickly realised that the detailed nature of fluid invasion could not be ignored [121]. The first theoretical efforts in front roughening with a *global* conservation law were done by Krug and Meakin [160]. They considered the roughening of a Laplacian front as discussed below, using a linear analysis. This is similar to the problem of Saffman and Taylor [291], for the stable case of a high viscosity fluid entering a low viscosity one.

Since the Laplacian one is a basis for later theories as well, it is worth considering it in some details. The starting point of such an analysis is based on the phenomenological law of Darcy for flow in porous media,

$$\mathbf{q} = -\frac{\kappa}{\eta} \nabla P \quad (22)$$

where \mathbf{q} is the flux of liquid, η the viscosity, and κ the permeability of the medium, essentially dependent of the size of the channels through which the liquid flows (c.f. Equations (15) to (11) in the Introduction). The incompressibility condition $\nabla \cdot \mathbf{q} = 0$ leads to a Laplace Equation for the pressure

$$\nabla^2 P = 0. \quad (23)$$

The front then propagates because of mass transport by the flow \mathbf{q} , whose component normal to the front determines the front velocity

$$v_n = -\frac{\kappa}{\eta} \partial_n P, \quad (24)$$

where ∂_n represents the normal derivative to the front.

We consider the situation described in Fig. 15. The interface, of average height H , is described by a single-valued function $y = h(x, t)$ with Fourier decomposition

$$h(x, t) = H + \sum_{k \neq 0} h_k(t) e^{ikx}. \quad (25)$$

At the level $y = 0$ the medium is in contact with an outer reservoir of liquid and the pressure is supposed to be controlled to $P(x, 0; t) = \mathcal{P}_0(t)$. At the interface the boundary condition for the pressure is

$$P_{\text{int}} = P(x, h(x, t); t) = P_0 - p_c - \sigma \mathcal{K} \quad (26)$$

where p_c is the coarse-grained capillary pressure, introduced in Section II A, P_0 is the atmospheric pressure of the ambient gas, and \mathcal{K} is the curvature of the front. Up to linear order in the interface fluctuations $\delta h(x, t) = h(x, t) - H$, the pressure field is given by

$$p(x, y, t) = \mathcal{P}_0 - \frac{\eta v}{\kappa} y - \sum_{k \neq 0} e^{ikx} \left(\frac{\eta v}{\kappa} + \sigma k^2 \right) \frac{\sinh ky}{\sinh kH} h_k \quad (27)$$

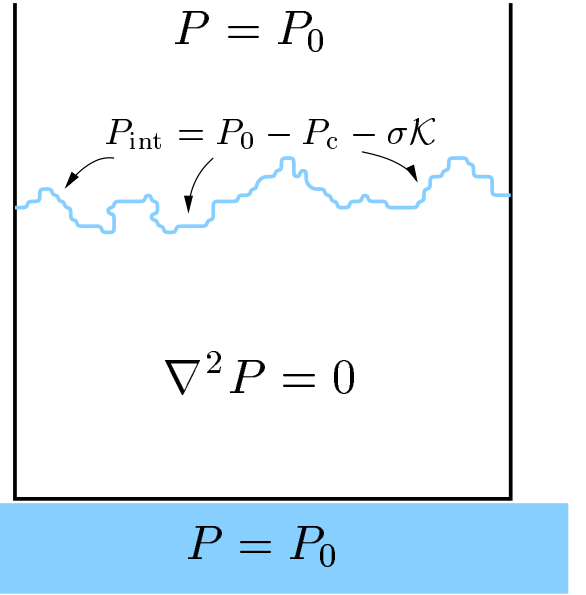


FIG. 15: Theoretical concepts of modelling imbibition. A rough front is situated at the average height H . A pressure field solves Laplace’s equation in the bulk, boundary conditions are given at the contact line to the liquid reservoir and at the rough interface. Pressure gradient is proportional to flux, and influx at the interface proportional to interface displacement velocity.

where the average displacement of the interface

$$v = \frac{dH}{dt} = \frac{\kappa}{\eta} \frac{\mathcal{P}_0 - P_0 + p_c}{H}. \quad (28)$$

The dynamical equation for the interface fluctuation [160] is then

$$\frac{dh_k(t)}{dt} = -\frac{|k|}{\tanh |k|H} \left(v + \frac{\kappa}{\eta} \sigma k^2 \right) h_k(t). \quad (29)$$

Several important conclusions can already be drawn from this analysis:

(i) The average behaviour of the interface is determined from the pressure at the bottom of the porous medium. A constant pressure gradient results in a constant average velocity of the interface v . On the other hand, if the porous medium is simply immersed into a reservoir at atmospheric pressure P_0 , the average interface velocity decreases with the average height

$$v = \frac{\kappa}{\eta} \frac{p_c}{H}. \quad (30)$$

Solving for $\partial_t H = v$ makes the Washburn-Darcy behaviour apparent,

$$H^2(t) - H^2(t_0) = 2 \frac{\kappa}{\eta} p_c (t - t_0). \quad (31)$$

(ii) There exists an intrinsic length scale

$$\xi_\times^2 = \frac{\kappa}{\eta v} \sigma \quad (32)$$

that separates two different modes for the relaxation of the interface fluctuations. If this interface moves at a constant velocity, this length is fixed and static, while it is dynamical ($\xi_\times \sim v^{-1/2} \sim t^{1/4}$) for spontaneous imbibition. Note that the capillary number $C_a = \eta v / \sigma$, relating the viscous and capillary forces, can be used to rewrite $\xi_\times = (\kappa / C_a)^{1/2}$.

(iii) There are odd powers in momentum, more precisely a dependence on $|k|$ in the dynamical Equation (29), which reflects non-locality in space arising from the conservation law. However, the truly non-local $|k|$ -dependence cancels for wave-vectors $|k| \ll 1/H$, meaning that the interface must be far enough from the reservoir of liquid to start to feel the effects of conservation. The surface dynamics is then local in the sense that points with mutual distance greater than H are essentially independent of each other.

(iv) This equation is in principle readily applicable to the case of fluid propagation in Hele-Shaw cells filled with glass beads [220], but the nature of the disorder remains ambiguous. Krug and Meakin [160] chose for their application to use non-conserved thermal noise, $\langle \eta_k(t) \eta_{k'}(t') \rangle \sim \delta_{k,-k'} \delta(t-t')$, which gives rise to asymptotic logarithmic roughness, not observed experimentally in imbibition. Nevertheless, this equation already gives some hint about the influence of the conservation law.

The simultaneous treatment of quenched disorder and liquid conservation was first attempted by Brenner and Ganesan [99]. They assumed that the capillary pressure was dependent on the spatial location \mathbf{x} and random, $p_c = p_c(\mathbf{x})$, as well as a constant mobility κ . Their end result is similar to that of Eq. (29), although it includes non-linearities and the quenched nature of disorder,

$$\frac{dh_k(t)}{dt} = |k| \left(\frac{\kappa p_c}{H} + \kappa \sigma k^2 \right) h_k(t) - \frac{\kappa p_c}{H} \int dk' k' [k - k'] h_{k-k'} h_{k'} - \kappa \sigma \int dk' |k'|^3 [k - k'] h_{k-k'} h_{k'} + \eta_k. \quad (33)$$

The noise term η_k is obtained by assuming that the boundary condition Eq. (26) can be modified by adding a random part $P_{\text{int}} \rightarrow P_{\text{int}} + \eta(x, h)$ with so-called random field correlations $\langle \eta(x, h(x, t)) \eta(x', h(x', t')) \rangle = \Delta \delta(x-x') \delta(h(x, t) - h(x', t'))$. These would amount to the fluctuating part of the capillary force at the interface. Note that the non-linearities also appear non-locally in space, contrary to the usual non-linear term introduced in the KPZ equation outlined in the next subsection. The noise term also enters the interface equation in a non-local way. It is however difficult to extract any results from this method, since Eq. (33) is not very well suited even for direct numerical integration. A Flory-type analysis (term-by-term comparison of typical magnitudes of the terms) yields a roughness exponent $\chi = 3/4$ but this result is questionable since it is well known that a similar analysis gives wrong results in the simpler case of the so called quenched Edwards-Wilkinson (QEW) equation discussed also below.

This analysis was pushed further by Pauné and Casademunt [261]. They considered the specific problem of fluid flow in a Hele-Shaw cell, where the only disorder is through variation in the thickness of the cell b . This implies that both the capillary pressure

$$p_c = \sigma \cos \theta \left(\kappa + \frac{1}{b} \right) \quad (34)$$

and the permeability $\kappa \propto b^2/\eta$ become random quantities. They then proceeded to derive a phenomenological equation that combines Eq. (33) and earlier equations derived by Hernández-Machado *et al.* and Dubé *et al.* (these are discussed in more detail later). This

work shows that disorder in the capillary pressure and in the mobility act on very different length scales depending on the velocity of the average interface, as will be discussed in details in Section (III G 5). At the simplest level the main source of disorder will come from variation of thickness $b \rightarrow b + \delta b$, which affects the capillary pressure $p_c \sim p_c + \delta p_c$ and the permeability $\kappa \sim \kappa + \delta \kappa$,

$$\frac{\delta p_c}{p_c} = -\frac{\delta r}{r_0} \quad \text{and} \quad \frac{\delta \kappa}{\kappa} = \frac{\delta r}{r_0}. \quad (35)$$

Based on a simple Darcy analysis, this would suggest that variations in the velocity due to permeability disorder δv_κ are of the same order of magnitude as those due to variation in the capillary pressure δv_{p_c}

$$\left| \frac{\delta v_{p_c}}{\delta v_\kappa} \right| \sim \left| \frac{\kappa \delta p_c}{p_c \delta \kappa} \right| = -1, \quad (36)$$

which would imply that both sources of disorder are equally important. This may be right for the specific case of a Hele-Shaw cell with varying thickness but not necessarily for more general random media such as paper.

C. Theoretical description of rough interfaces

1. The concept of roughness

The exact shape of a rough front or interface in a given dynamical process depends on the particular realization of randomness encountered and is unpredictable. The statistical properties of its shape fluctuations however

can be described in a controlled way. Quite often one observes statistical scale invariance in certain ranges of time and space. Naively this means that the interface “looks the same” when its parallel and perpendicular length scales are “blown up” or “shrunk” by certain factors. In this Section, as well as in the entire Article, we consider interfaces with translational invariance, meaning that they “look the same” no matter which part of them you consider. For an illustration see Figure 16.

Roughness need not be a static phenomenon but changes its properties in time. Typically, a growing or moving interface will increase its roughness with time, as single fluctuations are accumulated. We will also see scale invariance in time, i.e., an interface “behaves the same way” when time is speeded up or slowed down with an according spatial rescaling.

The relation to critical phenomena is evident. Statistical scale invariance over a certain range of length scales reflects itself in power law shapes of correlation functions. As with critical phenomena, one observes different types of power law behaviour of interfaces, which are therefore referred to as *universality classes* as well [20, 161, 218].

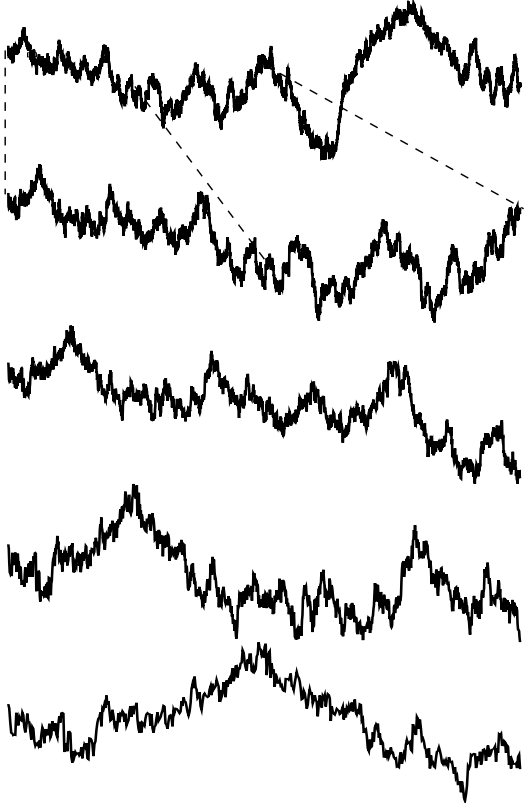


FIG. 16: Different aspects of an interface, magnified by a factor 2 in each step from top to bottom, as indicated by the dashed lines between the first two panels. No inherent length scale becomes visible, all surface pieces “look the same”

2. Formal description of roughness

Let us try to formalise the intuitive picture of shrinking and enlarging the aspect of an interface. Generally, an interface \mathcal{S} is an orientable d -dimensional object in $(d + 1)$ -dimensional space. A crystal surface is an example for $d = 2$ while a step separating two terraces on it is one for $d = 1$. Since the interface is orientable, we can define an indicator function $\varphi : \mathbb{R}^{d+1} \rightarrow \mathbb{R}$ which takes the value 1 on one side of the interface, -1 on the other, and 0 right on top of it. In the example of a crystal one can choose $\varphi = 1$ inside and $\varphi = -1$ outside.

To examine the roughness on various scales we use a smoothing kernel

$$f_{d+1}^L(\mathbf{x}) \equiv \frac{1}{B_{d+1}L^{d+1}} f\left(\frac{|\mathbf{x}|}{L}\right) \quad (37)$$

for some monotonously decreasing function $f(r)$ with the property $\int_0^\infty dr r^d f(r) = 1$, and the d -dimensional surface volume of the $(d + 1)$ -dimensional unit sphere $B_{d+1} = \frac{2\pi^{(d+1)/2}}{(d+1)\Gamma((d+1)/2)}$. By convolution one can obtain via the smoothed profile function

$$\varphi_L(\mathbf{x}) \equiv \int d^{d+1}y f_{d+1}^L(\mathbf{x}-\mathbf{y}) \varphi(\mathbf{y}) \quad (38)$$

the surface smoothed to a scale L

$$\mathcal{S}_L \equiv \{\mathbf{x} | \varphi_L(\mathbf{x}) = 0\}. \quad (39)$$

The profile function $\varphi_L(\mathbf{x})$ contains information about how far a point is away from \mathcal{S}_L : If \mathcal{S} is a hyperplane, \mathcal{S}_L remains identical to it and $\varphi_L(\mathbf{x}) = F(\delta/L)$ where δ is the distance between \mathbf{x} and \mathcal{S} , and $F(r) = \int_0^r ds s^d f(s)$. So, it is natural to define

$$\delta(\mathbf{x}, \mathcal{S}_L) \equiv L F^{-1}(\varphi_L(\mathbf{x})) \quad (40)$$

as a measure for the distance of a point \mathbf{x} from \mathcal{S}_L . When \mathbf{x} is taken on the original interface \mathcal{S} Equation (40) gives an access to its roughness fluctuations on scales smaller than L . For an illustration see Figure 17

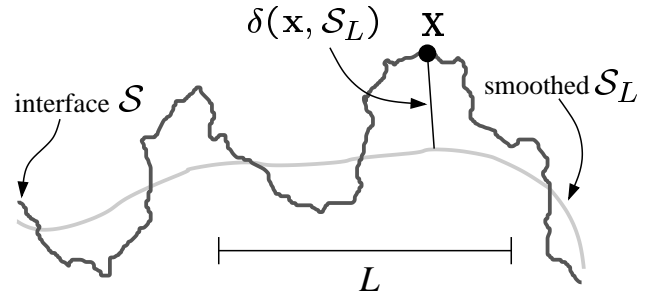


FIG. 17: Example for construction of \mathcal{S}_L and $\delta(\mathbf{x}, \mathcal{S}_L)$ in $d + 1 = 2$ dimensions.

Generally one observes power law scaling of the various moments of roughness,

$$w_q(L, t) \equiv \langle \langle \delta(\mathbf{x}, \mathcal{S}_L)^q \rangle_{\mathbf{x} \in \mathcal{S}} \rangle_{\mathcal{S}}^{1/q} \sim L^{X_q} \text{ for } L < \xi(t) \quad (41)$$

saturation to a constant for L larger than the so called *correlation length* $\xi(t)$. In this definition $\langle \cdot \rangle_{\mathbf{x} \in \mathcal{S}}$ takes the average over all points in \mathcal{S} . The outer brackets stand for the ensemble average over all possible interface configurations. The measure for these averages is inferred from the area of the interface and is straightforward to construct in most cases; χ_q is called roughness exponent of the q th moment.

In the case of multiscaling the χ_q differ from each other. A classical illustration of this is given by the concept of “turbulent interfaces” introduced by Krug in [162]. Its point is best illustrated on a discrete crystal lattice: The height fluctuations may be related to the *largest* step heights between two neighbouring points on the discrete lattice. This introduces a new length scale $\Delta h = |h_{x+1} - h_x|$ which then makes the scaling more complicated. The different momenta of w_q would show a relation to the largest values of Δh in L . Δh can then depending on the model exhibit various behaviours: E.g., its probability distribution can be directly a function of the system size [162, 303], or at least have a cut-off imposed by it [11, 235]. Many physical processes lead instead to (regular) or normal self-affine scaling with $\chi_q \equiv \chi = \text{const}$, to which we restrict ourselves for most of this article, omitting the index q and mentioning possible cases of multi-scaling by remarks when necessary.

In a roughening process the correlation length $\xi(t)$ increases with time, because physical coupling of different points in the interface spreads fluctuations. Again, in general one observes power law behaviour, which for historical reasons related to the theory of critical phenomena is written

$$\xi(t) \sim t^{1/z} \quad (42)$$

with z the dynamical exponent. The maximal extent of interface fluctuations is

$$w(t) \equiv \lim_{L \rightarrow \infty} w(L, t) \sim \xi(t)^\chi \sim t^{\chi/z} \equiv t^\beta, \quad (43)$$

which connects the relations (41) and (42) and defines the scaling exponent β .

All these relations can be combined into a scaling form

$$w(L, t) = \alpha(t) \xi(t)^\chi \mathcal{W}\left(\frac{L}{\xi(t)}\right). \quad (44)$$

with the scaling function $\mathcal{W}(x) \sim x^\chi$ for $x < 1$ and approaches a constant for $x \gg 1$. In many cases the amplitude $\alpha(t)$ is constant, which is referred to as normal scaling. It may however increase with time, causing one sort of so-called anomalous scaling [198]. This behaviour occurs for forced flow imbibition with columnar disorder, analysed theoretically in section III G 6 and experimentally in Section IV.

In most cases $0 \leq \chi \leq 1$, but it need not be restricted to that range. Interfaces with $\chi > 1$ sometimes are called “super-rough” [82, 198, 199]. One-dimensional interfaces in disordered two-dimensional media are examples for

super-roughness [144, 188, 189, 190, 191] and of particular interest for imbibition in effectively two-dimensional media such as paper or thin Hele-Shaw cells [82, 83, 84].

3. Height fields without overhangs

The quantitative description of interfaces can be simplified a good deal when overhangs can be neglected. An interface is then represented by a height field $h(\mathbf{x}, t)$ moving in time, $t \in \mathbb{R}$, over some d -dimensional substrate, whose points are $\mathbf{x} \in \mathbb{R}^d$. The roughness exponent χ is then linked to the *structure factor* or spatial power spectrum

$$S(\mathbf{k}, t) \equiv \langle |h(\mathbf{k}, t)|^2 \rangle \sim \begin{cases} k^{-(2\chi+d)} & \text{for } k \gg 1/\xi(t) \\ \xi(t)^{2\chi+d} & \text{for } k \leq 1/\xi(t) \end{cases} \quad (45)$$

where $h(\mathbf{k}, t)$ denotes the spatial (d -dimensional) Fourier transform of $h(\mathbf{x}, t)$. The scaling behaviour of Equation (45) is illustrated schematically in Figure 18. From this schematic representation the scaling form

$$S(\mathbf{k}, t) = \xi(t)^{2\chi+d} \mathcal{S}(\xi(t)|\mathbf{k}|) \quad (46)$$

of the power spectrum becomes evident. As in Equation (45), we have $\mathcal{S}(\kappa) \sim \kappa^{-2\chi-d}$ for $\kappa \gg 1$, and $\mathcal{S}(\kappa) \equiv \text{const}$ in the opposite limit.

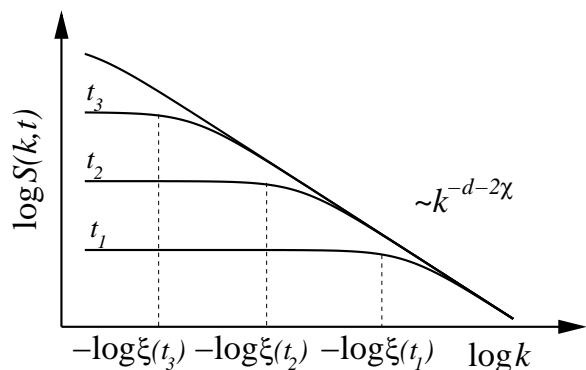


FIG. 18: Schematic plot of structure factors $S(k, t)$ of an interface at times $t_1 < t_2 < t_3$ in double logarithmic scale. The correlation length $\xi(t)$, as well as the intensity of long wavelength fluctuations $S(k \rightarrow 0, t)$ increase with time.

Often the height difference correlation function

$$G_2(\mathbf{x}, t) \equiv \langle |h(\mathbf{x}, t) - h(0, t)|^2 \rangle = \int_{\mathbf{k}} S(\mathbf{k}, t) (1 - \cos(\mathbf{k} \cdot \mathbf{x})) \quad (47)$$

is measured. It is self-averaging (unlike $S(\mathbf{k}, t)$), so “smooth curves” are easily obtained from spatial averaging, but one tends to neglect that the initial power law increase for $|\mathbf{x}| \ll \xi(t)$ reflects only the *local* roughness exponent χ_{loc} which due to convergence of the integral

in Eq. (47) is restricted to values ≤ 1 [164, 189]. Thus, to study a super-rough interface with $\chi > 1$, the power law decrease of $S(\mathbf{k}, t)$ should be analysed instead.

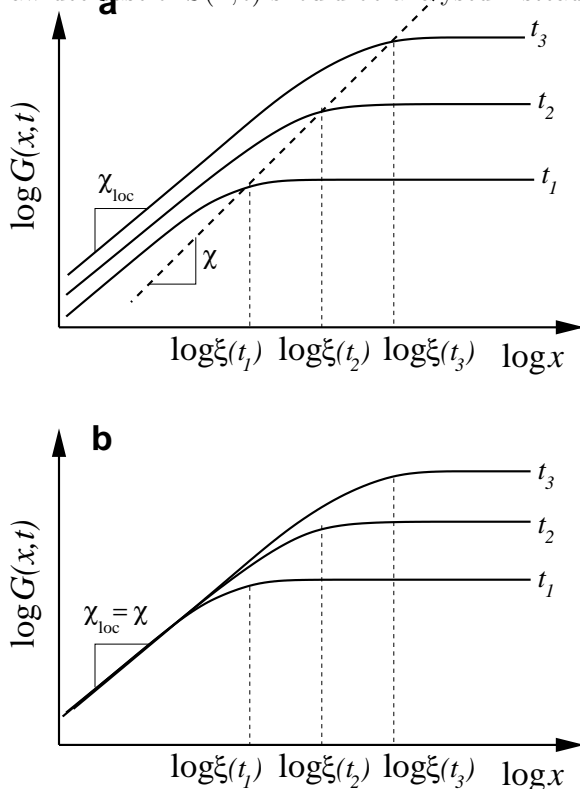


FIG. 19: Schematic plot of height difference correlation functions $G_2(x, t)$ of an interface at times $t_1 < t_2 < t_3$ in double logarithmic scale. Part **a** illustrates anomalous scaling of a super-rough interface with $\chi > \chi_{loc} = 1$, part **b** normal scaling with $\chi = \chi_{loc}$.

Figure 19 contains a schematic representation of $G_2(\mathbf{x}, t)$ for a super-rough (part **a**) and a normally rough (part **b**) interface. In part **a** it becomes clear why measuring the initial power law increase does not yield the global roughness exponent χ .

4. Temporal interface fluctuations

In the same way as in the spatial case, interface fluctuations can be studied in the course of time. We have already seen the increase of the interface width with time, $w(t) \sim t^\beta$ with $\beta \equiv \chi/z$ in Eq. (43), valid for early times as long as $\xi(t)$ is smaller than the lateral size of the system containing the interface.

Analogous to $S(\mathbf{k}, t)$ and $G(\mathbf{x}, t)$ one can construct quantities reflecting the temporal fluctuation of the interface height above a substrate point \mathbf{x} . These are conveniently defined for stationary processes at late times in a finite system, i.e., when $\xi(t) = L_{\text{system}} < \infty$, and contain, e.g., the power spectrum

$$S(\mathbf{x}, \omega) \equiv \langle |h(\mathbf{x}, \omega)|^2 \rangle \quad (48)$$

of the Fourier transform of the height field in time ($t \rightarrow \omega$), or the correlation function of the q th moment of height “jumps” over a temporal distance t

$$C_q(\mathbf{x}, t) \equiv \langle |h(\mathbf{x}, t+s) - h(\mathbf{x}, s)|^q \rangle^{1/q}. \quad (49)$$

Generally one finds an increase $C_q(\mathbf{x}, t) \sim t^{\beta_q}$ over “short” time distances t . In the case of (*conventional*) *scaling* it is related in a simple fashion to the early time increase of the width in Eq. (43), i.e., for all q -moments $\beta_q \equiv \beta = \chi/z$. For practical purposes $C_q(\mathbf{x}, t)$ is easier to measure than $w(t)$ at early times and therefore this relation is often used.

This simple picture does not hold if height fluctuations are intermittent, e.g., if the interface advances in avalanches with a non-trivial size distribution. In the experimental context this is known as Barkhausen noise, originally measured for the motion of boundaries between domains of different magnetisation in a solid with disorder [21]. It is not surprising that imbibition into a disordered medium also exhibits multi-scaling in time, and it will play a role in several parts of this Review.

5. Brief history of roughness

Roughness of interfaces and surfaces has been studied in many contexts and on all scales, and the interest in the roughness of imbibition fronts was based on these previous studies to a large extent. To name a few examples: cloud fronts, mountain rims, shore lines, rivers, forest ranges, sandpiles, biofilms, cell colonies, cancer, grain boundaries in polycrystals, crystal surfaces, crystal terrace steps, deposited thin films, flux lines in superconductors, fracture fronts ... (see again e.g. [20, 116, 224, 314]).

The theoretical interest arose from the observation that many completely different roughness phenomena exhibit the same (or similar) scaling exponents, and therefore be understood as belonging to the same “universality class”. Consequently a main theoretical emphasis has been to find the essential mechanisms behind the different universality classes by constructing the simplest possible models with the same roughness properties as a given observed process in nature.

To use a simple “classification” there are two kinds of models: Continuum equations, in most cases stochastic partial differential equations, are more suitable to an analytical approach, either by exact solution or by renormalisation and perturbative approaches. On the other hand, lattice or particle based models are well suited for simulations, often on large scales.

Among the continuum equations we name only the most classic ones. First, the linear Gaussian model of Edwards and Wilkinson (EW equation) for a surface relaxing by surface tension or downhill surface current and perturbed by noisy forces [89], which can in the stationary state be said to be in equilibrium. Second, introducing a preferential direction of growth to the surface,

Kardar, Parisi, and Zhang (KPZ) constructed a true non-equilibrium model. It (as they noted) is equivalent to Burger's equation for a vortex-free, compressible, randomly driven fluid [44, 147]. It reads

$$\partial_t h(\mathbf{x}, t) = \sigma \nabla^2 h(\mathbf{x}, t) + \lambda (\nabla h(\mathbf{x}, t))^2 + \eta(x, t), \quad (50)$$

where σ is a surface tension, and λ measures the strength of the celebrated KPZ nonlinearity, proportional to the squared local slope of interface. In the case $\lambda \equiv 0$ one obtains the EW case. $\eta(x, t)$ denotes here a simple delta-correlated "thermal" noise field, that roughens the interface. One has thus the correlator $\langle \eta(x, t) \eta(x', t') \rangle = 2T \delta(x - x') \delta(t - t')$. The main ingredient of Eq. (50) is that the interface always has a non-zero normal component of the local growth velocity, with respect to the local interface orientation. Also, the coupling between the noise field η and the non-linearity gives rise to the much-studied complex dynamics and morphology of the KPZ class. As it is in some sense the most fundamental non-equilibrium field theory this equation has gained much interest and was often thought to be the correct large scale description for most experimental and model systems for surface roughening, among them for imbibition — erroneously as we shall see in this review.

Similarly, among the discrete models we briefly mention the family of (driven) lattice gases and equivalent deposition or solid-on-solid models for crystal surfaces, with evaporation or surface diffusion. Discrete in the number of deposited particles, but continuous in space and time are, e.g., ballistic deposition models. A pedagogical overview of growth models can be found in the lecture notes of Krug and Spohn [161]. Covering only the earlier years of studies on kinetic roughening it nevertheless presents the types of models which were relevant for the approach of non-equilibrium statistical mechanics to imbibition and which are presented in this Chapter.

D. Interfaces in disordered media and avalanches

As already stated, there are several cases where the interface separates regions with common characteristics, distinguished by the field ϕ introduced in Section III C. The example of a step separating two terraces was used, but interfaces will also arise between magnetic domains, or in paper around regions that are either burned or wet; in some alloys, it can be the boundary between grains with different orientation of the crystal structure, or even with completely different structure, such as in martensitic materials.

These interfaces can move either spontaneously, under thermodynamic forces, or else through an applied force, such as a magnetic field or a pressure difference. The essential point however is the thermal influence of the environment is often negligible; fluctuations in the interface arise only from the presence of impurities or defects in the material structure itself. These impurities are quenched, i.e., static in time and the disorder felt by the interface

is thus intrinsically dependent on its *position* itself. For example, the KPZ equation, Eq. (50), is modified to

$$\partial_t h(\mathbf{x}, t) = \nu \nabla^2 h(\mathbf{x}, t) + \lambda (\nabla h(\mathbf{x}, t))^2 + F + \eta(x, h(x, t)), \quad (51)$$

where F is the force acting on the interface and the quenched nature of the disorder is reflected in the properties of the noise correlator. Two broad classes are usually distinguished: Random Bond (RB) disorder, where the correlator of η arises essentially from the fluctuations of the surface tension (like in an Ising magnet with random coupling constants). More important is Random Field (RF) disorder, also since in the QEW case discussed below (Eq. (55)) it can be explicitly shown that the Random Bond and Random Field correlators renormalise to the same under rescaling.

In the RF case, the effectively felt noise depends directly on the position of the interface and has correlations

$$\langle \eta(x, h(x, t)) \eta(x', h(x', t')) \rangle = \Delta(h(x, t) - h(x', t')) \delta(x - x') \quad (52)$$

where $\Delta(u)$ is a function which is strongly peaked around $u = 0$, often taken to be a delta function

$$\Delta(h(x, t) - h(x', t')) \rightarrow \delta(h(x, t) - h(x', t')) \quad (53)$$

For an interface moving at some velocity v , we can separate the average motion from the fluctuations $h(x, t) = vt + \delta h(x, t)$. For length scales $l_{\text{th}} > (vt)^{1/\chi}$, the quenched noise correlator

$$\delta(h(x, t) - h(x', t')) \rightarrow \delta(v(t - t') + \delta h) \rightarrow \frac{1}{v} \delta(t - t') \quad (54)$$

and the interface effectively feels an annealed thermal noise with effective strength $\tilde{\Delta} = \Delta_0/v$.

1. Avalanches

On length scales below l_{th} , the quenched nature of the noise is fully felt and a finite threshold force F_c is needed to get the interface in motion. The velocity then shows critical behaviour $v \sim (F - F_c)^\theta$ until $F \gg F_c$ for which $v \propto F$. Equation (51) is then just one example of a system which shows a *depinning transition* when a control parameter, in this case the force F , is tuned.

The physics in this case is best discussed in terms of avalanches, and it is useful to first consider the limit of vanishing nonlinearity $\lambda \rightarrow 0$ of Eq. (51), the so-called quenched Edwards-Wilkinson equation (QEW),

$$\partial_t h(x, t) = \nu \nabla^2 h(x, t) + F + \eta(x, h(x, t)), \quad (55)$$

which is appropriate if the anisotropy (λ) in the dynamics has a "kinematic" origin and vanishes in the limit $v \rightarrow$

0. See also the discussion in subsection III E about the origins of such behaviour and Figure 46 in Section IV.

The case $\lambda = 0$ has received lots of attention in the disordered systems community since it presents a stereotype for the renormalisation group treatments of such systems and associated problems. The QEW-equation is also an interesting candidate for a local description of liquid propagation in porous media since it contains three very important ingredients of the problem: surface tension, driving force, and variations in the local (capillary) force, e.g., due to pore structure fluctuations. This was indeed noticed in the mid-eighties by Koplik and Levine [157] who extended ideas of domain wall dynamics in random field Ising magnets [41] (see also [151]). And indeed, we shall show below that within the length scale ξ_{\times} (Eq. (32)), the physics of imbibition is very similar to the physics that comes from Eq. (55).

It is also worth keeping in mind that spontaneous imbibition exhibits something akin to a velocity-dependence: an interface that slows down experiences different average velocities depending on the distance to the reservoir. Thus, tilts in the interface should affect the local average velocity, again.

For forces just slightly larger than F_c , the interface dynamics in the QEW model is characterised by *avalanches*. This implies typically that large regions of the interface stay quiescent, while only parts move in a coherent manner. This is described by the correlation length $\xi_{\parallel} = (F - F_c)^{-\nu}$, which is related to the fluctuations of the interface via a roughness exponent such that $\xi_{\perp} \sim \xi_{\parallel}^{\chi}$. Temporal scaling, $\xi_{\parallel} \sim t^{1/z}$, is also assumed, and the length- and time scales are related via the relation

$$\theta = \nu(z - \chi), \quad (56)$$

defining the order parameter (velocity) exponent [192, 247, 249].

Since the disorder that the interface “experiences” has a history effect, it is clear that it is non-trivial to compute the correlator of the disorder in a coarse-grained QEW, as already was noticed in the beginnings [157]. Later functional renormalisation group calculations have resolved this issue by pushing perturbation theory up to second order. For uncorrelated disorder the original one-loop functional RG results read $\chi = (4 - d)/3$, and $z = 2 - (4 - d)/9$, with $\nu = 1/(2 - \chi)$. These, together with the θ -exponent, manifest the fact that there is only one temporal and one spatial scale at the critical point. Later work by Chauve, LeDoussal, and Wiese on much more tedious higher-order RG expansions [53, 184] have yielded corrected expressions for the exponents.

For example with $\epsilon \equiv 4 - d$ the original $\zeta = \frac{\epsilon}{3}$ changes to $\zeta = \frac{\epsilon}{3}(1 + 0.14331\epsilon + \dots)$. In particular in $d = 1$, this means that the RG beyond one loop is better able to adhere to the numerical results [188, 192, 249, 286]. These imply that $\chi_{\text{QEW}, d=1} \sim 1.2 \dots 1.25$, i.e., the pinned interface is super-rough. This approximate value makes for an interesting piece of numerology, since the exponent agrees

with the phase field model result for the global roughness exponent as discussed below.

The usual discussion of depinning in the QEW takes place by considering the limit $F \rightarrow F_c^+$ and concerns the values of such critical exponents. One may of course ask questions about the behaviour for a slightly larger driving force, or in particular consider the *avalanches* right at the critical point. For $F > F_c$ one has a cross-over to the thermal EW on large enough scales, Eq. (54), and for the avalanches it holds that they start to overlap, eventually, signalling such a cross-over. It is possible that one can define here effective exponents [157], perhaps analogous to imbibition in many ways. For $F \leq F_c$ in a finite system the velocity goes to zero, into an “absorbing state”.

Avalanches can be observed in the vicinity of a critical point (for a general discussion about phase transitions with an absorbing state see [216], and for an overview of avalanches in similar, critical systems [260]) by imposing a suitable ensemble. With the caveat from above (overlap of avalanches) there are two set-ups that give rise to well-defined avalanches:

- *constant velocity* ensemble, resembling forced fluid flow imbibition,
- *self-organised* critical ensemble, induced by a combination of slowly increasing F and boundaries that pin the interface.

The former is useful in this context since it exhibits translational invariance; one may thus proceed to study in this ensemble the statistics of avalanches and the character of the critical point, as e.g. [175, 248]. SOC, self-organised criticality was coined originally by Bak, Tang and Wiesenfeld [15], in a context that is actually directly related to an interface description or model of charge-density waves. Recent work has expanded and clarified much the picture of SOC as an interface depinning transition [3, 4] or as an absorbing state phase transition as such [75].

The geometric picture of “avalanches” considers a generalised situation where the interface has “pinning paths”, akin to paths on the backbone of a percolation cluster. Assuming that there is a “punctuation event” if the interface is pushed at any particular spot, the interface is released and propagates locally till another connected pinning path is encountered. The geometric properties of avalanches set now the size distribution of avalanches: it is determined by the usual critical exponents and (except perhaps in the SOC ensemble) does not involve other physics. The important quantity is the scaling of voids, between two such paths that pin the interface, or their relation of size vs. area, which immediately involves the roughness exponent. The size distribution of avalanches is then expressed as

$$P(s) \simeq s^{-\tau_s} f(s/L^D). \quad (57)$$

where, if *translational invariance* exists (see above), $D = d + \chi$ and it usually holds that $\tau_s = 2 - 2/D$ [5].

In the DPD case [135] (see next Section and Fig. 20), it is possible to derive the avalanche size exponent τ_s in $d = 1+1$ dimensions as

$$\tau_s = 1 + (1/(1 + \chi))(1 - 1/\nu). \quad (58)$$

Similar scalings can be attempted for the SOC case.

Note, finally, that such scaling laws as Eq. (57) can be established for the duration and support as well, not only for the size or area/volume. The presence of long-range interactions instead of the Laplacian surface tension in Eq. (55) might present some interesting twists [322].

E. Cellular automata for imbibition

Since the apparent failure of the usual kinetic roughening framework to account for the large value of the roughening exponent was partially due to the thermal nature of the disorder, specific models were then developed to account for the influence of *quenched* disorder. In particular, the ‘‘Directed Percolation Depinning’’ (DPD) [7, 45] model completely ignores all effects of liquid conservation to focus only on the quenched nature of disorder. The algorithm that advances the front in this model is essentially similar to the sandpile (and forest fire) models [15] and has three main ingredients, also illustrated in Figure 20:

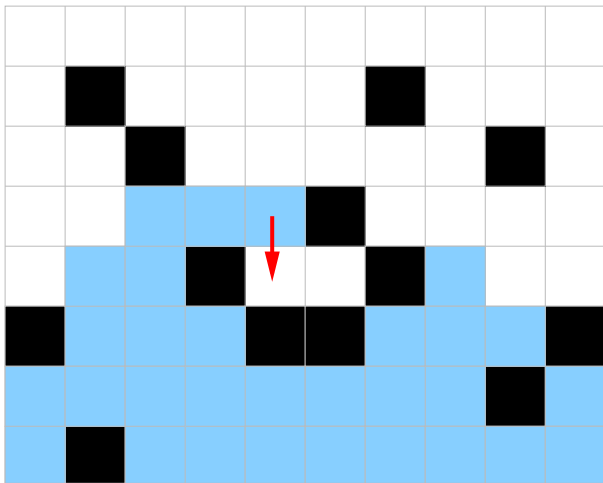


FIG. 20: Schematic representation of the DPD model after [7, 45]. The medium is divided into regular cells. Blocked cells are black, invaded (wet) cells grey, invadable (dry) cells white. Any dry cell adjacent to a wet one can be invaded in the next time step. The arrow indicates a cell which gets wet immediately in order to erase an overhang.

- (i) The porous medium is divided into cells that are either blocked or open for fluid flow. This model was first applied to imbibition of ink into paper, the ink pigment then being instrumental in blocking the flow progression.
- (ii) The progression of the front takes place only in open cells, with overhangs being erased instantaneously. A

later development of the model introduced a linear gradient in the density of blocked cells to phenomenologically mimic the effects of evaporations through an increasing difficulty of propagation [7].

(iii) The progression of the front stops when no neighbouring open cell is available, i.e., when a percolating line of blocked cells is encountered. If p represents the probability of a cell being blocked, interface pinning occurs at the percolating threshold $p_c \approx 0.47$.

The statistical properties of the interface are related to the properties of the percolating path. Close to p_c the directed percolating path is characterised by the parallel and perpendicular length scales $\xi_{\parallel} \sim |p - p_c|^{-\nu_{\parallel}}$ and $\xi_{\perp} \sim |p - p_c|^{-\nu_{\perp}}$, with values $\nu_{\parallel} \approx 1.7$ and $\nu_{\perp} \approx 1.09$. The saturated width of the interface then is $W \sim \xi_{\perp} \sim \xi_{\parallel}^{\nu_{\perp}/\nu_{\parallel}}$, which defines a roughness exponent $\chi = \nu_{\perp}/\nu_{\parallel} \approx 0.63$. It was argued that the right continuum description of this automaton is the quenched KPZ equation, given above in Eq. (51).

The physical justification to the main feature of the DPD model, the erosion of overhangs has already been approached by experimentalists [130]. It is plausible that propagation of the fluid in a direction parallel to the reservoir, if it has a chance to occur, will be favoured over the motion of the fluid away from it, since this does not result in any change in the average capillary pressure. In that sense, any overhangs will eventually be removed, although the question of the different time scales involved in such dynamics is certainly extremely complex. As shall be seen below, phase-field models, which include this possible effect do not show any kind of DPD roughening. Other specific predictions of the DPD or quenched KPZ class would be that of the DPD critical point, a front moving with constant velocity has an effective roughness exponent $\chi = 0.7$ and a dynamical exponent $z = 1$. Leschhorn [191] has moreover shown numerically that the DPD model consistently gives rise to multi-scaling.

A variation of the DPD idea, introduced by Sneppen [306], allows invasion always at sites of lowest resistance. An interesting aspect of this model is temporal multi-scaling [307], due to avalanche motion [190, 256]. Avalanches are also present in the process of spontaneous imbibition, although the conservation law imposes a natural cutoff on their size and distribution [81]. It is nevertheless interesting that a similar lack of temporal scaling is also seen in the phase field model of imbibition, thus surviving the introduction of a conservation law. We refer to that in Section III G below.

The DPD model in its simplest form may or may not describe well the statistical properties of a pinned interface. However, this model cannot describe the whole dynamical motion of the interface, since it does not account for liquid conservation. It already fails by predicting a *constant* average interface velocity, contrary to Washburn’s law. This also holds for dyed liquids, for which the DPD model was originally developed, since the conservation law governing the motion of the fluid must be

reflected on the motion of the dye particles. We conclude that any such *local* interface equation, as for instance the QKPZ one, is not appropriate for imbibition. Note that this extends to interface equations where the coupling between the interface points is non-local [150, 243, 322].

F. Microscopic simulations

The normal alternative approach to imbibition is based on pore network models. The porous medium is represented by an assembly of pores and throats connecting pairs of pores. A simplified case is a network (in 2d) of horizontal and vertical capillary tubes with a stochastic distribution of cross-sections. The nodes between the tubes are structureless in order to avoid all the possible complications described in Chapter IV or by Lenormand in [187]. With this simple structure, the flow within each capillary is of Poiseuille type and the progression of the overall front is dictated by the global pressure difference and local fluid conservation at each node of the network.

Note that there are recent lattice-Boltzmann simulations of multiphase flows that have also tackled flow in porous media and imbibition. The main advantage of the method are easy-to-implement boundary conditions. Other phases such as surfactant are easily added and questions such as Onsager transport coefficients can be analysed from a first-principle viewpoint. Actual examples both in 2d and 3d however highlight the technical challenges [200, 207] associated with the method. A natural idea is to study the front properties exactly as for coarse-grained models and the authors present some examples of rough interfaces with unfortunately little analysis that would compare to usual kinetic roughening measures. However, it seems to us that the capacities of such models have to be augmented considerably before one can expect “realistic” results.

A recently much practised approach is to construct network geometries that attempt to mimic the statistics of the porous media more faithfully via statistical laws for the pore sizes, and fluctuating connectivities (pore throats) for neighbouring pores. Other dynamical aspects (behaviour of residual gas pockets related to saturation, prewetting layers, Bosanquet-flow — see Section IV) can also be added [25, 32, 49, 52, 63, 238, 279, 281, 298]. Simulations can be either quasi-static — the dynamics is applied at the “weakest link”, and no other processes are allowed — or dynamic so that the pressure balance is maintained dynamically at the single pore level [29, 30, 51, 65, 74, 136, 157, 238]. Such simulations are closer to describing the reality of flow through porous media but are naturally heavier computationally. In addition, quasi-static simulations have no time scale, which poses a genuine limitation for many comparisons with experiments and makes studies of kinetic roughening impossible. Only for dynamical simulations are time-dependent mass flows included explicitly using Darcy’s laws and possibly more complicated effects on the pore

level [32, 136].

Both kinds of models have already been used extensively to study the forced and slow displacement of a wetting liquid by a non-wetting liquid, often in connection with oil recovery techniques. Generally there are difficulties for such methods to study interfacial dynamics since the wetting front is a very non-compact object - one has to pay attention to the definition of the interface. Questions that are of relevance from the interface viewpoint and that have been addressed include pore-scale phenomena as broad pore size distributions [300] and the role of the fluid viscosity ratio of the two fluids in controlling micro-fingering for low C_a [335], studies of relative permeabilities [221]. Of major interest is the use of micro-structural parameters (from tomography or from other experimental sources) and the analysis of correlations in the pore scale [10, 42, 125, 141, 153, 212, 257, 258, 308, 326]. Typical quantities considered are relative permeabilities and capillary pressures as well as saturation curves. These all tend to highlight the fact that *in the presence of correlations* the imbibition-related quantities change much more readily than, e.g., single-phase permeability.

Concerning “interfacial aspects” it is of course true that any mass flux into the system in imbibition arises due to and is controlled by the interfacial area between the two different phases. Thus it is a natural quantity to compute, and consider [108]. A related problem is the presence of initial saturations [141], and some network simulations have been done to address exactly this question [106, 255, 276].

Direct interfacial studies in network models [30, 136]. Given complicated — or realistic enough — rules the boundary between completely non-wet (occupied by the non-wetting fluid) and partially saturated regions can be quite complex due to the effects discussed already in detail (film flow, initial presence of wetting fluid etc.). This is of course the strength of network models. Figure 21 illustrates the problems that ensue even in qualitative comparisons with simplistic laboratory setups. The generic features in the Figure show the agreement between dynamical network simulation results and the experimental snapshots as the fronts get more and more complex with decreasing C_a . Nevertheless, it is clear that the similarity is mostly superficial (given the many free choices in the details of such simulations as here). It would seem to be of both practical and theoretical interest to apply such network models to at least two tasks at hand.

The first concerns analysing the detailed dynamics of the saturation in the presence of relatively well defined fronts — what is the actual coarse-grained driving mechanism here, if the mass flux is used as the “order parameter”? Second, the morphology of such fronts, the noise affecting them and the relation to coarse-grained models as the phase field approach seems like an interesting avenue, in particular in the presence of pore-level details as snap-offs and film flow. We underline that the

first of these suggestions has to do with the very basic physics of imbibition, while the second would bridge the gap between any analytical theory and models that contain much of the microscopic effects actually in action.

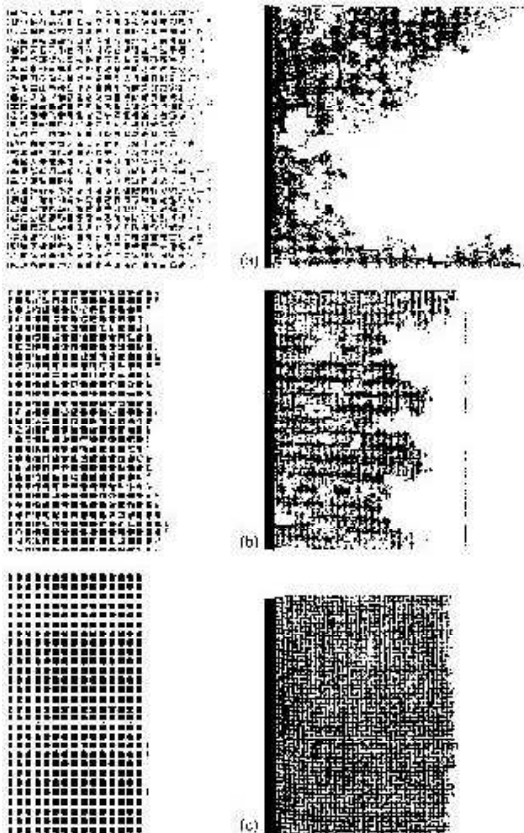


FIG. 21: Simulations of a dynamic network model vs. experimental results from a laboratory channel network [136, 185]. The capillary numbers are $C_a = 6 \times 10^{-7}$, $C_a = 1.4 \times 10^{-5}$, and $C_a = 3 \times 10^{-4}$, in the simulations, from top to bottom. Notice the transition to a compact front with increasing capillary number. The ratio of average pore throat conductivity to that of wetting layers is about 2000, controlling the “percolation” of the fronts.

To circumvent the difficulty of obtaining well-defined interfaces, conditional wetting rules, depending on the state of nearest and next-nearest neighbours may be introduced [31, 178]. These produce a more compact front so that a single-valued interface may be defined. This approach is discussed below, as it was used by Lam and Horváth [178], with the goal of reproducing the experimental results of Horváth and Stanley [130] discussed in Chapter IV. This is a priori not obvious since one of the main characteristics of this experiment is progression of the interface different from Washburn’s law, $v \sim H^\Omega$ with $\Omega \approx 1.6 \neq 1$. It was found that a very specific distribution of pore radii would give rise to the desired relation of average front height and velocity, although no plausible physical reason was given. In particular, it is not clear, that what appears to be some power law, is in

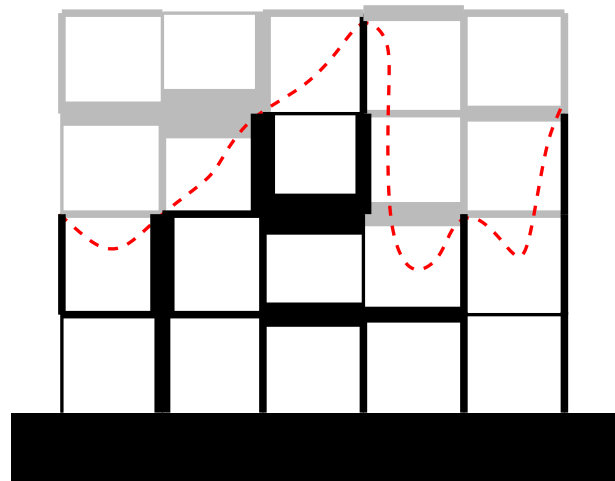


FIG. 22: Schematic representation of the pipe network model of Lam & Horváth [178]. A regular grid of pipes is invaded by a fluid. Pipe diameter is random and independent for each pipe, determining capillary pressure at invasion and conductivity for transport when invaded. Dark pipes are invaded, grey ones dry. The dashed line highlights the “interface”.

fact transient behaviour.

The scaling behaviour of the temporal fluctuations was found to be similar to the experimental results. The temporal correlation function (defined in Eq. (49), here the moment $q = 2$ is considered) could be described by the scaling function

$$C(t) = v^{-\kappa} f\left(tv^{(\theta_t + \kappa)/\beta}\right) \quad (59)$$

with exponents $\kappa = 0.49$, $\theta_t = 0.38$, and $\beta = 0.63$.

Spatially, the roughening process shows clear anomalous scaling. The stationary two-point correlation function (cf. Eq. (47)) had the scaling behaviour

$$G_2(r) = v^{-\kappa} g(rv^{(\theta_l + \kappa)/\chi}) \quad (60)$$

where $g(u) \sim u^\chi$ for small u tending to a constant at larger values. The values $\theta_l = -0.25$ and $\chi = 0.63$ were reported. Based on the assumption that a single time scale controls the roughening process, Lam and Horváth propose the exponent identity

$$\beta = \frac{\Omega}{\Omega + 1}(\theta_t + \kappa) \quad (61)$$

which, for both theory and experiment, agrees with about 15 % error margin.

These results raise several questions from a theoretical point of view. First, it is unclear why such a particular choice of the distribution of radii could give rise to universal scaling behaviour. The exponent Ω does not seem to depend in any controllable way on the disorder, so a long transient towards an asymptotic Washburn behaviour is not to be excluded.

The value $\chi = 0.63$ for the local roughness exponent can be interesting since it could indicate that the imbibition process belongs to the DPD class of roughening. The anomalous nature of roughening and the continuously slowing down of the interface of course do not support this view, and only a measurement of the structure factor could give some further insight.

In fact, the most questionable result is Eq. (61), that relates the different scaling exponents. We shall show below how this identity conflicts with the picture of imbibition that emerges from the phase field models, and how the results of Lam and Horváth can be interpreted within this approach.

G. Phase-Field Models

1. General concept

A continuum approach different from interface equations and conceptually related to the reasoning of Sections IIIB and IIIF was taken by Dubé et al. and Hernández-Machado et al. [82, 84, 85, 122]. This approach concentrates on the bulk of the porous medium rather than on a hypothetical interface equation and presents the following advantages:

- (i) Interface equations for particular models arise naturally from the sharp interface limit of the model. Simulations using the phase field approach thus include automatically the relevant interface equation, with all possible non-linearities. Equally, non-local interactions between different parts of the interface arise naturally.
- (ii) Disorder is directly introduced at the level of the bulk of the porous medium and thus does not need to be postulated in the interface equation.

The simplest phase field approach to imbibition starts from the observation that all coarse-grained descriptions of flow in porous media, based on Darcy's Law Eq. (22), are essentially diffusive. All inertial effects of hydrodynamics are neglected and only pressure determines the flux of liquid \mathbf{q} . The dynamical equation for the fluid concentration c is then defined through a continuity equation [295]

$$\frac{\partial c}{\partial t} + \nabla \cdot \mathbf{q} = 0 \quad (62)$$

where the concentration is related to the saturation through the porosity $c = s\mathcal{P}$. The concentration refers to both the wetting and non-wetting fluids. The two phases are differentiated by the field $\phi(\mathbf{r}, t)$, defined over all space and related to the saturation concentration of either liquid or air as ϕ_e . The total concentration field over the porous medium is then

$$c(\mathbf{x}, t) = \frac{1}{2}c_w \left(1 + \frac{\tilde{\phi}(\mathbf{x}, t)}{\phi_e} \right) + \frac{1}{2}c_n \left(1 - \frac{\tilde{\phi}(\mathbf{x}, t)}{\phi_e} \right) \quad (63)$$

where c_w and c_n are the respective concentrations of the wetting and non-wetting fluids and the values $\tilde{\phi} = +\phi_e(-\phi_e)$ are associated to the wetting (non-wetting) phases.

The field is locally conserved, which is reflected in a continuity equation that controls the dynamical evolution of the field

$$\frac{\partial \tilde{\phi}(\mathbf{x}, t)}{\partial t} + \nabla \cdot \mathbf{j} = 0 \quad (64)$$

where the current is taken to be proportional to the gradient of a chemical potential, $\mathbf{j} = -M(\mathbf{x}, \tilde{\phi})\nabla\mu$, with a mobility that may be a function of both space and concentration. The chemical potential has a thermodynamic origin, $\mu = \delta F/\delta\tilde{\phi}$, with the free energy functional

$$F = \int d\mathbf{r} \left[V(\tilde{\phi}) + \frac{c}{2}(\nabla\tilde{\phi})^2 - (\tilde{\alpha}(\mathbf{x}) - \alpha_0)\tilde{\phi} \right], \quad (65)$$

and the potential

$$V(\tilde{\phi}) = -\frac{r}{2}\tilde{\phi}^2 + \frac{u}{4}\tilde{\phi}^4. \quad (66)$$

For $\tilde{\alpha} = 0$, this free energy represents two liquid phases, described by the values $\phi_e^2 = r/u$ at chemical potential $\mu = \alpha_0$. The double-well nature of the free energy, combined with the square gradient term ensures that a well defined interface (of width $\zeta \sim (c/r)^{1/2}$) exists between the regions with $\phi = \pm\phi_e$. The fluids described by Eq. (66) have a slight compressibility ($\sim r^{-1}$) but since the model does not consider hydrodynamical effects explicitly, this represents only a minor correction to the overall dynamics of the interface.

Notice that the ‘‘saturation dynamics’’ described by the phase field model is diffusive. Attempts have been made to look at this aspect separately by Mitkov et al. [236] (see also refs. [109] and [237]). This is similar to the approach based on Richard's equation that incorporates a non-linear (and non-trivial) mobility M_w (see Eq. (20)) usually determined empirically for each particular case [22].

The model is defined in terms of the chemical potential, so as to make close contact with theories of critical dynamical phenomena with conserved field (Model B in the nomenclature of Halperin and Hohenberg [115]. See [38, 112] for general reviews on phase fields), used to study binary fluids as well as the liquid-gas transition. The correspondence between pressure p and chemical potential μ is easily accomplished in this limit through $p \sim \mu\phi_e$. Notice that Eq. (65) is also a continuum limit of a random field Ising lattice gas with locally conserved magnetisation.

Disorder enters the problem naturally though the transport properties of the porous medium and we can identify three main sources:

- (i) **Capillary disorder.** The term $\tilde{\alpha} - \alpha_0$, sets the local value of the chemical potential and thus effectively represents the pressure difference due to capillary forces,

$$p_c = \phi_e\tilde{\alpha}, \quad (67)$$

If this quantity is taken to be random it is natural to assume the following correlations

$$\begin{aligned}\langle \tilde{\alpha}(\mathbf{x}) \rangle &= \bar{\alpha} > 0 \\ \langle \tilde{\alpha}(\mathbf{x})\alpha(\mathbf{x}') \rangle - \bar{\alpha}^2 &= (\Delta\alpha)^2\delta(\mathbf{x}-\mathbf{x}').\end{aligned}\quad (68)$$

(If one assumes a Gaussian distribution for $\tilde{\alpha}$, as one usually does when defining a random variable by its 1st and 2nd moment, one has to exclude negative values by hand. However, the model results do not depend on the precise shape of distribution, only on the moments quoted above.)

(ii) Mobility disorder. The local mobility $M(\mathbf{x})$ (neglecting any dependence on the fluid density $\tilde{\phi}$), which controls the ease of flow of the liquid, is related to the permeability of a porous medium through the relation

$$\frac{M}{\phi_e^2} \equiv \frac{\kappa}{\eta}. \quad (69)$$

and is random and characterised by the correlations (again the precise shape of distribution does not matter)

$$\begin{aligned}\langle M(\mathbf{x}) \rangle &= M_0 > 0 \\ \langle M(\mathbf{x})M(\mathbf{x}') \rangle - M_0^2 &= (\Delta M)^2\delta(\mathbf{x}-\mathbf{x}').\end{aligned}\quad (70)$$

There is a priori no reason to expect any simple relation between the two fluctuating quantities and they are kept independent.

Since the chemical potential is analogous to pressure, it also enters the model in the boundary conditions. We next outline the choice in two spatial dimensions, the only one studied so far in the literature. In the case of spontaneous imbibition the chemical potential obeys the boundary conditions $\mu(x, y=0) = \alpha_0$ (equivalent to atmospheric pressure) and $\partial_y\mu(x, y=L) = 0$ (closed at the upper end) [82]. The boundary conditions on the phase field $\partial_y\phi(x, y=L) = 0$ and at $y=0$, the field's value is the solution to

$$-\tilde{\alpha} - \tilde{\phi} + \tilde{\phi}^3 = 0. \quad (71)$$

Since the term α_0 simply corresponds to a constant shift in the chemical potential, we consider $\alpha_0 = 0$ from now on. In order to model imbibition situations at constant flow rate, as in [311], constant flux boundary conditions $M\partial_y\mu = \gamma_0$ are imposed. Both situations, spontaneous imbibition and constant flux shall be examined in details below.

When the effects of evaporation or gravity are sufficiently strong, they act in a way that stops the imbibition front and produce a pinned interface. Both effects can be taken into account in a generalised imbibition model of the form [85]

$$\frac{\partial\tilde{\phi}(\mathbf{r}, t)}{\partial t} - \tilde{G}\frac{\partial\tilde{\phi}(\mathbf{r}, t)}{\partial y} = \nabla(M(\tilde{\phi}, \mathbf{x})\nabla\mu) - \frac{1}{2}\tilde{\epsilon}\left(\phi_e + \tilde{\phi}(\mathbf{r}, \tau)\right) \quad (72)$$

The convective term is included to describe gravity. Although gravity can only be introduced properly through

an hydrodynamical field [140, 149], one can argue that this term reproduces the correct equation of motion for the average position of the imbibition front. The connection to Darcy's law is established through

$$G \equiv g \frac{\kappa}{\eta}. \quad (73)$$

When $\tilde{\epsilon} \neq 0$, a non-conserving term is introduced into the equation of motion, which, to a first approximation, describes evaporation of liquid (the $\tilde{\phi} = \phi_e$ phase), at a rate $\phi_e\tilde{\epsilon}$ and proportional to the total area covered by the fluid. Note, that in this case one thinks of a thin medium from which the fluid can evaporate on the sides, as in the case of a wet paper sheet.

Taking the mobility to be $M(\tilde{\phi}, \mathbf{x}) = M_0 m(\mathbf{x})$ (here we have neglected explicit dependence on the field value), the basic scales for length, energy, and time of the problem are

$$\begin{aligned}\zeta &= (c/r)^{1/2}, \\ \mu_0 &= (r^3/u)^{1/2}, \\ \tau_M &= \frac{\phi_e\zeta^2}{M_0\mu_0}.\end{aligned}\quad (74)$$

Equation (72) can then be put in a dimensionless form by defining

$$\begin{aligned}\alpha &= \frac{\tilde{\alpha}}{\mu_0}, \\ \gamma &= G\frac{\tau_M}{\zeta}, \\ \epsilon &= \tau_M\tilde{\epsilon},\end{aligned}\quad (75)$$

which leads to a dynamical equation

$$\frac{\partial\phi(\mathbf{x}, \tau)}{\partial t} - \gamma\frac{\partial\tilde{\phi}(\mathbf{x}, t)}{\partial y} = \nabla(m(\phi, \mathbf{x}) \cdot \nabla\mu(\mathbf{x}, t)) - \frac{1}{2}\epsilon(1 + \phi(\mathbf{x}, t)) \quad (76)$$

where the chemical potential $\mu = -\phi + \phi^3 - \nabla^2\phi - \alpha(\mathbf{x})$.

For slow enough motion of the interface the chemical potential is adjusted quasi-statically to the interface positions [38], which themselves are driven by the difference between incoming and outgoing current $\mathbf{j} = -m\nabla\mu$. In the sharp interface limit, and for a slowly moving front, the concentration ϕ is approximately constant in the bulk, changing only at the interface. The chemical potential μ thus satisfies the equivalent of a Poisson equation

$$\nabla \cdot \nabla\mu = \epsilon \quad (77)$$

in the bulk. At the interface, μ must obey the Gibbs-Thomson boundary condition

$$\Delta\phi\mu|_{int} = \Delta V - \sigma\mathcal{K}, \quad (78)$$

where \mathcal{K} is the curvature, σ the effective surface tension of the model, the miscibility gap $\Delta\phi = \phi_+ - \phi_-$ and

$\Delta V = V(\phi_+) - V(\phi_-)$. The quantities ϕ_{\pm} are the *equilibrium* values of the phase field, defined by the usual tangent construction [38, 181]. The interface motion is then determined by the normal velocity

$$(\Delta\phi)v_n = -\partial_n\mu|_{\pm} - \gamma. \quad (79)$$

These conditions are of course completely equivalent to the description based on capillary pressure and Darcy's law in the context of Eq. (22) in Section III B.

2. Interface equation

To extract the interface equation from Eq. (72), it is convenient to use a local coordinate system (u, s) close to the interface [140, 332]. Two-dimensional space is parametrised by $\mathbf{x}(u, s) = \mathbf{X}(s) + u \hat{\mathbf{n}}(s)$, where $\mathbf{X}(s)$ is a point of the interface, $\hat{\mathbf{n}}$ is a unit vector normal to the interface pointing towards the side where $\phi > 0$, and s is the arc-length coordinate along the interface [91]. In terms of the phase field, this corresponds to $\phi(u=0, s) = 0$. The time derivative of the field then becomes

$$\frac{\partial\phi(u, s, t)}{\partial t} = V_n(s) \frac{\partial\phi}{\partial u} \quad (80)$$

where $V_n(s)$ is the normal velocity of the interface at position s . If the interface thickness, $\zeta = 1$ in dimensionless units, is much smaller than the typical radii of curvature of the interface (the sharp interface limit), the Laplacian term of the chemical potential may be expanded such that

$$\nabla^2 = \frac{\partial^2}{\partial u^2} + \frac{\partial^2}{\partial s^2} + \mathcal{K}(s) \frac{\partial}{\partial u} \quad (81)$$

where $\mathcal{K}(s)$ is the curvature of the interface. For $\alpha = 0$, the one-dimensional kink solution is $\phi(u, s) = \phi_0(u) = \tanh(u/\sqrt{2})$, with corrections of order $\mathcal{O}(\alpha)$ from the finite compressibility of the model. Therefore, to first order, $\mu \approx -\alpha(u, s) - \mathcal{K}(s)\partial\phi_0(u)/\partial u$. Still in the sharp interface limit $\zeta\mathcal{K} \ll 1$, the derivatives of the kink solutions have properties $\partial\phi_0(u)/\partial u \approx \Delta\phi\delta(u)$ and

$$\sigma = \int du \left(\frac{\partial\phi_0(u)}{\partial u} \right)^2 = 2 \frac{\sqrt{2}}{3} \quad (82)$$

where $\Delta\phi \approx 2$ is the miscibility gap and σ is the dimensionless surface tension or, for the fully dimensional expression,

$$\tilde{\sigma} = 2 \frac{\sqrt{2}}{3} \zeta\phi_e\mu_0. \quad (83)$$

Note that this quantity represents an average surface tension associated with the interface and does not necessarily bear any relationship to the microscopic surface tension that gives rise to capillary pressure. Nevertheless, assuming $p_c \sim \sigma/r_0$, with r_0 the typical pore size and using Eq. (67) yields

$$\alpha = \frac{\zeta}{r_0}, \quad (84)$$

i.e., the dimensionless parameter α corresponds to the ratio between the interfacial width and the typical pore size.

The capillary number $C_a = \eta\tilde{v}/\tilde{\sigma}$, \tilde{v} denoting the fluid velocity, represents the ratio between the viscous and capillary forces. Strictly speaking, this cannot be defined in the phase field model since the fluid is not explicitly taken into account, only the ratio η/κ . Nevertheless, the capillary number itself does not play a direct role in the roughening of the interface, but enters the problems only through the length scale ξ_x . Assuming that the permeability can be related to the average pore radius $\kappa \sim r_0^2$, it is easy to show that,

$$C_a \sim \frac{r_0^2}{\zeta^2} \frac{v}{\sigma}, \quad (85)$$

where v is the velocity of the *interface* – unlike the fluid velocity \tilde{v} . For spontaneous imbibition, this is easily related to the capillary pressure, from Eq. (84), to the dimensionless parameter α to give $C_a = v/(\sigma\alpha^2)$.

For constant mobility $m(\phi, \mathbf{x}) = 1$, the dynamical phase field equation may be inverted with the use of Green's function, defined by

$$\nabla^2 G(x, y|x', y') = -\delta(x-x')\delta(y-y'), \quad (86)$$

for the range $-\infty < x, x' < \infty$, $0 < y, y' < \infty$, with Dirichlet boundary conditions. The half-plane Green's function

$$G(x, y|x', y') = \frac{1}{4\pi} \ln \frac{(x-x')^2 + (y-y')^2}{(x-x')^2 + (y+y')^2} \quad (87)$$

must be used, since the presence of an reservoir at position $y = 0$ breaks the translational symmetry in y . This yields the equation

$$\int d\mathbf{x}' G(\mathbf{x}|\mathbf{x}') \left(\frac{\partial\phi(\mathbf{x}', t)}{\partial t} - \gamma \frac{\partial\phi(\mathbf{x}', t)}{\partial t} + \frac{1}{2} \epsilon (1 + \phi(\mathbf{x}', t)) \right) = \mu(\mathbf{x}, t). \quad (88)$$

Multiplying Eq. (88) by $\int du (\partial\phi_0(u)/\partial u)$ then effectively projects the phase field dynamics onto the interface $u = 0$. A translation $u \rightarrow u + h(s, t)$ then yields

$$\int ds' G(s, h(s, t)|s', h(s', t)) (V_n(s') - \gamma) + \Delta\phi \epsilon \int ds' \int_0^{h(s', t)} du' G(s, h(s, t)|s', u') = \eta(x, h(x, t)) + \sigma\mathcal{K}. \quad (89)$$

where $\eta(x, h) \equiv \int dy \phi'_0(y - h(x, t)) \alpha(x, y) \sim 2\alpha(x, h)$.

Without disorder, the advancing liquid front interface remains flat, $\mathcal{K} = 0$, with position described by $H(t)$ and the value of the chemical potential at the interface $\mu|_{\text{int}} = -\alpha$, c.f. Eq. (78). It is then straightforward to obtain the dynamical evolution

$$\frac{dH(t)}{dt} = \frac{\bar{\alpha}}{2H(t)} - \gamma - \frac{1}{4} \epsilon H(t). \quad (90)$$

Without gravity or evaporation, the interface then progresses in a typical Lucas-Washburn behaviour, $H(t) \sim t^{1/2}$ while non-zero values of γ or ϵ eventually stop the interface at an equilibrium height $H_p(\gamma, \epsilon)$ given by the zero of the right-hand side of Eq. (90) with limiting cases $H_p(\gamma, \epsilon=0) = \bar{\alpha}/(2\gamma)$ and $H_p(\gamma=0, \epsilon) = \sqrt{2\bar{\alpha}/\epsilon}$.

At early times $t \ll t^* \equiv \min(\bar{\alpha}\gamma^{-2}, \epsilon^{-1})$, the rise of the interface follows Washburn behaviour, $H(t) = (\bar{\alpha}t)^{1/2}$. For $t \gg t^*$, the pinning height is approached exponentially. In cases where gravity is absent, the average interface, of initial height $H(t=0) = 0$, is described at all times by

$$\left(\frac{H(t)}{H_p} \right)^2 = 1 - e^{-\epsilon t/2}, \quad (91)$$

while for $\epsilon = 0$, the rise follows the transcendental equation

$$\frac{H(t)}{H_p} + \ln \left(1 - \frac{H(t)}{H_p} \right) = -\frac{2}{\bar{\alpha}} \gamma^2 t. \quad (92)$$

Although both gravity and evaporation pin the interface at a given height, it must be kept in mind that

the physics behind these two effects is quite different [84]. Spontaneous imbibition, without external influences, is characterised by a Laplace equation for the chemical potential $\nabla^2\mu = 0$ in the bulk (i.e., far away from the interface). When solved with boundary conditions $\mu(y=0) = 0$ and $\mu(y=H) = -\bar{\alpha}$, this yields a gradient $\partial\mu \propto -1/H$ in the liquid phase. The gravity term of Eq. (72) thus has the effect of stopping the interface when $\partial\mu \simeq -\gamma$.

On the other hand, the non-conserving term introduced by evaporation is such that the chemical potential in the bulk must be a solution of the Poisson equation $\nabla^2\mu = \epsilon$ and at pinning height, the gradient in the chemical potential $\partial\mu = 0$. This simply represents the fact that the flux of liquid from the reservoir exactly balances the losses due to evaporation.

The time and length scales coming from gravity and evaporation can however be very different. Studies of capillary rise with light organic liquids (for which evaporation is presumably an extremely weak effect compared to ordinary water) imbibed in filter papers [104] have found a pinning height of the order of 1 m, with time scales on the order of days. In contrast, evaporation effects can cause the pinning height to be of the order of 15–50 cm, with correspondingly much faster time scales.

When capillary disorder is introduced, the interface equation is best expressed in terms of the Fourier modes of the interface fluctuations h_k . A straightforward expansion of Eq. (89) yields the linear equations

$$\left(\dot{h}_k + \frac{1}{2} \epsilon h_k \right) \left(1 - e^{-2|k|H} \right) + |k|(\dot{H} + \gamma) h_k \left(1 + e^{-2|k|H} \right) = \frac{1}{4} |k| (\{\eta\}_k - \sigma k^2 h_k). \quad (93)$$

The quenched noise enters in a somewhat non-standard way, by a Fourier transform of the disorder values at the interface, $\{\eta(t)\}_k \equiv \int_x e^{-ikx} \eta(x, h(x, t))$. Immediately

apparent is the presence of the modulus of the wavevector, $|k|$, arising from the conservation law. Non-linear terms, similar to those in Eq. (33) obtained by Ganesan

and Brenner [99] can also be obtained from Eq. (89).

3. Spontaneous imbibition without pinning

In this section, we specialise to the case of spontaneous imbibition, where the porous medium is simply put into contact with a liquid reservoir. In this setup the interface follows the typical square root behaviour in time for the average interface height, $H \sim t^{1/2}$. It is worth mentioning that similar thermodynamical non-equilibrium states are found in other systems. An example is the invasion of a type II superconductor by magnetic field vortices. Indeed, lattice models similar in spirit to the phase field formalism have been developed, and it is an interesting question how the understanding of imbibition (dynamics, roughening, continuum equations) would find applications in that context [138, 252].

Disorder enters the model in very different ways, and changes in the local capillary pressure enter directly into the chemical potential through the Gibbs-Thomson boundary condition. This term is present independently of the velocity of the interface. On the other hand, it is easy to show that changes in the chemical potential $\delta\mu$ from its constant mobility value μ_0 due to changes in the mobility δm can be estimated as

$$\nabla^2(\delta\mu) \sim \nabla(\delta m)\nabla\mu_0 \sim \nabla(\delta m)v_0, \quad (94)$$

which means that the effects of disorder in the mobility are essentially proportional to the interfacial velocity, a quite intuitive result.

In the case of spontaneous imbibition, the interface continuously slows down and the effect of mobility disorder becomes smaller and smaller until finally disorder in the capillary forces completely controls the roughening process. In this Subsection, we thus consider a constant mobility $m(\phi, \mathbf{x}) = 1$, and refer to the implications of mobility variations in the next Subsection.

The limit $\gamma = \epsilon = 0$ of Eq. (93) shows that there exists a lateral length scale separating two different modes of damping of the interfacial fluctuations. The changes in the chemical potential due to curvature (Gibbs-Thomson effect) and those due to slowing down of the front balance at a length scale

$$\xi_\times \simeq \left(\frac{\sigma}{v}\right)^{1/2} = \left(\frac{\sigma H}{\bar{\alpha}}\right)^{1/2}. \quad (95)$$

The front is smoothed on length scales larger than ξ_\times since parts of the interface further away from the reservoir have a slower velocity. Large fluctuations are constantly suppressed.

A convenient way to study this case is to adapt the model to the experimental setup invented by Horváth and Stanley [130] where a steady state is reached by pulling a paper sheet at a constant velocity $\mathbf{v} = -v\hat{\mathbf{y}}$ towards a reservoir, or (almost) equivalently by monitoring the average interface height to remain at a constant

value. In this case, the equation of motion reads

$$\partial_t\phi = -\nabla^2 [\nabla^2\phi + \phi - \phi^3 + \alpha(\mathbf{x} - \mathbf{v}t)] + \mathbf{v} \cdot \nabla\phi. \quad (96)$$

The corresponding interface remains at a fixed average height $H = \bar{\alpha}/2v$, where a freely rising interface would have velocity v .

A simple spatial discretisation of Eq. (96) on a square lattice yields satisfactory results. The Laplace operator is then discretised in the standard way of finite differences

$$(\Delta\phi)_{i,j} = \sum_{|(i,j)-(i',j')|=\Delta x} (\phi_{i',j'} - \phi_{i,j}). \quad (97)$$

The grid spacing Δx has to be adapted to the variation in the phase field and should not be larger than 1/3 of the interface width.

It would be interesting to apply a finite element method to imbibition problems which could resolve the interface on a finer scale and remain coarse in the bulk phases. One has however to be careful to keep track of the quenched disorder field $\alpha(x)$ when rearranging the mesh. Also, a slightly modified version of the phase field equations, where the disorder acts only at the interface and not in the bulk is better suited. This could be achieved by, e.g., changing the noise term to $(1 - \phi(x))^2\alpha(x)$.

For the slow diffusive motion an explicit Euler time integration is also satisfactory, even if the fourth spatial derivative requires relatively small time steps $dt \sim 0.01$. Recent developments on semi-implicit schemes, where the nonlinear terms are treated explicitly, but the linear ones implicitly, might prove useful for models of this type [88].

The steady-state structure factor $S(k, H)$ for the stationary setup of Eq. (96), shown in Fig. 23(a), shows that there is a maximum length scale for the fluctuations, independent of the lateral system size, with the global roughness exponent extracted from the power-law decay $\chi \approx 1.25$. It is slightly intriguing, that the value is so close to the QEW one, again (c.f. Section III D 1).

All the data can be rescaled using $\xi_\times \sim v^{-1/2} \sim (H/\bar{\alpha})^{1/2}$. For the second moment height difference correlation function (defined and schematically shown in Fig. 19 in Section III C) one obtains the scaling function

$$G_2(r, H) = \Delta\alpha v^{-\chi/2} g\left(r v^{1/2}\right). \quad (98)$$

The dependence of the interface velocity v (and equivalently on the average height H) follows from the above analysis. The relatively simple scaling dependence on the noise strength $\Delta\alpha$ is found numerically and shown in Fig. 23(b), but a convincing explanation is to our knowledge missing [82, 84].

The scaling function $g(u)$ is constant for $u \gg 1$ and $g(u) \sim u^{\chi_{\text{loc}}}$ if $u \ll 1$, with $\chi_{\text{loc}} \approx 1$ [82, 84, 164, 198].

The same scaling picture applies in the freely rising case, where the average interface height $H(t) = (\bar{\alpha}t)^{1/2}$ provided that a dynamical correlation length $\xi_\times \sim (t/\bar{\alpha})^{1/4}$ is used. There appears a complete equivalence between the interfacial fluctuations at an instantaneous height $H(t)$ and the saturated fluctuations of a

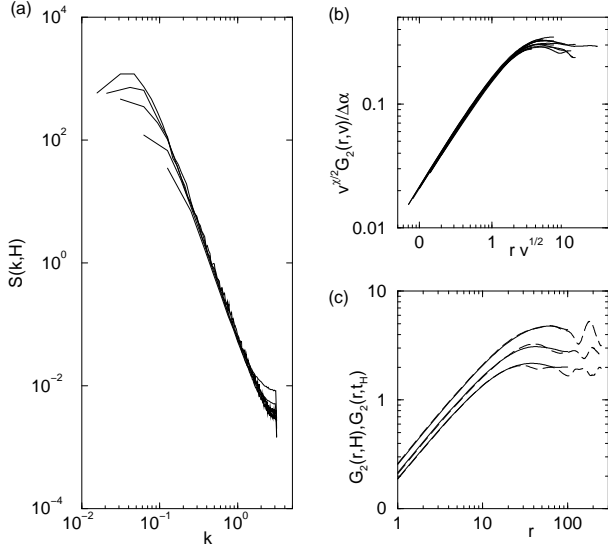


FIG. 23: (a) Structure factors for systems of height $H = 50, 100, 150, 200$ and lateral size $L = 2H$. Note that for large system sizes the power spectrum is *not* cut off by the system size, but by some other length scale $\xi_x < L$. (b) Correlation functions $G_2(r, H)$, scaled according to Eq. (98) for various $v \sim H^{-1/2}$ and $\Delta\alpha$. (c) Comparison of the correlation functions in the steady state, $G_2(r, H)$ (solid lines) for $H = 25, 50, 100$ and of the rising case $G_2(r, t_H)$ (dashed lines), at times $t_H = H^2/\bar{\alpha}$.

stationary interface. The length scale ξ_x is thus *conceptually different* from the intrinsic time dependent lateral correlation length ξ_t commonly found in models of kinetic roughening (see Section III C). Here ξ_x merely fixes the maximum range of correlated roughness and can only occur if the “natural” dynamical exponent $z < 4$, so that the interface fluctuations can always catch up instantly with the available area of correlation. This also implies a dynamical behaviour of the total width of the freely rising interface $W \sim \xi_x^x \sim t^{x/4} = t^\beta$, with $\beta \approx 0.31$ [82, 84]. It cannot be overemphasised that the exponent β found here is conceptually completely different from the usual exponent in traditional descriptions of kinetic roughening introduced earlier in Eq. (43).

The temporal correlations in the steady state, obtained from Eq. (96), can be analysed through the q^{th} order height difference correlation functions $C_q(t, H) = \langle |h(x, t+s) - h(x, s)|^q \rangle^{1/q}$. For small time differences t there appear logarithmic slopes (that have been interpreted as “effective” exponents β_q) which are independent of H and *decrease* with q , as shown in Fig. 24 and its inset. Note that the exponent $\beta_2 \approx 0.85$ is fundamentally different from the growth exponent associated with the width of a freely rising front. Standard concepts of multi-scaling are not easily recovered in this system, even if the only reason is the restriction in the system sizes simulated.

It seems however certain that the reason for the de-

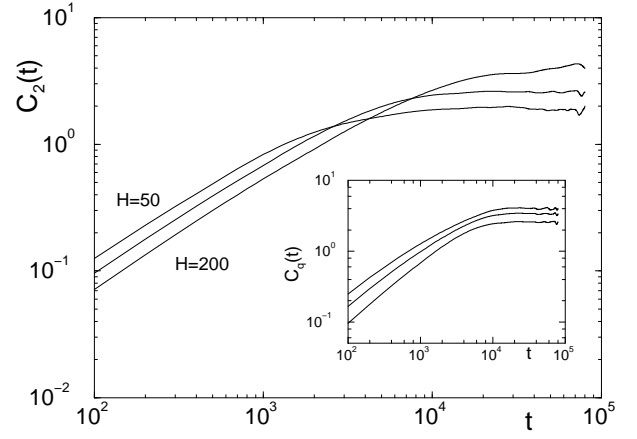


FIG. 24: Steady state temporal correlation functions for systems of size $L_x = 400$, at heights $H = 50, 100, 200$. Saturation level and overall roughness increase with H , whilst short time differences and typical velocities decrease. The inset shows the correlation functions of moments $q = 2, 4, 6$ (from bottom to top) for $H = 100$, which decrease in their logarithmic slopes.

crease of β_q is linked to the propagation of the front by avalanches, which in the QEW equation (55) leads to similar statistics in temporal correlations [190]. In Figure 25 we show a few dozen interface configurations at equidistant times which apparently propagate by effective avalanches. Zones where interfaces get blocked for

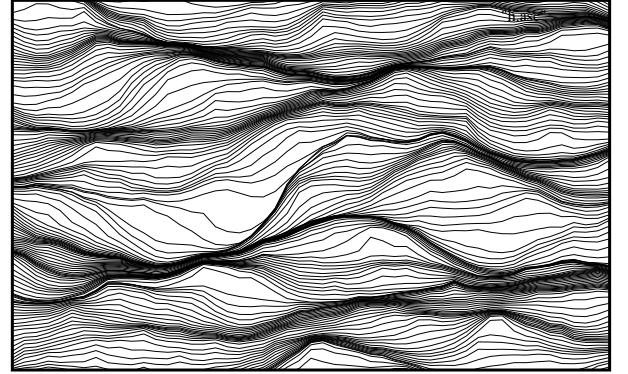


FIG. 25: An example of an interface in the phase field model propagating by avalanches. Configurations at equidistant times are plotted together. Regions with “avalanche sweeps” become visible (low density of lines), as well as pinning zones (high density).

a longer time appear as thick dark lines which are separated by regions through which the interface sweeps in a fast avalanche.

The precise nature of the decrease of β_q has not been studied thoroughly. An answer to the origins of such behaviour may lie in the *distribution functions* of the fluctuating variables. In Fig. 26a) we show the distribution of the normal interface velocity in the phase field model.

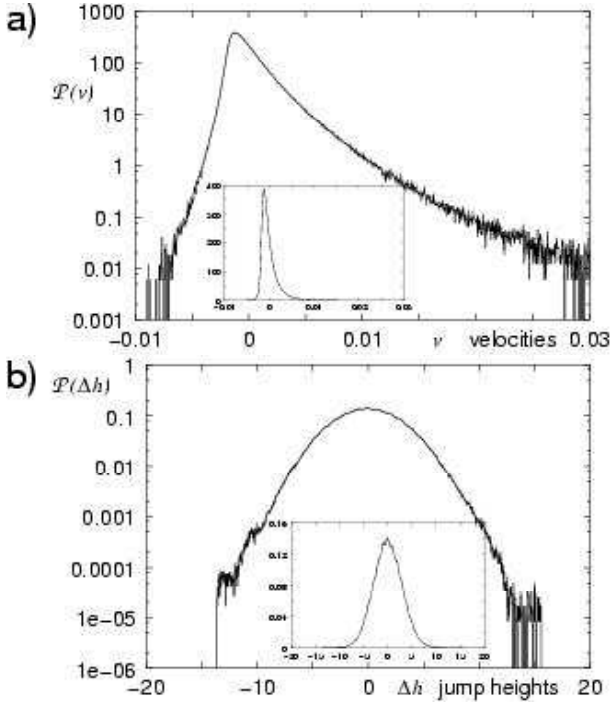


FIG. 26: a) probability density function of the interface velocity in a numerical simulation of the phase field model Eq. (96). b) Distribution of height differences taken at two different times. The insets show the same data on a linear scale.

It is kept in a steady state by shifting the system towards the reservoir at constant velocity $\mathbf{v} = -v\mathbf{e}_y$, as in the experiments of Horváth and Stanley [130] expressed by the modified phase field equation (96).

The velocity distribution is related to the distribution of differences $h(x, t + \tau) - h(x, t)$ in the height profile in the limit of small time steps $\tau \rightarrow 0$. For large $\tau \rightarrow \infty$, when both profiles are essentially uncorrelated the shape of the height difference distribution crosses over from that of Figure Fig. 26a) to that of 26b). It seems plausible that the characteristics of this crossover become more apparent from the probability distributions themselves than from the behaviour of their moments $\langle |h(x, t + \tau) - h(x, t)|^q \rangle^{1/q}$. The behaviour of the velocity distributions gives rise to analogies with other systems (with “local” Langevin equations) that exhibit interesting probability distributions [37]. The deviations from Gaussian distributions relate to the existence of correlations, and make the question pertinent why self-averaging fails.

Anomalous roughness with a global roughness exponent $\xi \approx 1.25$ has been found in the spatial structure factor or power spectrum $S(k, t)$. For the second moments of temporal fluctuations or the exponent β_2 a similar phenomenon is found: Figure 27 shows the velocity power spectra

$$S_v(\omega) = \langle |v(x, \omega)|^2 \rangle \quad (99)$$

obtained from simulations of steady state distributions

of Eq. (96) at different average heights $H = 40, 80, 120,$ and 160 . The overbar denotes a spatial average over the system, the brackets and ensemble average, and $v(x, \omega)$ is the Fourier transform of $v(x, t) = \partial_t h(x, t)$ which leads to the obvious identity $S_v(\omega) = \omega^2 S_h(\omega)$. From the power spectra one can read a global temporal exponent β_2^{global} : A possible power law behaviour goes like

$$S_v(\omega) = \omega^{1-2\beta_2^{\text{global}}}. \quad (100)$$

It cannot be overemphasised that this is the global counterpart to the local exponent defined via $C_{q=2}(t, H)$ in Figure 24, and **not** the exponent related to the early time increase in interface roughness when starting from an initially flat configuration.

The crossover observed in the velocity distributions, Fig. 26, will of course prevent a “pure” power law in $S_v(\omega)$, but we can nevertheless observe three regions giving rise to “effective” exponents. (i) For low frequencies, long times, the fluctuations are stationary, $S_v(\omega) \sim \omega$ and therefore $\beta_2 = 0$. (ii) Fluctuations at short times and high frequencies, on the time scale of avalanche duration, are “turbulent” in the sense of [162]: We find $S_v(\omega) \sim \omega^{-3/2}$ and thus $\beta_2^{\text{global}} = 5/4$. It certainly would be of interest to examine these in greater detail and pin down the connection to the velocity distributions shown in Fig. 26. (iii) Last we can identify an intermediate regime with an apparent behaviour between $S_v(\omega) \sim \omega^{-3/4}$ and $\omega^{-2/3}$, which would correspond to $\beta_2^{\text{global}} = 7/8$ or $5/6$. We would however suggest not to put too much emphasis on the power law nature of this regime, which probably is caused by an interplay of several different mechanisms during the crossover from avalanche propagation to the stationary fluctuations at long time scales.

The different regimes appearing in $S_v(\omega)$ exhibit different scaling behaviour with respect to the average interface velocity $|\mathbf{v}|$. The stationary regime with $S_v(\omega) \sim \omega$ ends at $\omega_0 \sim |\mathbf{v}|^{\beta_2^{\text{global}}}$. A possible interpretation is to take the typical duration of avalanches $\tau_{\text{ava}} \simeq \Delta h_{\text{ava}}/v_{\text{ava}}$ from their vertical extent $\Delta h_{\text{ava}} \sim \xi_x^x$ and their “sweeping velocity” $v_{\text{ava}} \sim |\mathbf{v}|^{-\beta_2^{\text{global}}/2}$. The velocity v_{ava} also appears in the large frequency tail where $S_v(\omega) \sim \omega^{-3/2}$ with an amplitude $\propto v_{\text{ava}}^2$. The lower bound of this tail, ω_1 , at the crossover to the intermediate regime seems to be independent of the average velocity $|\mathbf{v}|$. Also these findings certainly need to be examined more thoroughly.

Interestingly we find the exponent $\beta_2^{\text{global}} = 5/4$ in the short time regime to be the same as the global roughness exponent χ . Assuming that these short time fluctuations follow a standard scaling picture we can combine them to $z = \chi/\beta_2 \approx 1$ which means linear or ballistic propagation of fluctuations along the interface. At first sight this is plausible: We are dealing with the advancement of the front in the course of single avalanches, between encountering regions of stronger pinning. Here the front can propagate freely with some typical velocity, and it is easy to imagine that fluctuations will be carried along

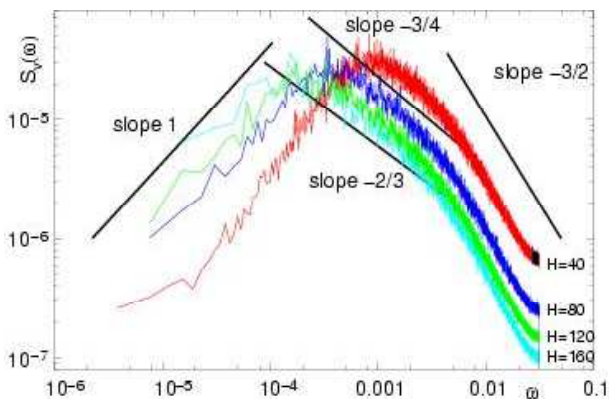


FIG. 27: Power spectra for the interface velocities in the steady state of Eq. (96). At low frequencies $S_v(\omega) \sim \omega$, at high frequencies $S_v(\omega) = \omega^{1-2\beta_2^{\text{global}}}$ with $\beta_2^{\text{global}} \approx \chi \approx 5/4$ indicating a dynamical exponent $z \approx 1$. The behaviour in the intermediate frequency range is not clear. Data were obtained in systems with size $L = 500$ at average interface heights $H = 40, 80, 120,$ and 160 respectively.

the interface with a constant velocity during that process. Again, this would be an interesting topic for further studies. We have not pursued an analogous direction, by computing the power spectrum of the interface velocity (recall Fig. 26). In the context of microscopic models - related to e.g. Barkhausen noise - with avalanches that are easier to define than in imbibition, the $S(\omega_{v,int})$ can be related to the exponents describing the avalanches which in turn relate to those that describe the underlying critical point itself [167].

It is worth remembering here both with respect to the correlation functions C_q and the β -exponents, that the deviations from ordinary kinetic roughening stem from the memory or history effects in imbibition. In local models the central question in this respect concerns whether the local fluctuation $\delta h(x, t) \equiv h(x, t) - \bar{h}(t)$ defines effectively a Markovian process. Imbibition is different, since, among others, clearly the dynamics measured by the two-point functions C_q depends on both the fluctuating field $\delta h(x, t)$ and also on \bar{h} , the distance to the reservoir. Secondly, it is clear though only on a qualitative level that the existence of ξ_x implies memory effects that are valid also beyond the particular details of spontaneous imbibition.

In any case, the model results shown in Figure 24 reproduce several experimental features found by Horváth and Stanley [130]: First, the late time saturation level of C_q increases with H indicating larger overall roughness, and second, $C_q(t, H)$ at fixed small t decreases with H , indicating a faster intrinsic avalanche velocity for a smaller H .

However, the picture developed so far contradicts strongly with the exponent identity, Eq. (61) proposed by Lam and Horváth [85]. This identity is derived under the assumption that the dynamics are controlled by a single time scale which can be obtained by two means.

For a moving interface, a width w is reached after a time $t_1 \sim w^{(\Omega+1)/(\kappa\Omega)}$. On the other hand, the form of the time correlation function, Eq. (59) suggests a time scale $t_2 \sim v^{-(\theta_t+\kappa)/\beta} \sim w^{(\theta_t+\kappa)/\kappa\beta}$, where $\theta_t = 0.38$ and $\beta = 0.63$ are found. Assuming that $t_1 \propto t_2$, the exponent identity is obtained. This is trivially true in usual kinetic roughening but wrong for spontaneous imbibition since t_1 and t_2 describe two distinct physical time scales. It takes a time t_1 for the correlation length to have value $\xi_v(t_1)$. This in turn controls the width as $w \sim \xi_v^\chi$. On the other hand, t_2 is the relaxation time of the fluctuations when the interface is kept at a fixed height. In this case, the correlation length ξ_v is a predetermined constant and the saturation within this zone is obtained when the spatial extent of the correlations equals ξ_v . We emphasise that the growth of the width in spontaneous imbibition is controlled by the increase of ξ_x , the zone available for correlated fluctuations, and not from the intrinsic dynamical fluctuations of the interface.

In fact, the correlation function, Eq. (60), clearly defines a length scale $\xi_v \sim v^{-\gamma}$, where $\gamma \equiv (\theta_t + \kappa)/\alpha \approx 0.4$, which then implies $G_2(r) \sim \xi_v^\chi g(r/\xi_v)$. Thus, $\xi_v \sim v^{-0.4}$ is analogous to the $\xi_x \sim v^{-1/2}$ discussed for the ideal case of spontaneous imbibition with Darcy-Washburn behaviour. Equation (60) also defines a *global* roughness exponent, $\chi = \kappa\alpha/(\kappa + \theta_t) = 1.25$, again very similar to the results obtained from the phase field model.

The scenario proposed by Lam and Horváth could only occur if the fluctuations were slower than the increase of ξ_x , which implies $t_2 \gg t_1$. Recall the point that for $z < 4$, in the case of the phase field model, this is never true. Indeed, the numerical data indicate $t_2 \sim w^{2.8}$ and $t_1 \sim w^{3.25}$ which shows this assumption to be false asymptotically.

4. Spontaneous imbibition with pinning

In presence of the pinning effects of gravity or evaporation, numerical simulations of the phase field model show that the behaviour of the average interface height is well described by the transcendental equation, Eq. (91) and Eq. (92). The actual pinning heights deviate only slightly from the predictions due to the presence of disorder [85].

It is convenient to analyse the effects of gravity and evaporation separately. In the absence of evaporation, the linearised equation of the fluctuations Eq. (93), immediately shows the existence of a length scale $\xi_g(t)$ restricting the range of the spatial fluctuations and evolving in time as

$$\xi_g(t) = \frac{1}{2} \left(\frac{\sigma}{2(\dot{H} + \gamma)} \right)^{1/2} = \frac{1}{2} \left(\frac{\sigma H(t)}{\bar{\alpha}} \right)^{1/2}, \quad (101)$$

where $H(t)$ is given by the solution of Eq. (92) (minor corrections of order $\mathcal{O}(\xi_g/H)$ are also expected). The length scale $\xi_g(t)$ is thus analogous to the length scale $\xi_x(t)$ in spontaneous imbibition without external influences, but it does not increase in time according to a

simple power law any more. At pinning, this length scale becomes

$$\xi_g(H_p) = \frac{1}{2} \left(\frac{\sigma}{2\gamma} \right)^{1/2} = \xi_x(H_p). \quad (102)$$

As in spontaneous imbibition without gravity, dynamical scaling relations can be established by assuming a single correlation length $\xi_g(t) \sim \gamma^{-1/2} (\sigma H/H_p)^{1/2}$, where, from Eq. (92), the quantity H/H_p is a function of $\gamma^2 t$ only. The temporal behaviour of the width of the interface $W(t)$ can then be scaled as

$$W(t) = \gamma^{-\chi/2} w(\gamma^2 t) \quad (103)$$

where $w(x) \sim x^{\chi/4}$ for $x \ll 1$ and tends to a constant for large arguments. Numerically, the global roughness exponent $\chi \approx 1.25$ has the same value as for spontaneous imbibition without external influences [85].

The scaling picture at pinning is confirmed from the structure factor. Figure 28 shows the structure factor for systems with different pinning heights (arising from different values of the constant γ). The structure factor decays as $k^{-3.5}$ at large values of wave-vector, consistent with the value $\chi = 1.25$ and the curves can be collapsed on the common scaling form by setting $\xi_g(H_p) \sim \gamma^{-1/2} \sim H_p^{1/2}$:

$$S(k, H_p) = (\xi_g(H_p))^{1+2\chi} s(k \xi_g(H_p)). \quad (104)$$

The scaling function $s(k\xi)$ is the same as in the freely rising case and thus relates to the scaling function g in Eq. (98).

As for pure spontaneous imbibition the concept of a dynamical exponent z describing the propagation of fluctuations along the interface does not apply to imbibition with gravity. The fluctuations always catch up to the available zone of correlated roughness, correlation lengths cannot exceed ξ_g .

Dynamical roughening of the interface in the presence of evaporation (and absence of gravity) is the most complex case. Although the average interface dynamics is well described by the mean-field equation, the extra term in $\epsilon(1 - e^{-2|k|H})$ means that a single correlation length $\xi = \xi(t, H(t))$ cannot be unambiguously identified.

The situation becomes clear only in the pinned interface limit, where a simple correlation length can be defined as

$$\sigma \xi_e^{-3} = 2\epsilon(1 - e^{-2H_p/\xi_e}). \quad (105)$$

In the limit $\xi_e \ll H_p$, $\xi_e \sim (\sigma/\epsilon)^{1/3}$ while in the opposite limit $\xi_e \gg H_p$, $\xi_e \sim (\sigma^2/(\bar{\alpha}\epsilon))^{1/4}$. The first case corresponds to weak evaporation, defined by $\epsilon \ll \bar{\alpha}^3/\sigma^2$, while the second case is that of strong evaporation, $\epsilon \gg \bar{\alpha}^3/\sigma^2$. The value of the roughness exponents is established from the decay of the structure factor, with again the result $\chi = 1.25$ [85].

The prediction for the pinned correlation length can be checked by considering the scaling behaviour of the

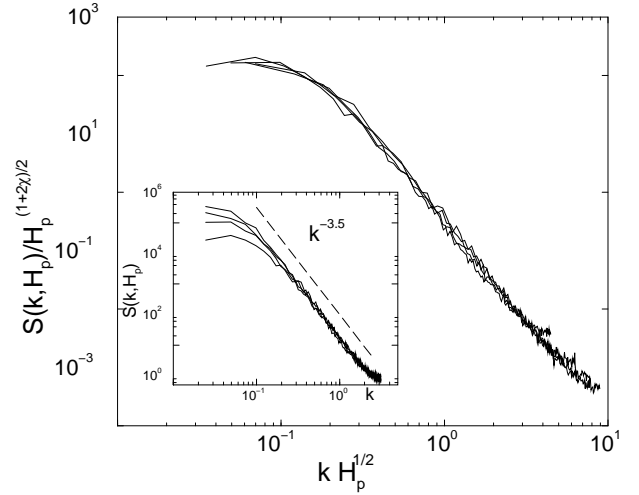


FIG. 28: A log-log plot of structure factors of the pinned interface in presence of gravity. The inset shows the value of $S(k, H_p)$ for pinning heights $H_p = 20, 40, 60$ and 80 . The main figure shows the collapse of the data under the assumption of a correlation length $\xi_g(H_p) \sim H_p^{1/2}$. The dashed line indicates a roughness exponent of $\chi = 1.25$. All quantities are taken in the dimensionless units of Eq. (72).

pinned structure factors $S(k, H_p)$ as shown in Fig. 29. The data with the highest evaporation rate can all be collapsed assuming a correlation length $\xi_e \sim (\bar{\alpha}\epsilon)^{-1/4}$, while for lower evaporation $\xi_e \sim \epsilon^{-1/3}$. The crossover occurs roughly for parameters $\bar{\alpha} = 0.2$ and $\epsilon = 10^{-4}$. The complete set of data can be reduced to a common scaling form by solving Eq. (105) numerically (using a value of $\sigma = 2\sqrt{2}/3$). As a result the structure factor at pinning has a scaling form similar to Eq. (104), although care must be taken in identifying the correlation length.

To summarise, the main result of the analysis presented here is that the fluctuations of the interface are intimately coupled to the average position, through the length scale ξ_x . Both ξ_x and H should be studied simultaneously. Experimentally, the existence and dynamical behaviour of this length scale can be inferred from the saturation of the spatial and temporal correlation functions and should be easier to observe than the precise values of the scaling exponents on scales $r < \xi_x$.

5. Constant flow

Imbibition with a constant flow rate can easily be performed, e.g., in Hele-Shaw cells with disorder and can be modelled within the phase field approach by a simple modification of the boundary conditions. So far we have had for the average velocity of the interface $2v = |\langle \nabla \mu |_{y=0} \rangle|$ (the factor 2 coming from the miscibility gap). If now the disorder is in the mobility, its effect on the interface dynamics is proportional to the flow influx, so a priori it cannot be neglected. This adds

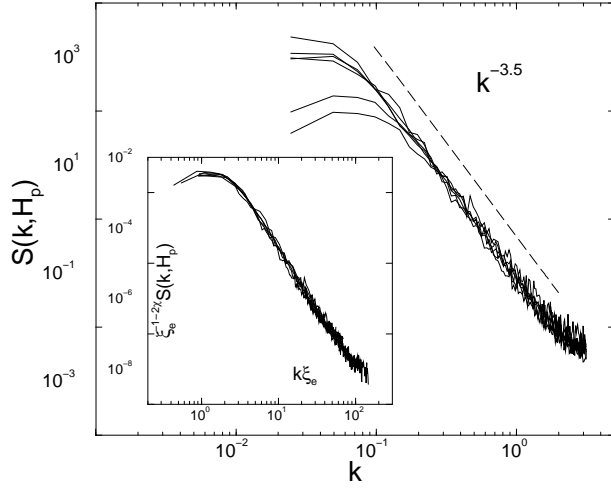


FIG. 29: A log-log plot of structure factors of the pinned interface in the presence of evaporation. The main figure shows the value of $S(k, H_p)$ for pinning heights (from bottom to top) : $H_p \simeq 20$ ($\bar{\alpha} = 0.2, \epsilon = 10^{-3}$); $H_p \simeq 28$ ($\bar{\alpha} = 0.2, \epsilon = 5 \times 10^{-4}$); $H_p \simeq 45$ ($\bar{\alpha} = 0.1, \epsilon = 10^{-4}$); $H_p \simeq 63$ ($\bar{\alpha} = 0.2, \epsilon = 10^{-4}$); $H_p \simeq 77$ ($\bar{\alpha} = 0.3, \epsilon = 10^{-4}$); $H_p \simeq 109$ ($\bar{\alpha} = 0.3, \epsilon = 5 \times 10^{-5}$). The structure factors for $\epsilon \sim 10^{-4}$ all collapse on the same curve, independent of the value of $\bar{\alpha}$. A complete collapse of the data can be accomplished by solving Eq. (105) numerically, as shown in the inset. The dashed line indicates a roughness exponent of $\chi = 1.25$. Again, all quantities in the dimensionless units of Eq. (72).

a term to the interface equation, of the form

$$\int d\mathbf{x}' G(\mathbf{x}|\mathbf{x}') (\nabla \cdot m(\mathbf{x}) \nabla \mu). \quad (106)$$

The usual projection technique becomes quite involved in this case. However, for a linear analysis, it is sufficient to relate the gradient of the chemical potential to the average interface velocity $\nabla \mu \sim v$, which yields

$$\dot{h}_k = - (v + \sigma k^2) |k| h_k + \frac{1}{4} |k| \{\eta\}_k + v \{m\}_k \quad (107)$$

where $\{m\}_k \approx 2 \int_x e^{-ikx} m(x, h(x, t))$ represents the noise induced by the mobility. In contrast to the capillary disorder, represented by $|k| \{\eta\}_k$, this noise is non-conserved, but with a strength proportional to the mean velocity of the interface.

This equation, also derived in [261] and partly in [122] shows that mobility and capillary disorder influence the fluctuations on different length scales. Small length scales are dominated by capillary disorder while the effect of mobility disorder becomes dominant on large scales. This is evident and natural, since the latter reflects fluctuations in the local fluid flow in the bulk, which obviously have an effect beyond local pore randomness. A crucial point however is that the crossover length-scale ξ_{mob} between the two regimes is velocity dependent, in

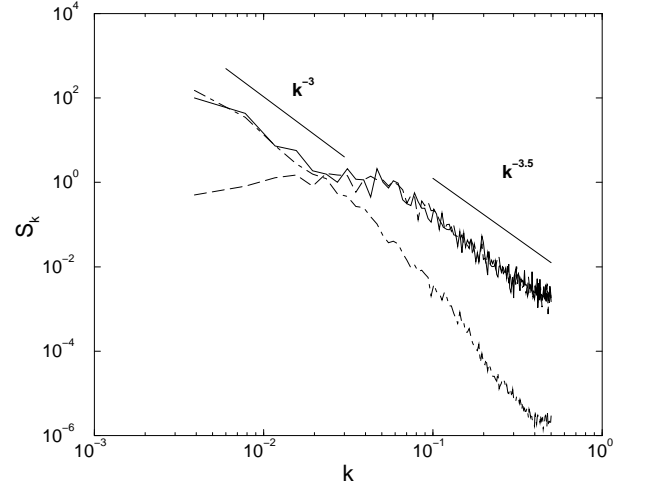


FIG. 30: Comparison of roughness spectra (structure factors) for capillary and mobility disorder. The dashed line represents capillary disorder only, the dot-dashed line mobility disorder only and the full line to both sources of disorder present. The simulation is done at $v = 0.005$, taken at an average height $H = 50$. Beyond a length scale ξ_{mob} (cf. Eq. (108)) mobility disorder, with $\chi \approx 1$ gives the dominant contribution to roughness, on smaller scales disorder in capillarity, with $\chi = 1.25$ is more important.

terms of dimensional quantities

$$\xi_{\text{mob}} \sim \frac{\kappa^2}{v\eta} \frac{\delta p_c}{\delta \kappa}. \quad (108)$$

In the simple model of Pauné and Casademunt, where both permeability and capillary pressure are related to an effective pore radius r_0 , $\xi_{\text{mob}} \sim r_0/C_a$ [261].

The length scale ξ_{mob} can be seen in Figure 30, where the roughness spectra of three model setups are plotted on top of each other: (i) capillary disorder only, which gives the main contribution to roughness on short scales $< \xi_{\text{mob}}$, (ii) mobility disorder only, which roughens the opposite regime, and (iii) including both, which gives an envelope of the other two curves. The comparison between the structure factors corresponding to different average interface velocity is shown on Fig 31. An effective exponent $\beta \simeq 0.4$ can be defined, but it is strongly influenced by cross-over between the capillary and mobility regimes of disorder.

The behaviour of the interfacial fluctuations is a lot clearer at *low capillary number*, where only capillary disorder is relevant. The intrinsic length scale $\xi_\infty = (\sigma/v)^{1/2}$ is still present but it is now static, and does not play an explicit role in the dynamics of the fluctuations. Figures 32 and 33 show the numerical results obtained from a simulation of the phase field model with constant flow, $m(\mathbf{x}) = 1$ and without pinning ($\gamma = \epsilon = 0$). The structure factor at saturation shows that the short wavelength exponent $\chi \approx 1.25$ with a much smoother roughness at large length scales. The dynamical behaviour of the width shows first a steep increase, with exponent

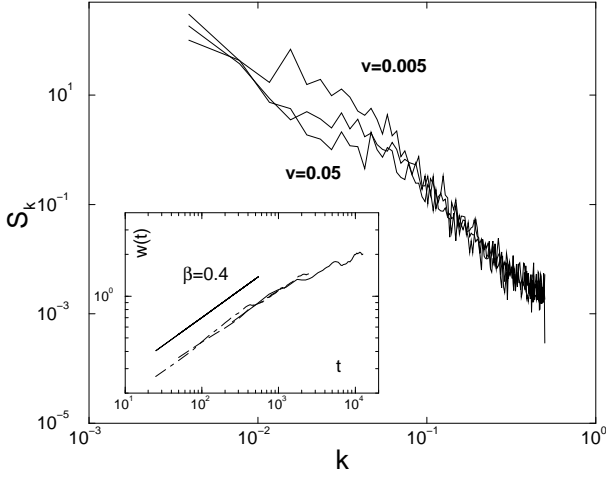


FIG. 31: Comparison structure factors for both capillary and mobility disorder at different velocities. The simulations are done for three different velocities, $v=0.005, 0.01$ and 0.05 with the structure factors taken at the same average height $H=50$. A clear separation between the two roughening regimes occurs only if $\xi_{\text{mob}} \sim 1/v \rightarrow \infty$. Beyond a length scale ξ_{mob} (cf. Eq. (108)) mobility disorder, with $\chi \approx 1$ gives the dominant contribution to roughness, on smaller scales disorder in capillarity, with $\chi = 1.25$ is more important.

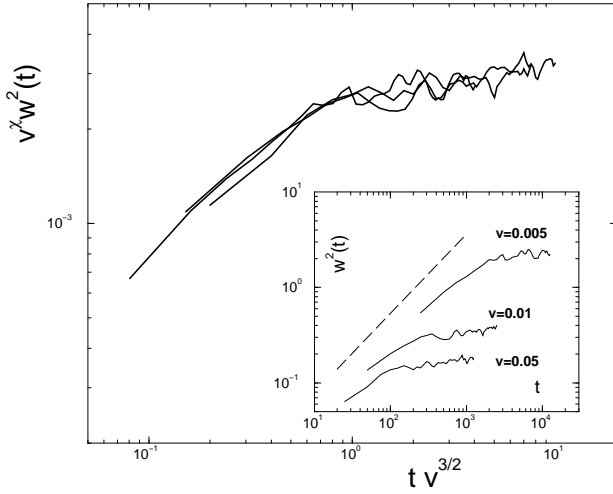


FIG. 32: Growth of the width for interfaces moving at constant velocity $v = 0.005, 0.01$ and 0.05 . The inset shows an initial growth exponent $\beta \approx 0.42$ followed by a weak logarithmic regime. The main figure shows the rescaling of the data using Eq. (109) and a crossover time $t_x \sim v^{-3/2}$. The roughness exponent $\chi = 1.25$.

$\beta \approx 0.42$ which is indicative of a dynamical exponent $z = \chi/\beta = 3$. At later times, the width flattens out, to an effective exponent (only defined on the small window available) $\beta \approx 0.1$, more representative of logarithmic roughening than true power-law behaviour, a trend confirmed by the form of the structure function.

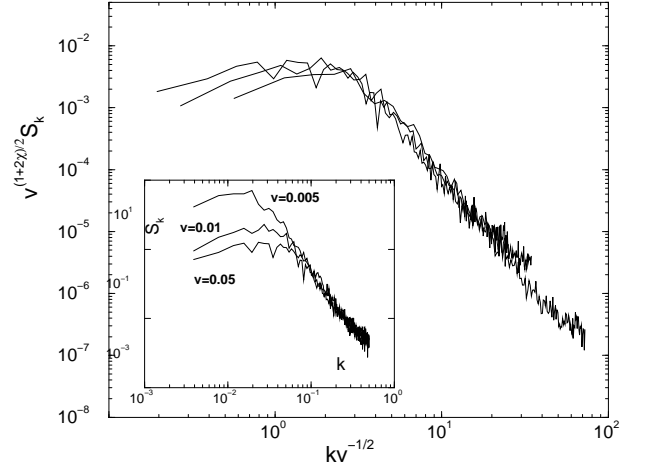


FIG. 33: Structure factor at saturation for interfaces moving at constant velocity $v = 0.005, 0.01$ and 0.05 taken in the logarithmic regime for the growth of the width (nearly saturated regime). The inset of the Figure shows the structure factors, the faster velocity have the smaller range of correlated roughness. The main Figure shows the rescaled data using the correlation length $\xi_x \sim v^{-1/2}$ and the roughness exponent $\chi = 1.25$.

The dynamics is thus controlled by two correlation lengths, $\xi_1 \sim vt$, which dominates the dynamics for wave-vectors $k \ll \xi_x^{-1}$, and $\xi_3 \sim (\sigma t)^{1/3}$, which controls the scale $k \gg \xi_x^{-1}$. The time development of the width is determined by the ξ_3 term as long as $\xi_3 \ll \xi_x$ while the slower ξ_1 is only effective at times when $\xi_1 \ll \xi_x$:

$$\begin{aligned} w(t) &\sim \xi_3^\chi(t) \sim t^{\chi/3} & t \ll t_x, \\ w(t) &\sim w(t_x) + \mathcal{O}(\log(t/t_x)) & t \gg t_x. \end{aligned} \quad (109)$$

The crossover time between the two dynamical regimes is $t_x \sim \sigma^{1/2}/v^{3/2}$ and the width after saturation of the rough zone $w(t_x) \sim \xi_x^\chi$.

6. Columnar Disorder

Recent experiments have also dealt with the case of imbibition with columnar disorder [311, 312], defined by

$$\langle \alpha(\mathbf{x})\alpha(\mathbf{x}') \rangle - \bar{\alpha}^2 = (\Delta\alpha)^2 \delta(x-x'). \quad (110)$$

An example is shown in Figure 39 (Section IV A 1). The main characteristic of this type of noise is that the dimension perpendicular to the reservoir does not come into play, it corresponds to imbibition on “stripes” of different properties. Thus, at the level of the interface equations, the position of the interface does not enter the quenched noise. The linear interface equation is thus

$$\frac{\partial h_k(t)}{\partial t} = -(v + \sigma k^2) |k| h_k + \frac{1}{4} |k| \eta_k \quad (111)$$

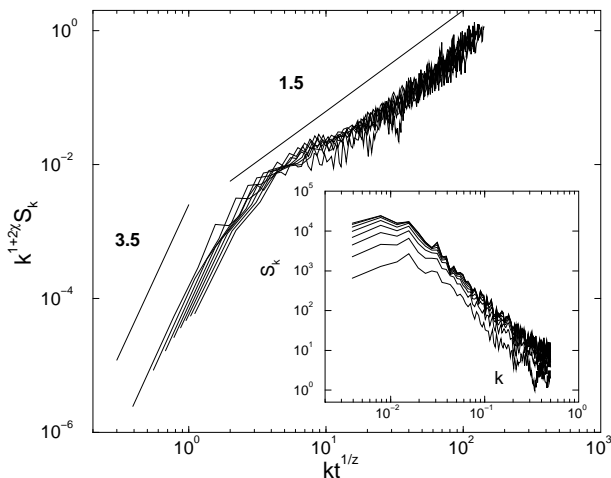


FIG. 34: Structure factor obtained from the phase field model with columnar capillary disorder and constant flow rate. Intrinsic anomalous roughening [198] is visible in the inset. The scaling plot (main graph) indicates a roughness exponent $\chi \approx 1.25$ and dynamical exponent $z \approx 2$. The scaling plot indicates an anomalous exponent $\theta_a \approx 0.75$, similar to the value found experimentally [312]. The simulations were done with a imposed velocity $v = 6.25 \times 10^{-4}$ and capillary disorder only.

where now $\langle \eta_k \eta_{k'} \rangle = (\Delta\alpha)^2 \delta_{k,-k'}$. With this simple nature of the disorder, the roughening process can be studied analytically at the linear level. At saturation, the structure factor

$$S_k \sim \frac{1}{(v + \sigma k^2)^2} \quad (112)$$

indicates a short-wavelength roughness exponent $\chi = 3/2$ and a flat interface at large distances. However, due to the development of fingers in the interface, separated by large slopes, the linear approximation of Eq. (111) breaks down and experiments (Figure 41), as well as simulations of the phase field model (Figure 34), show instead intrinsic anomalous roughening [198]. In this case, there is a time-dependent increasing amplitude of the structure factor, characterised by an exponent θ_a , due to steepening of local slopes on the interface.

$$S_k(t) \sim \begin{cases} \xi^{2\theta_a} k^{-2(\chi+\theta_a)-1} & \text{for } k \gg \xi^{-1} \\ \xi^{2\chi+1} & \text{for } k \ll \xi^{-1} \end{cases} \quad (113)$$

and $\xi = t^{1/z}$. Indeed, the experimental distribution of slopes shows a power law tail [311, 312], similar to what is observed for roughening in fractal structures [11]. At this point it becomes clear that the linear interface equation fails to appropriately describe this case.

IV. EXPERIMENTS ON IMBIBITION

In the following we summarise the current experimental situation in imbibition with regard to the theoretical

ideas presented earlier. The main goal of this section is to give some experimental substance to theoretical ideas presented earlier. Beyond this we want to understand where further interesting avenues exist, and to outline which of the recent advances in models have been confirmed. From the existing works one can see some clear directions for further investigations.

The introduction presented already some experimental complications associated with both spontaneous and forced imbibition. Since our approach is predominantly based on an interfacial approach, where the advancing front of liquid has an effective surface tension, it is important to discuss in which cases the simplifications of the theoretical models are expected to be valid.

To recapitulate the viewpoint of a statistical physicist interested in the front roughening, the main issue is whether an interface description actually makes sense at all. In our case this is considered to be true if the large-scale geometry of the boundary between the “dry” and “wetted” parts of the system can be described with the aid of self-affine concepts. Exceptions can arise if the saturation of the imbibing fluid is a very smooth function, in the coarse-grained sense. Then the transport dynamics are determined on the level of individual pores, and coarse-graining to an interface is not possible. When an interfacial description is possible, pore-scale phenomena can be embedded in the noise contained in the interfacial equation of motion. A second question to be asked is whether the Darcy-Washburn behaviour is valid (recall that it is based on a idealised picture of fluid flow), even in the presence of a well-defined imbibition front. Failure of simple Darcy-flow concepts can stem from fluid-matrix interactions, from hydrodynamical reasons (inertial and transient effects, as Bosanquet-flow), and from contact-line physics, like the change of the contact angle over time [266, 304].

In this section, when appropriate, we also point out analogies between kinetic roughening in imbibition and other experimental systems, (see [20, 116, 224] for early reviews of the subject). We first discuss the specific problem of paper, or fibre networks, and then continue with results on interface dynamics for constant flow rate (forced fluid flow) imbibition, followed with the spontaneous case.

Before embarking on this task, it is worth keeping in mind some basic facts of roughening in nature. The theoretical models are always a “coarse-grained” description of the experimental system considered, that is the microstructure enters only via an effective description, most often encoded in the noise terms. Several length scales are also usually present and many cross-over phenomena can occur. In real systems, as well as in simulations, one encounters a typical structural length-scale l_c (e.g., the bead size in a Hele-Shaw cell) so that real scaling behaviour is established only for $l \gg l_c$. Cross-over behaviours are also due to the finite size L of system itself which enters the scaling function of any measure of roughness or correlations. Finally the boundary condi-

tions can induce boundary effects by suppressing or enhancing local dynamics. It is customary to neglect these by considering only a part of the system (to use a window in space), but there is of course no guarantee that this procedure works a priori. In particular, it is often assumed that one needs to subtract the ‘tilt’ (linear trend) from the height profile $h(x, t)$ to avoid long-wavelength effects (see e.g. [297] for a discussion). For all these three reasons it is clear that one should take any exponent values measured for a fixed l/l_c with a grain of salt. Indeed, the effect of boundaries on the behaviour of systems exhibiting criticality is a very complex topic by itself, with many facets, e.g., for directed percolation [183] and the KPZ universality class [163].

A second important point is that true scaling behaviour is observed only if good averaging, in the “thermal” sense is obtained [245]. The interface must see several different realisations of disorder before any scaling behaviour can be observed. This is intuitively clear even in a simulation, where one run just considers a particular noise history and representative scaling is established only within a statistical ensemble. There are two ways around this problem. The simplest, brute force approach, is simply to do a large enough number of experimental runs with different noise configurations. This is however difficult with imbibition since, analogous to fracture experiments, it is often impossible to repeat the experiment very many times. The other option is to consider long enough experimental runs, so that the interface fluctuations reach a steady state [130, 245]. This is again very difficult in imbibition, due to the slow time scales involved. Also, in the theoretically interesting case of spontaneous imbibition the front slows down constantly and there is no steady state. In cases where thermal noise becomes irrelevant (slow, avalanche- or activation-like dynamics) the situation is in practical terms even more precarious than in usual kinetic roughening when it comes to obtain reliable data.

7. Difficulties inherent to paper imbibition: a case study

In many statistical physics experiments on imbibition the medium of choice has been either a Hele-Shaw cell filled with (transparent) beads up to a certain volume fraction or, for obvious simple practical reasons, paper. The first approach is perhaps less subject to accidental experimental complications. To both assist with the interpretation of actual scaling results and to highlight the difficulties that could arise in various media we now discuss the specific case of paper and its impact on studies of imbibition. Sheets have been used to study striped media [351] and *radial* propagation [225], and two fronts can be made to collide [246], in addition to the papers cited below in later sections.

Experiments have demonstrated that clear, Washburn-like behaviour can only arise if there is not much interaction (swelling, prewetting) between the fibre networks

and the penetrating liquid [104]. Ordinary paper is made from wood fibres and, in many cases, chemical additives and filler materials like talc and clay, arranged in a disordered structure [253]. There is a wide distribution of pore sizes (this can be simulated by computer models [254], or studied via, e.g., X-ray tomography [293]) with a high effective tortuosity. The actual mass distribution per unit area varies (due to a phenomenon called flocculation [253]) and the resulting structure has on the top of this power-law correlations up to a cut-off of a few average fibre lengths [269].

The surface of paper sheets is extremely uneven and the concept of surface pore is itself ill-defined. This gives rise to problems in defining static and dynamical contact angles as is typical of inhomogeneous substrates and implies that there will be large fluctuations in the capillary pressures. In commercial papers, there is also an anisotropy between the “machine-direction” (MD, parallel to the web) and “cross-direction” (CD, perpendicular to the web), which may also influence the liquid penetration in the structure. For industrial papers there are often residues of chemicals, which may induce drastic changes in the effective viscosity or surface tension of the invading liquid.

In paper, the whole fibre structure may be modified by swelling of the fibres in contact with the liquid [39]. Cellulose fibres show a great affinity to water and can absorb large quantities in millisecond time-scales, giving rise to concomitant changes in fibre volume and pore structure. By nuclear magnetic resonance (NMR) it is possible to observe the simultaneous intake of water into pores between fibres but also *inside* the fibres themselves. However, this is not the case for many organic fluids and oils. Any intuitive picture of fibres (or the network) as capillary tubes is thus often false: the pore structure is highly non-trivial and in some cases time-dependent (see also [158, 323]). If swelling occurs, the volume to be filled with liquid increases and the flow resistance of the pore network changes, which leads possibly to non-Washburn behaviour.

There can also be an exchange of liquid between the inside of a fibre and the “surface” pores, important in particular since the imbibition takes place “along” the sheet. This complicates enormously the fluid flow since there are no well defined “structures” (either the pores, or the fibres) responsible for the capillary forces [12, 153, 263]. The fluid may very well undergo imbibition as such only on the rough paper surface. This is a mechanism that has been studied itself by various authors in other contexts [28, 213, 289], but not for such rough surfaces. All this makes it questionable as to whether it is possible to easily find a representative network description [186, 300]. Mathematically, the problems amount to defining the essential effective properties of a pore for the imbibition process. Classical applications of imbibition to study the flow properties of porous media hope to answer this unequivocally, but correlations in the pore-scale properties may however render the starting point useless, since both

the typical scale of pores and the effective correlations need to be mathematically specified in any model of a “typical” pore [153, 308].

A. Forced flow imbibition

Simultaneously to the development of the theoretical picture of “local” kinetic roughening several groups attempted to measure the properties of a fluid-gas interface in Hele-Shaw cells [95, 121, 288]. These were typically done in planar cells of thickness between one and a few bead diameters. The general outcome is that no really convincing link could be established with such “local” descriptions. Quite recently this has been taken up by the group of Ortín, Hernández-Machado, and co-workers, using specially prepared substrates with controlled disorder [122, 311, 312, 313]. We outline below the current experimental situation.

1. Interface roughening

The early works [95, 121, 288] measured typically the temporal exponent β and the roughness exponent χ by using digitised pictures of interfaces and two-point correlation functions (c.f. Eqs. (47) and (49)). This method has many natural limitations: the typical resolution available for spatial structure was of the order of 250 points of $h(x, t)$ and the two-point correlation function cannot measure roughness exponents larger than 1. Representative values for the exponents would be $\beta = 0.65$ and $\chi = 0.80 \dots 0.9$. These are substantially higher than standard KPZ exponents $\beta_{\text{KPZ}} = 1/3$ and $\chi_{\text{KPZ}} = 1/2$.

He et al. [121] observed the roughness in a Hele-Shaw cell with capillary numbers $10^{-5} < C_a < 10^{-2}$. They determined a large roughness exponent $\chi \sim 0.8 - 0.9$ (as illustrated in Fig. 35, from [121]) and a decrease of the global width with increasing capillary number with a possible saturation of the width at very low capillary number (Fig. 36 [121]). The roughness exponent was obtained from the two-point correlation function and is probably indicative of a super-rough ($\chi > 1$) interface. They also made the important point that the dynamics is non-local and introduced a simple scaling argument to relate the total width of the interface to the capillary number C_a

$$w \sim C_a^{-q} \quad (114)$$

where $q = 2\chi/(2\chi + 1)$ in 2D. This argument is obtained by balancing the local (pore level) capillary forces to the global viscous pressure drop driving the interface and agrees qualitatively with the experimental results at large capillary numbers, although it cannot fit with the plateau at low capillary numbers.

However, this argument does not take into account any large scale curvature of the interface, from which

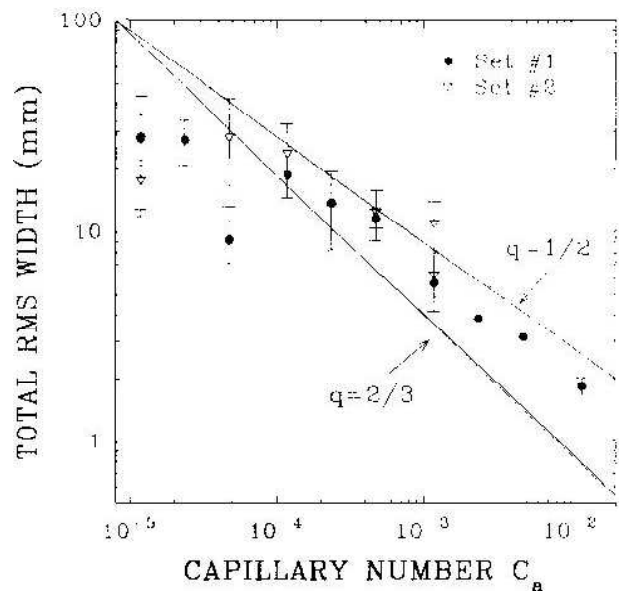


FIG. 35: Interface width vs. the capillary number C_a in a Hele-Shaw cell with a constant flow rate. (Experiment by He et al. [121]). The lines show scaling predictions (see text).

the length scale $\xi_x \sim C_a^{-1/2}$ in Eq. (21) arises. The experimental results can then also be explained with the theoretical picture developed in the preceding section. Since the experimental capillary number is small, we assume that only capillary disorder is important and that the mobility has a negligible effect. At very small capillary numbers, the length of the cell $L \ll \xi_x$ and so the width is independent of C_a . As the capillary number increases, $\xi_x < L$ and, neglecting the small logarithmic correction at large scales, $w \sim \xi_x^\chi \sim C_a^{-\chi/2}$. A roughness exponent $1.0 < \chi < 1.25$ yields $0.5 < 0.625$ which is also in qualitative agreement with the experimental results.

At large capillary numbers, Horváth et al. noted that there seemed to be a cross-over in χ to values ~ 0.5 [128] at large length scales (a clear example is depicted in Fig. 37, from the same reference) which would be consistent with a regime where either mobility disorder or the “thermalisation” of the quenched disorder becomes relevant. The measured dynamical exponent $\beta = 0.65$ is also indicative of a smaller value of z .

Lately the forced flow case has been studied intensively both theoretically (see the preceding section) and experimentally by the group of Ortín, Hernández-Machado and co-workers [122, 311, 312, 313]. The central idea, different from earlier approaches, was to use Hele-Shaw cells with a pattern of copper tracks or islands placed on a substrate of fibre glass. An illustration of the experiment is shown in Fig. 38, together with the way of introducing randomness into the samples. Here such disorder is given simply by the fluctuations in the cell gap. A definite advantage of this setup is that the disorder is under better qualitative control. In particular it allowed for the first time the study of “columnar disorder”, where the gap

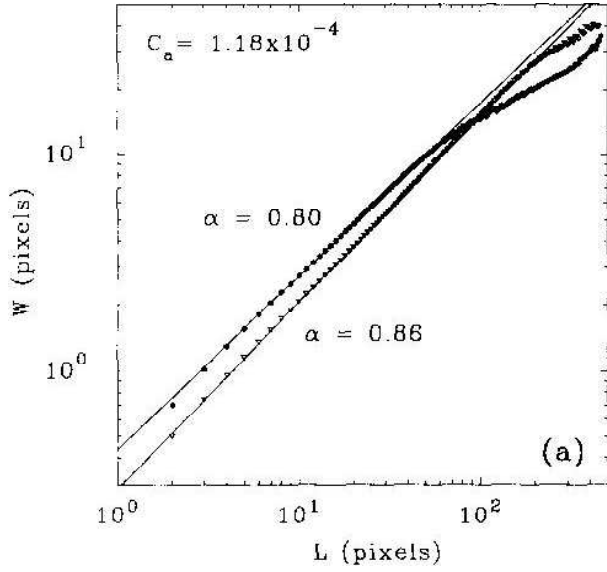


FIG. 36: Two examples of the local width (called W here) for the experiment of He et al. [121]. For L small the effective roughness exponent is about 0.8, whereas for larger scales the scaling changes.

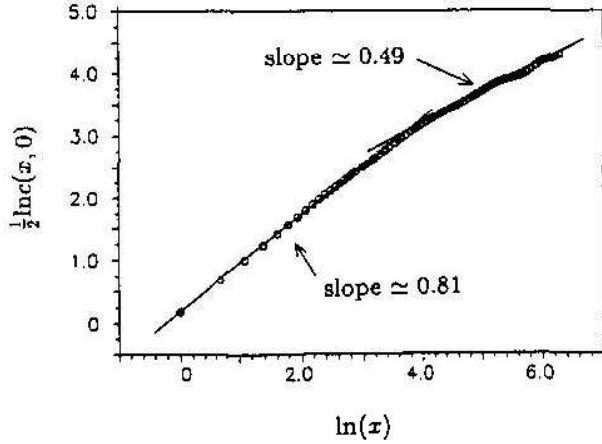


FIG. 37: The spatial two-point correlation function in a forced fluid flow experiment by Horváth et al. [128]. Notice the presence of two scales in the data, with a larger exponent at small scales.

value is quenched and does not vary in the direction of interface propagation, for the first time (see Eq. (110)). On the other hand this very interesting work also highlights the standard experimental difficulties in this field: the need for many samples (disorder averaging) and the problems in attaining reasonable scaling windows for the possibly critical quantities are difficult to circumvent. The in practice achievable length-scales are obvious in Fig. 39, and one should note in particular the case with columnar disorder.

Hele-Shaw cells with a pattern of square islands (square disorder) is similar to using cells with randomly packed beads. Intuitively one may perhaps expect a bet-

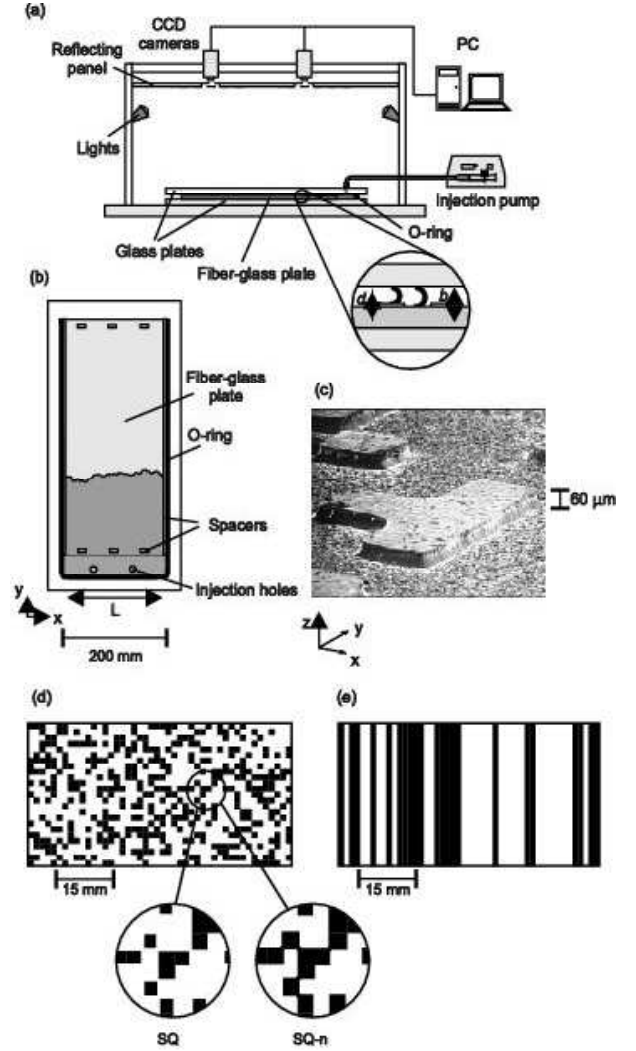


FIG. 38: Sketch of the experimental setup of [311]. a) and b) present views of the experimental apparatus, c) a SEM image of the copper islands on the fibre-glass plate, and d) and e) present views of the disorder pattern for “point-disorder” and “columnar disorder”, such that copper islands are denoted by the black regions.

ter qualitative picture of the porosity (gap) fluctuations than in such earlier setups. For capillary numbers in the range $1.33 < C_a < 17.0$, the cross-over phenomenon already observed by Horváth et al. [128], together with exponent $\beta \sim 0.5$ was also present. The structure factor of Fig. 40 clearly shows a short-range exponent $\chi_{SR} \sim 1.0$. At large scales, it appears that the roughness exponent changes continuously as a function of velocity, but this behaviour should be contrasted to the theoretical results of Section III. From the phase-field simulations (see Figs. 30 and 31), it is known that roughening due to capillary forces gives rise to a large roughness exponent but only up to a length scale ξ_\times . At larger length scales, mobility disorder dominates, but there can be a very long crossover between the two regimes, particularly

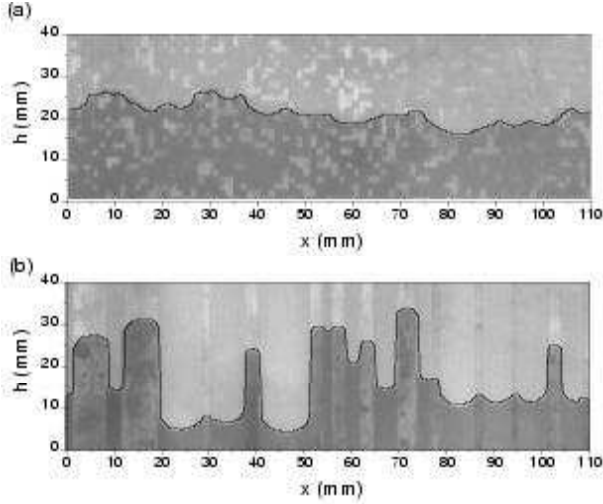


FIG. 39: Interface profiles for examples of disorder, point-like in a), columnar in b), with the original images included. Notice in particular the scale of the vertical “discontinuities” in b). From [311].

at large capillary numbers (i.e., for a large interface velocity). The experimental data of Fig. 40 are then more indicative of a well-defined long-range roughness exponent $\chi_{LR} \sim 1.0$ and of a cross-over behaviour, than a true velocity-dependent roughness exponent.

For columnar disorder, analysed theoretically in Section III G 5, the papers brought up the idea of a phase diagram, which depends on the strength of the capillary forces (gap in the cell in the experiments being the control parameter) and the forced flow velocity. If the capillary forces are of major importance, *anomalous scaling* is found [198, 312]. This results from another length-scale, the “lag” between neighbouring columns due to the difference in local mobility. The usual signs of anomalous behaviour could be extracted: correlation functions for the spatial fluctuation would exhibit different scaling exponents χ_q depending on the order (or moment) of the correlations measured, the local and global exponents for the roughness would differ, and finally the global width would in addition exhibit “super-rough” behaviour, $\chi > 1$ [198]. The scaling of the structure factor of the interfaces also pointed out the possibility of several χ values, as shown in Fig. 41 for the experiments: for short scales the roughness exponent would exhibit such anomalous, super-rough scaling ($\chi \approx 1.2$) while on more macroscopic scales the same cross-over behaviour as for square disorder would be observed. Again, this may be a crossover effect between capillary and mobility disorder. For the other exponents $\beta \approx 0.5$ and $z \approx 2.0$ were obtained (see Fig. 42). Again, higher order correlation functions show different effective exponents, a possible indicator for multi-scaling. Fig. 43 gives evidence for this, for interfaces with columnar disorder and at saturation. A distinction between the various phases for multi-scaling is illustrated in Fig. 44. Such signs are similar to what is

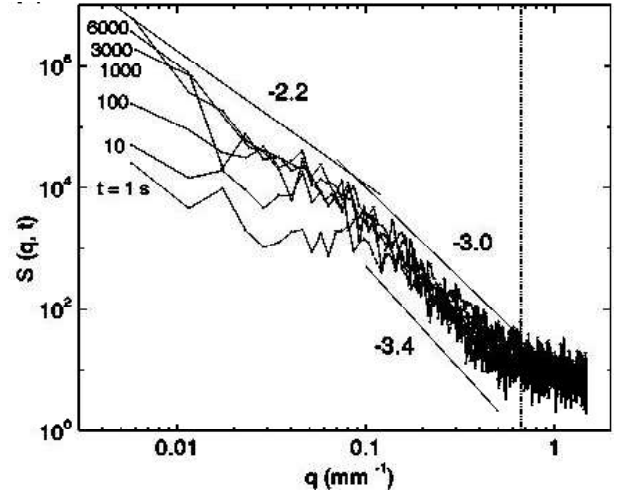


FIG. 40: Results from Ref. [311] for the power-spectra of the interfaces at different times approaching a steady state under point disorder as in Fig. 39(a).

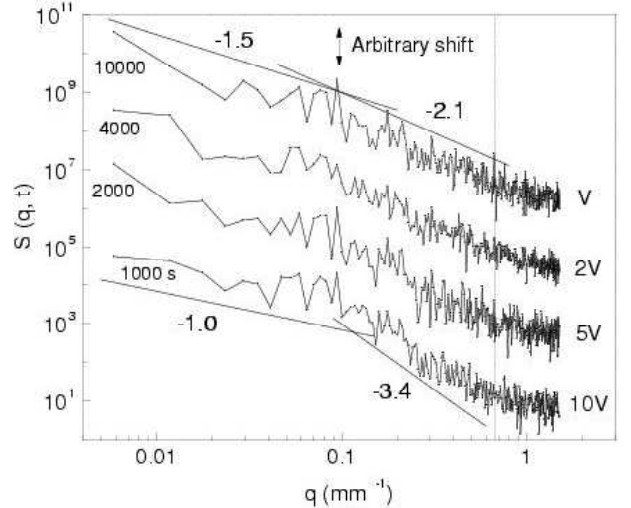


FIG. 41: Results from [311] for the power-spectra of the interfaces at four different imposed velocities and columnar disorder. The curves are shifted for clarity. The vertical line gives the scale corresponding to the typical width of the columnar tracks, and the other lines are fits to determine roughness exponents. Notice how a large velocity seems to imply in particular a larger short-range roughness exponent (recall that the structure factor decays as $k^{-(1+2\chi)}$).

seen in the phase-field description of interface dynamics (though the actual exponent values may not agree), and indicates that the presence of non-local dynamics invalidates simple scaling.

2. Avalanches and depinning

All the early works in particular in Hele-Shaw cells pointed out more or less directly the difficulty in observ-

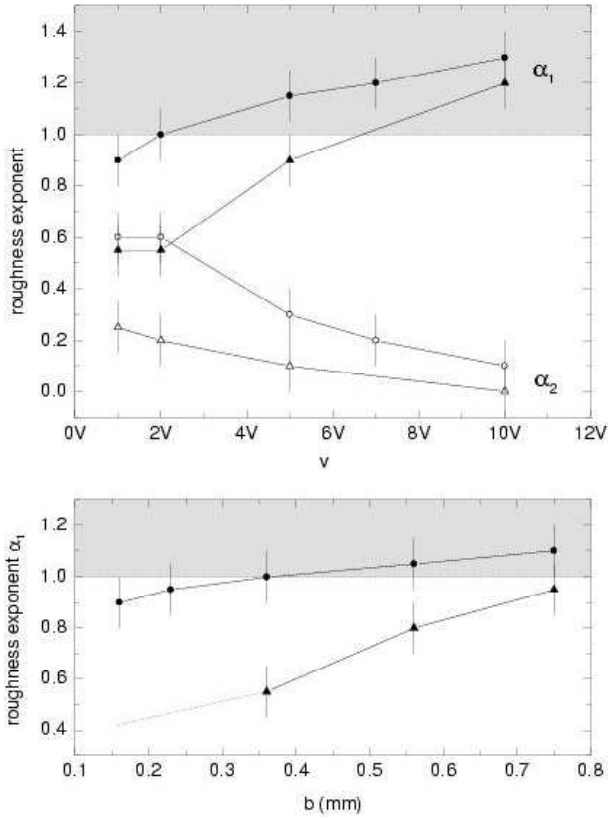


FIG. 42: Results from [311] on the roughness exponents, where the type of disorder is varied (circles: point-like, triangles: columnar). The top one shows variation with imposed velocity, and the bottom one with the gap between the plates between which the advancing liquid is confined. Solid and open markers correspond to short and long range exponents, respectively. For $\chi > 1$ (or α in the notation of the figure, from [311]) denoting “super-roughness” the region is shaded in grey.

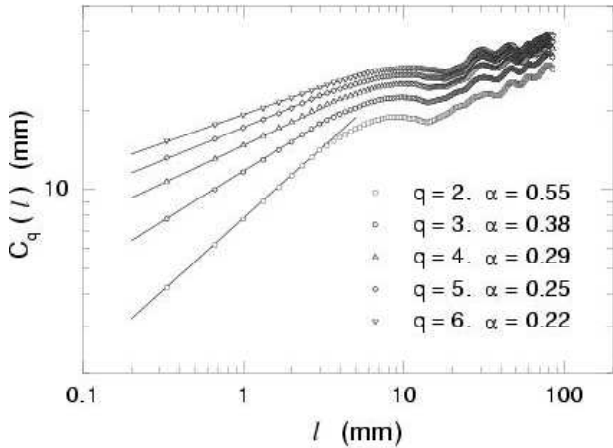


FIG. 43: q -th order two-point correlation functions of the interfaces in the experiment of Soriano et al. show at saturation some type of effective multiscaling as their logarithmic slope (taken as χ_q) is clearly q -dependent. Here the disorder used was of columnar type [312]. The long-range scaling is not reliable due to poor statistics.

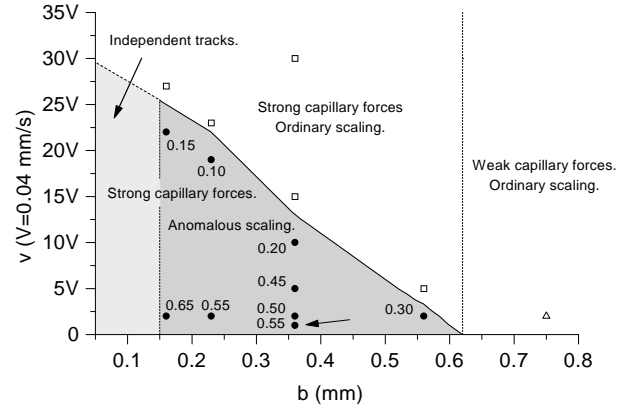


FIG. 44: An experimental phase diagram for anomalous scaling in the setup of Soriano et al. [312]. The symbols indicate the points explored. The numbers next to the symbols tell the difference between the “global” and “local” roughness exponents, χ and χ_{loc} . The effect is strongest for slow interface progression and small values of the gap — which renders the disorder strong and would perhaps indicate a simultaneous decrease of the effective interface tension.

ing the slow, avalanche-like motion for small C_a , due to the lack of self-averaging. Further experiments then concentrated on the study of avalanches and noise properties. Horváth et al. studied the *noise distribution* $P(\eta(x, t))$ [129]. For *local interface equations*, this can be obtained directly from the local increments of the interface height ($v(x, t) \sim \eta(x, t)$), as can easily be seen from, e.g., the slope-averaged KPZ equation. This quantity, turned out to have a power-law tail which is in qualitative agreement with the fact that no standard exponents were observed either. Fig. 45 shows the power-law-like shape of $P(\eta)$.

In later papers by Dougherty and co-workers, the avalanche-like motion of the interface was studied in more detail [6, 81] by looking at the average interface velocity as a function of the local average slope $|\nabla h|$ (inside a measurement window). It would be first assumed that, for a fixed average interface velocity, the function $\langle v \rangle$ is parabolic in the interface gradient. This is a consequence of the non-linear, KPZ-like terms in the interface equation which imply $\langle v(\Delta h) \rangle \propto \lambda(\Delta h)^2$ in the ensemble-averaged sense. As the velocity of the interface approaches zero, depinning models predict that the quantity $\langle v(\Delta h) \rangle$ can either vanish, which indicates the isotropic depinning universality class (QEW-like), or not, meaning that the depinning is anisotropic (QKPZ-like) if one considers local interface equations. The parabolic dependence of the velocity on the slope was indeed obtained experimentally, and the results further indicated that the depinning process was isotropic [6], consistent with the value $\chi = 1.25$ obtained from the phase field simulations (see Fig. 46).

Meanwhile in another paper, using the same setup, it was established that the avalanche statistics are not quite akin to normal depinning models: the area distribution was close to an exponential one and not a power-law,

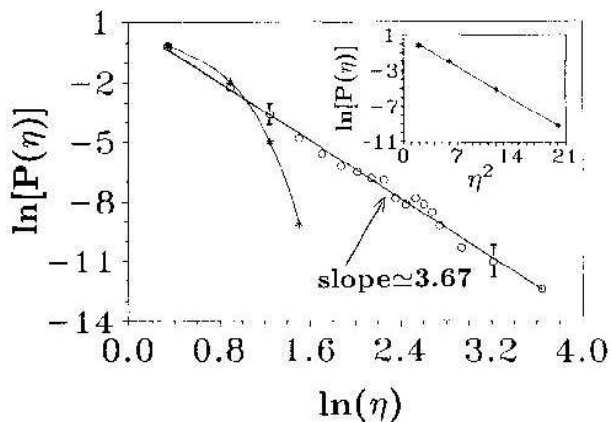


FIG. 45: The effective noise distribution $P(\eta)$, or equivalently the distribution of the local interface velocities in a 2d forced fluid flow imbibition (open circles). Clearly, there is a wide range of local rates of advancement. For comparison the data include the result from the RSOS model (stars), that belongs to the KPZ universality class (see text, figure from [128]).

which also was manifest in the fact that the avalanches spread mostly laterally [81]. One constructs from images of interfaces (Fig. 47) typical avalanches by using time steps (Fig. 48) to recover the areas, locally, swept by the interface. Clearly, the data in Fig. 49 are more in line with an exponential distribution.

This is in clear distinction from critical behaviour found in self-organised systems (e.g., SOC sandpiles or QEW). Criticality in these systems is measured in terms of the order parameter (average velocity) going to zero. An interface is then expected to exhibit avalanche-like motion with a wide distribution of scales *both* perpendicular and parallel to the orientation of the interface. Another landmark would be a power-law distribution of avalanche sizes that also is a signature of the lack of an intrinsic scale. These experimental results imply at least indirectly that the non-locality of the interface dynamics, which provides a definite length scale for the avalanche dynamics, was of importance, as one would expect in particular in the limit $v \rightarrow 0$. They also highlight the difference to other scenarios (theoretical and experimental) where the details of microscopic physics upon coarse-graining yield a “local” (KPZ) interface equation [64, 214, 245].

In this respect we also would like to point out the possibility of measuring directly (in model media) quantities that relate to the non-local properties as pressure fluctuations and saturation [331]. These could be perhaps *combined* with various analysis of the interface dynamics in future experiments.

B. Spontaneous imbibition

So far, both the theoretical and experimental developments in imbibition highlight the specific features of

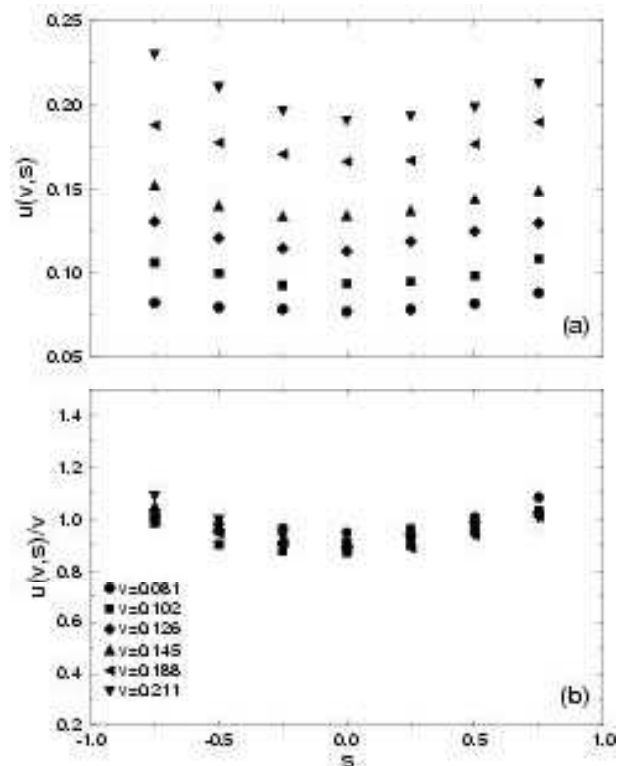


FIG. 46: a) Dependence of the local velocity $u(v, s)$ on the local slope s . The average velocity is given in bead diameters/second. In b) the same data is represented after rescaling by the velocities [6]. The parabolic shape of $u(v, s)$ would imply the presence of a KPZ-like nonlinearity in the effective dynamics.



FIG. 47: Typical interface in a forced fluid flow experiment by Dougherty and Carle [81]. The velocity was $13.7 \mu\text{m/s}$, which should be compared with the scale in the figure.



FIG. 48: The contrasted image (from [81]) shows where the interface has moved during a 4 s interval. As can be deduced, the motion takes place rather uniformly in small patches, without the presence of a wide variety of sizes of “avalanches”. This might be taken to indicate the presence of a correlation length, due to the non-locality of the dynamics.

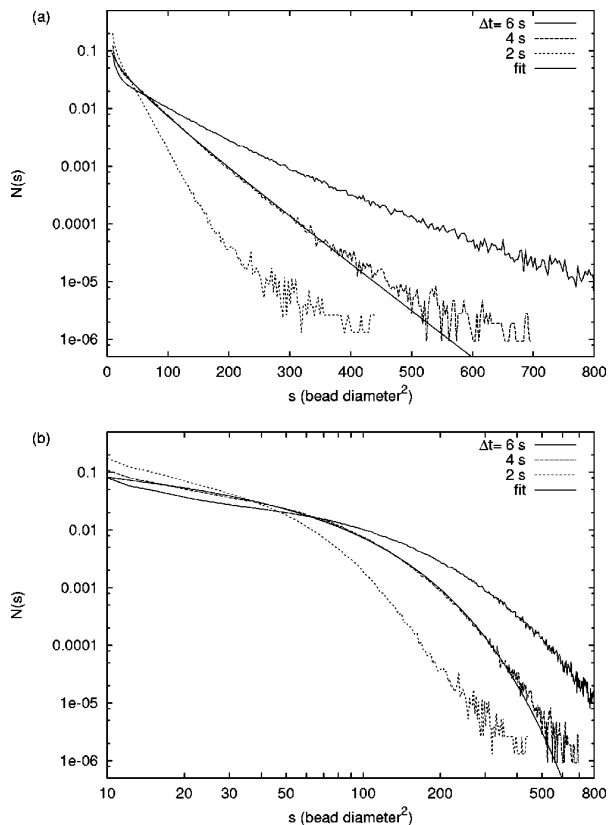


FIG. 49: The distribution of avalanche sizes in the experiment of ref. [81]. The tail resembles more an exponential than a power-law.

fluid invasion together with quenched roughness, and it is important to outline what in particular one should look for in the case of an interface that spontaneously slows down. Some of the specific ideas are:

- a length-scale, as ξ_x , separating regimes of effectively local and non-local interface dynamics,
- multi-scaling, or anomalous scaling, absence of simple scale invariance,
- the interface velocity and its variations as the interface approaches an equilibrium height,
- scaling functions for fluctuations, including the properties of pinned interfaces.

Next we overview both the older experiments and the more recent ones, while trying to relate them to the background established.

1. Pinned interfaces

A set of statistical physics imbibition experiments were done by Buldyrev et al. [19, 45, 46] and Family et al. [95].

The first one was performed with a dye solution in a vertical capillary rise setup. The rising front moved from the reservoir, until eventually, the dye front stopped, due to gravity and/or evaporation (no dynamical measurements were done), and the roughness of the pinned interface was measured. The main experimental finding was a roughness exponent $\chi = 0.63$, consistent with the DPD/KPZ model. It should be noted, however, that the length scale of the scaling behaviour was extremely small: For a total lateral extent $L = 40$ cm, $C(l) \sim l^\chi$ only for length scales l smaller than $l_{\max} \approx 1$ cm, with a cross-over to a constant or to logarithmic behaviour at larger l . This scaling region is only a few times larger than the average fibre length in paper, so the result should be taken with some care. A similar experiment was done in a three dimensional sponge-like material [46]. The stopped interface yielded a roughness exponent $\chi^{(2d)} \approx 0.5$, again consistent with the 2d DPD model.

Amaral et al. [7] studied the role of evaporation induced pinning, by controlling the pinning height via the evaporation rate (presumably by modifying the humidity during the experiment). The result is that the width of the pinned interface is related to the pinning height h_p (and thus to the evaporation strength) through a novel exponent γ , as $w_{\text{sat}} \sim h_p^\gamma$. The experimental value was found to be $\gamma = 0.49$, which could also be related to a modified version of the DPD model [7] as shown in Fig. 50 together with the scaling ansatz used. This result can also be related to the length scale $\xi_x(h)$: if the role of evaporation is to stop the interface, with little or no influence on the statistical fluctuations, then $w(t) \sim \xi_x^\chi(h_p) \sim h_p^{\chi/2}$ and $\gamma = \chi/2$.

Kumar and Juma [166] also performed an experiment in presence of varying evaporation conditions, with the claim that the roughness exponent depended strongly on the evaporation rate, i.e., $\chi = \chi(\epsilon)$.

The last results in this respect are those by the Mexican group [16, 17]. Here, the pinned interfaces in paper-ink wetting experiments were analysed. The main idea was to compare the front roughness (after usual digitisation procedures from a digital picture) between samples of different size. The pinned interface width vs. sample width was stated [16] to follow an exponent of the order of 0.75 or 0.63 ... 0.64 depending on the paper grade (type of sample). It is worth noting that the Washburn-behaviour was absent, i.e., the measured interface heights vs. time increased much slower. In such conditions it is no surprise that the interfaces possess lots of overhangs. Such a result is, in any case, qualitatively in accordance with the fact that Washburn-scaling is not observed - this must imply, that the pinning height can, as again was observed, vary with the sample size as well. However the later interpretation [17] that the actual exponent value would relate to the correlations in porosity and thus on the local “force” acting on the interface must be questioned. Unlike in many rocks etc. the pore space in paper is constrained by the finite thickness (of the order of 0.1 mm) and a typical pore thus has a size of a few

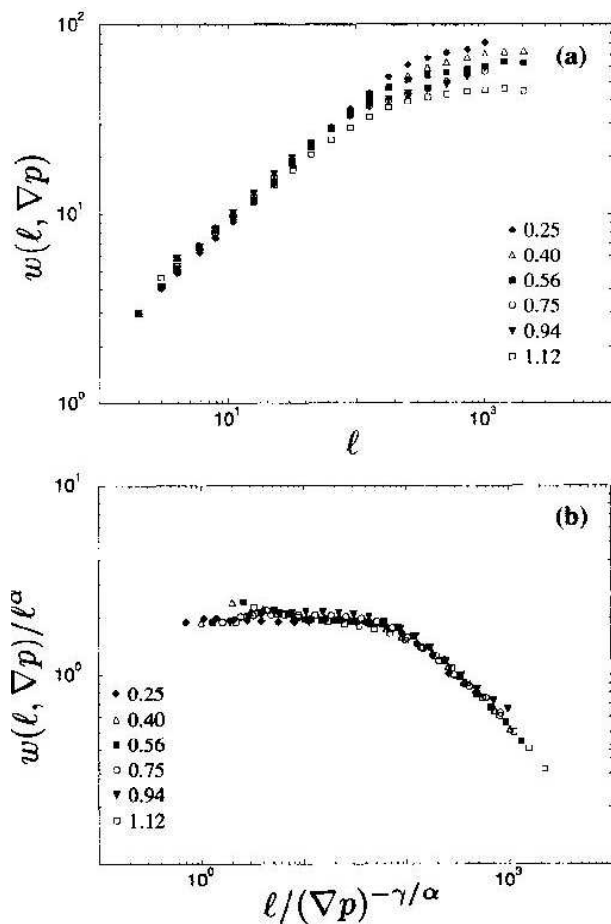


FIG. 50: The scaling of the interface width for a pinned interface as a function of the evaporation rate, related to the equilibrium height of the interface. Both the “raw data” and the scaling used by Amaral et al. are depicted [7].

tens of $\mu\text{ m}^3$, while the pore space is not expected to have fractal properties on any sizeable scale. There is no evidence that pores are correlated in paper. (Note that ref. [269] discusses *areal mass* fluctuations and the correlations there in, not pores.)

These results highlight the fact that the slow dynamics close to pinning are very difficult to understand. Indeed, Delker, Pengra and Wong, and later Lago and Araujo, have demonstrated in Hele-Shaw cells that the approach to pinning can follow a power-law, similarly to depinning transitions at the critical point in general [71, 176, 177]. This would follow after a Washburn-like temporal regime has been observed. With pinning allowed or included, Washburnian dynamics would imply an exponential law, also in contradiction with such experiments.

Recall that at the critical point of an absorbing state phase transition, or a depinning transition, the velocity often follows a power-law decay in time. The actual exponents of the experiments are perhaps not very surprisingly close to any standard depinning models. The attained values found by Delker and Wong for the decay

exponent of the interface velocity were in excess of unity, and dependent on many factors. Indeed, similar power-law behaviour has been reproduced for a contact line inside a capillary tube. The Hele-Shaw one may of course also simply demonstrate how local evaporation or slow surface flows lead to creep-like motion of the interface [47]. Other experiments on spontaneous imbibition in such systems have addressed saturation and cross-overs to fingering flow [120, 282]. These results do not seem to be in line with any of the standard local models, which does not seem to be too surprising, either.

2. Moving interfaces

In analogy with the pinned interfaces, the results on moving ones are also quite varied. Family et al. performed an experiment in a horizontal capillary setup with water, with the position of the air-water interface recorded both temporally and spatially [95]. The main results were an average interface progression $\bar{h} \sim t^\delta$, with $\delta = 0.7$ (faster than the Washburn one) and a self-affine interface described by a Family-Vicsek scaling relation, and characterised by the exponents $\beta = 0.38$ and $\chi = 0.76$. Concerning $h(t) \sim t^{0.7}$ it may be so that the details of the setup were at play: a reservoir was placed underneath the paper used, to combat evaporation. This may have caused condensation, or prewetting, thus increasing the velocity of the front. It is of course no news that water penetration in paper can be non-Washburn-like. The spatial scaling regime was rather small, for distances below $l_{max} \approx 2$ cm for a 40 cm wide sheet of paper.

The temporal scaling of the interface was studied in detail by Horváth and Stanley [130]. A paper sheet was moved so as to keep the interface always at a fixed distance h above a reservoir. A power law behaviour for the time correlation function $C_2(t)$ was established, with $\sim t^\beta$, $\beta = 0.56$. The experimental result is shown in Fig. 51. The velocity v at which the paper must be moved towards the reservoir varied as $v \sim h^{-\Omega}$, $\Omega = 1.6$. This implies that the interface propagated slower than $t^{1/2}$, $h(t) \sim t^{1/(\Omega+1)}$, from $v = dh/dt$. No spatial scaling results were reported. The value of β was independent of h , in contrast to the saturation time of $C_2(t)$. The correlation function was brought into a scaling picture,

$$C_2(t) \sim v^{-\Theta_L} f(tv^{(\Theta_t + \Theta_L)/\beta}), \quad (115)$$

where $f(y)$ is a scaling function such that $f(y) \sim y^\beta$ for $y \ll 1$ and $f(y) \sim \text{const}$ for $y \gg 1$. The values of the independent exponents were $\Theta_L = 0.48$ and $\Theta_T = 0.37$. One can again try to rewrite this in terms of ξ_\times by relating the lateral length ξ_\times to the velocity at h , so that

$$C_2^2(\tau \rightarrow \infty) \sim \int_{1/\xi_\times(h)}^{1/a} \frac{dk}{k^{2\chi+1}} \quad (116)$$

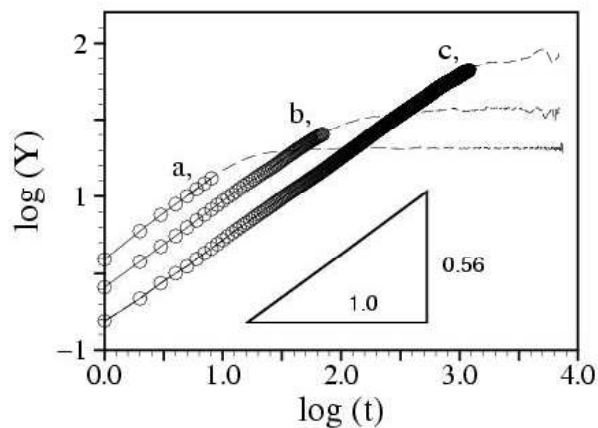


FIG. 51: The temporal two-point correlation function from the stationary height experiment of Horváth and Stanley, [130]. The apparent roughening exponent is about 0.56 regardless of the speed ($V = 4.03 \times 10^{-2}$, 1.32×10^{-2} and 1.40×10^{-3} cm/sec). Saturation takes place the sooner the larger the velocity.

which yields $C_2(\tau \rightarrow \infty) \sim h^{\chi/2} \sim v^{-\chi/2}$. As long as $\xi_x < L$, the correlation function $C_2(t)$ is *independent* of the total width of the system. Horváth and Stanley used only paper of one, fixed, size.

A similar velocity result was obtained by Kwon et al. [170]. A paper towel was set on an inclined glass plate, to follow the capillary rise of a dye solution. This gave $\bar{h}(t) \sim t^{0.37}$. Two scaling regimes were present in the saturated width; on small length scales (≤ 2 cm), $\chi = 0.67$ while on larger length scales (up to 20 cm) $\chi \approx 0.2$. Within the simple Family-Vicsek picture they obtained $\beta = 0.24$ on the short length-scale regime. It is conceivable again that the cross-over is simply due to non-local effects.

The only experiment so far on horizontal front roughening was performed by Zik et al. [350]. They obtained rough interfaces only with what was called “highly anisotropic” paper, with $\chi = 0.4$. For isotropic paper, the roughness was at best logarithmic. It is remarkable, that the scaling for the anisotropic paper was observed through a large range of length scales, not only up to a few fibre lengths.

There are two recent, intriguing experiments on spontaneous imbibition that have shown promise with respect to agreement with theory. First, Soriano et al. also used the Hele-Shaw setup to explore the effects of $v = 0$ by preparing the interface by finite-velocity transients. This means that the interface was first forced, as in a fixed flow rate experiment, until a certain height, and then let to relax to $v = 0$ [312]. It was established, with columnar disorder, that the local progression *inside* the copper tracks (with preferential wetting properties) followed Washburn-like dynamics. This setup and, possibly, experiments on regular assemblies of tracks would certainly be useful to investigate the cross-over between

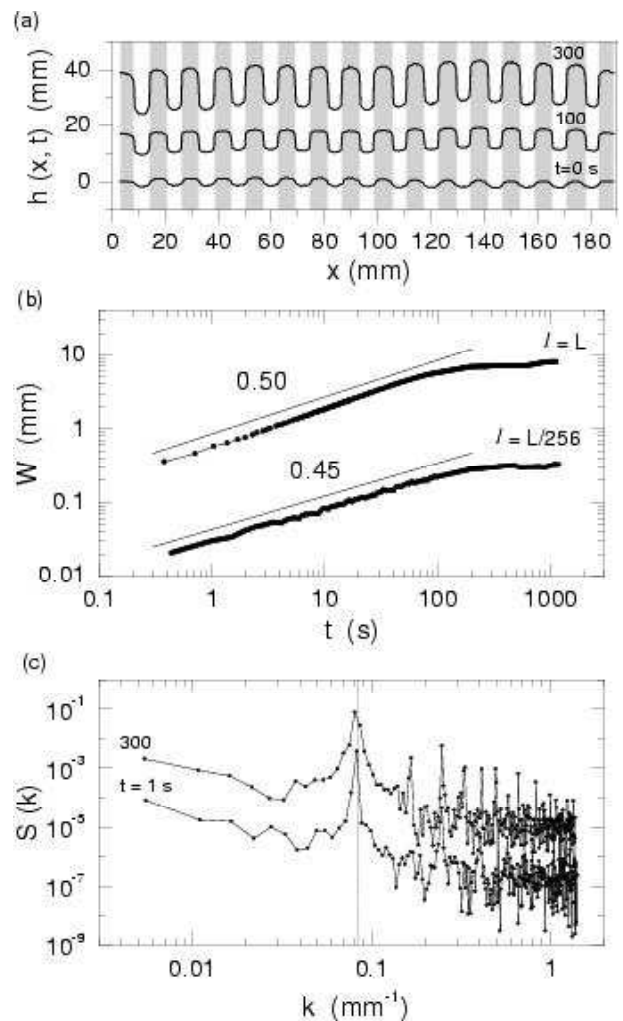


FIG. 52: Interfaces with a regular spacing of the tracks (or disorder columns) 6 mm wide. a) snapshots at different times, b) local width $w(l, t)$ for two values of l , and the power spectrum at saturation. The vertical line indicates wavelength of the pattern. From [312].

local and non-local dynamics (again, ξ_x) and the role of annealed (thermal) disorder by repeating the test in the same fixed geometry, as illustrated in Fig. 52 where the effect becomes visible in the local width $w(l, t)$ and the saturation power-spectrum.

In a recent paper Geromichalos et al. explicitly demonstrate the existence of a scale-length similar to ξ_x by studying rising liquid fronts between two rough glass plates [101]; we reproduce examples in Fig. 53. First, the Washburn-scaling of the velocity was established, although with standard prefactor-problems: the dynamic contact angle is unknown quantitatively. Measurements of the spatial two-point correlation function indicated the presence of two kinds of scaling, with $\chi_{SR} \approx 0.8$ and $\chi_{LR} \approx 0.6$ (see Figure 54). Maybe coincidentally, the values and the existence of the cross-over are similar to what has been established in a number of forced-flow ex-

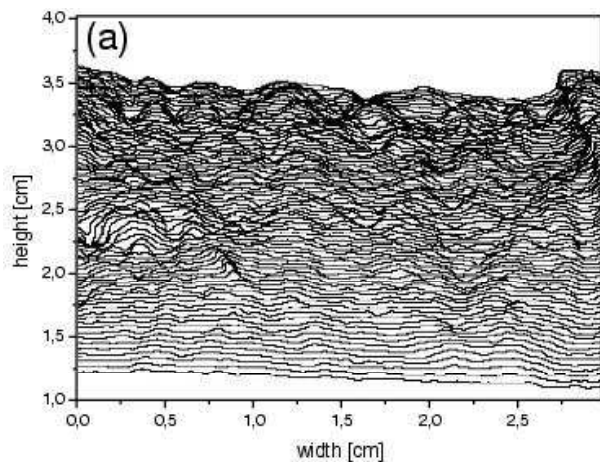


FIG. 53: A rising spontaneous imbibition front in an experiment with two rough, parallel glass plates. The snapshots are separated by 10 seconds [101].

periments discussed above [121, 128, 312].

The cross-over scaling should follow, as a function of the cell gap d the law

$$\xi_x \sim \sqrt{d} \quad (117)$$

which was in line with the results for dodecanol and water as the rising liquid. The exponents differ from most of the models except for perhaps that of Ganesan and Brenner [99], and also one should note that χ_{LR} is numerically close to the quenched KPZ value of 0.63. Unfortunately the published results do not consider the other exponents, as e.g. β (unpublished data may imply, that $\beta \sim 0.5 \dots 0.6$ [102]) nor the structure factor or higher order correlation functions that could be used to study multi-scaling. The authors pointed out that fronts sometimes had clearly visible dynamical structures or “kinks” one of which is shown in Figure 55. This would be certainly worth further study as would be the repeatability of the measurements and correlations between runs using the same glass plates several times.

C. Imbibition, wicking, and liquid transport in living organisms

Transport of water and solubles, and water entering parts of an organism are essential processes of its life. We finish this Section by giving a (very) short overview on recent studies of imbibition and water transport in plants, focussing on those which by their methods or subject come close to the physics aspects, as presented in this Review.

In a plant water flows through capillaries in the stem, roots, branches, and leaves, in vessels forming a fractal structure. Perhaps not too surprising from a Statistical Physics point of view, scaling behaviour can be observed in this structure for various quantities, among them the

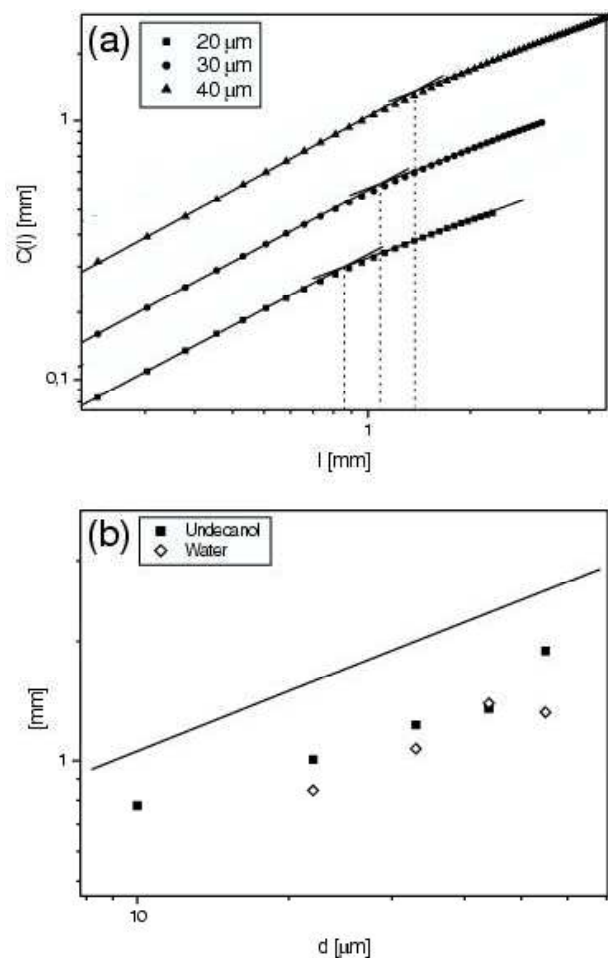


FIG. 54: In a) the spatial correlation functions of the experiments of Geromichalos et al. [101] are demonstrated, with varying separations of the two glass plates. The presence of two scaling regimes is apparent, as is a cross-over length-scale that decreases with the separation. In b) the length-scale is shown, both water and undecanol, as a function of the gap width. The square-root scaling of Eq. (117) is roughly reproduced by the data.

vessel diameters in relation to the biomass, the ratios of biomasses between roots and leaves, between stem and leaves, etc. Some simple arguments indicate that the plant structure, as it is found, optimises the supply of cells with respect to resource use [93].

One has to be careful to apply concepts of physics to biological systems, e.g., Darcy’s law connecting pressure gradient to flux, because living organisms may, and generally do *actively* influence all kinds of processes — so the exchange of water and solubles between a cell and its surroundings. Interestingly, the term *imbibition* is used for the soaking of water into seeds and grains, a mainly passive process and therefore in line with the models and experiments presented above. Imbibition to seeds starts germination through different mechanisms. Anybody is familiar with the swelling of a wet grain, which breaks the outer hull and thus enables or eases the seedling’s growth.

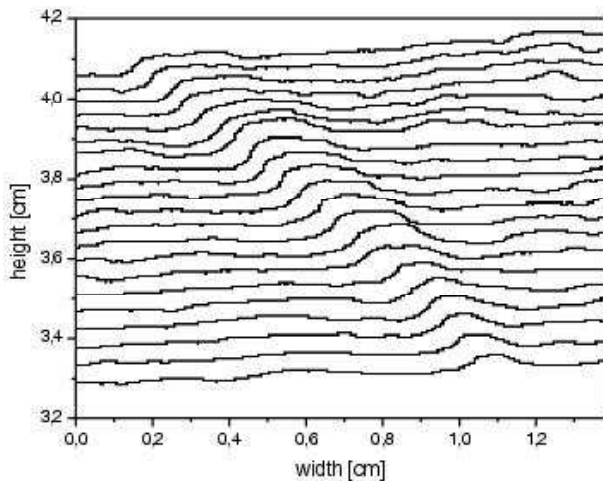


FIG. 55: A detailed look of some fronts (with undecanol), showing the presence of coherent features or deterministically moving “kinks” in the front dynamics ([101]).

But water entering the grain also starts physiological and developmental processes necessary for the early development of the embryo [1, 78, 194, 259]. It is influenced among other parameters crucially by temperature and water supply [35, 344]. Surface properties influence wettability and imbibition [26]. Besides these agricultural issues knowledge about grain imbibition has great importance in food processing and food storage [111, 139, 290].

Nuclear magnetic resonance allows for a direct measurement of water flow inside the grain. Generally, the hydration of a seed is a multistage process. For example in soy beans the water concentration keeps increasing on the time scale of days with water entering different compartments one after another and reaching the embryonic axis relatively late [264]. Similar results are found for cereals in detailed studies, so for barley [110, 223], oats [131], maize [222].

It is of considerable interest for agricultural applications to understand the interaction of a seed and its surrounding soil during imbibition. It would allow for optimal preparation of the soil structure (grain size distribution) and its humidity and give an estimate measure for successful germination. Bruckler has built a model based on a Darcy ansatz for imbibition of maize grains and was able to determine essential parameters such as, e.g., grain wall permeability by direct measurements of single grains which were kept in well defined conditions [40]. Subsequent tests in seed beds yielded good correspondence of observations and model predictions under variation of soil moisture and soil grain size, but difficulties in estimating the role of temperature variation [34]. This is in fact not too surprising, as temperature has substantial influence on physiological properties. As stated above, *active* processes in living organisms involve many details, often too complicated to be captured by simple thermodynamics or generally physical reasoning.

V. CONCLUSIONS

A. Overview

In this Article we have reviewed various aspects of front roughening in imbibition. To us, with a statistical physics viewpoint, it is striking that imbibition appears in many different fields, from the most abstract statistical physics of rough interfaces to detailed engineering studies in, e.g., paper fabrication or oil recovery. Many years have passed since the original work of Washburn [339], but perhaps it can be stated that the general understanding of imbibition has advanced relatively little.

This work has aimed at collecting the knowledge accumulated so far, grouping it into fields, and stating the most urgent and interesting open questions and advances from the theorist’s viewpoint. By far the most work has been done in numerous detailed technical applications, as the references to engineering literature on the subject that we have gathered should bear witness to.

Imbibition has attracted a good deal of interest among statistical physicists, in great part due to the presence of experiments on interface roughening that (still) remain unexplained. As usual in this context, it is of particular interest to look for the simplest possible model that captures the essential ingredients of the problem. This however implies the presence of the usual dichotomy between theory and experiment: The simplified approaches of statistical mechanics predict scaling behaviour but have difficulties to make quantitative predictions and there is often no satisfactory connection between experiment and theory. This is true in part for imbibition and it remains to be seen how quickly the distance between theory and experiment can be overcome. This also holds for the comparisons between numerical simulation models that contain microscopic details - as outlined in the Introduction - and more coarse-grained ones like the phase field approach. We next summarise the main theoretical issues that have been resolved so far and then point to a number of topics and issues that remain open and deserve further attention.

Theorists, in evaluating experiments and model simulations, have quite uncritically been looking for power laws in surface roughness without looking at the global picture. In our opinion, this has in many cases obfuscated the view for the essential features of imbibition. For example, it is of primary importance to observe and quantify the lateral length-scale ξ_x (c.f. Eqns. (21) and (95)), coming from the interplay of surface tension and pressure gradient in the liquid bulk. We note that this comes out of theoretical considerations [82, 83, 84], and that there is recent experimental proof for its existence in the case of spontaneous imbibition [101], while forced fluid flow in Hele-Shaw cells yielded indications even earlier [121].

Imbibition problems are of a broad general theoretical interest since they present a field in which usual “non-local” interface models (here referring to equations

of type $\partial_t h(x, t) = \int_{x'} K(x', x) h(x', t)$ fail to describe the problem properly. As noted in the theoretical section one may then proceed systematically by studying the origins of the effective noise terms, e.g., on the basis of an assumption of Stokes' flow everywhere in the bulk. This is not only useful for the particular case of roughening in imbibition but will also advance the understanding of the permeability properties, multi-phase flow and the role of capillary effects; for disordered porous media these are all very challenging problems (see among others [32, 86, 137, 234, 292, 330]).

The fact that quantitative understanding of kinetic roughening should also involve considering the solutions to these problems again point to the complications present in imbibition phenomena. We might then conclude that this merits a statistical physics approach, in which one eschews detailed considerations in favour of basic symmetry and scaling principles, but it is also important to realise that imbibition represents an important meeting point for statistical physics and actual applications to disordered media.

B. Future issues for theorists

The primary importance of imbibition points to a number of directions for theorists' future work. We now outline briefly three separate topics, that stress quite different aspects.

Interface roughness: from the viewpoint of general interface dynamics it would of course be most interesting to develop models that correctly describe the experimental results on interface roughness properties. One of the fundamental questions remaining open is of course the value (or possible values) of the roughness exponent χ in a "most clear-cut" imbibition experiment. In the theory section the idea of "dynamical noise" was brought forward to explain some of the scaling regimes of the phase field-type models corresponding to constant fluid flow setups. This kind of reasoning is an analogy of the quenched-annealed cross-over in ordinary interface depinning (QEW or QKPZ), which results from the fact that the noise becomes decorrelated due to the finite velocity. This highlights the point that, as in local models, it is the noise and the symmetries of the effective interface dynamics that dictate the "critical" exponents - however with the proviso that the scaling range might be limited due to the intrinsic nature of imbibition.

In this sense, attempts to quantitatively describe a variable-gap Hele-Shaw cell give rise to some optimism that the quenched features of the noise could be described, even quantitatively, in some simple cases. Lest it be forgotten we should emphasise that the theoretical and numerical results presented in Section III are inspired by simple experiments and computational ease: no work exists so far on imbibition-like models in, say, three dimensions. In the context of various numerical (lattice Boltzmann or network) models this is a challeng-

ing task. It is clear that the presence of an extra dimension makes analytical work more challenging, and perhaps presents new scenarios as in the case of anisotropic depinning [321]. It is also rather obvious that this would be of experimental and practical interest.

Washburn behaviour: it is clear that in many instances of spontaneous imbibition Washburn-like scaling is not observed, and other (velocity) laws are obtained. This can ensue from the dynamic response of the medium (swelling), from microscopic physics at the meniscus level (surfactant dynamics, inertial flow in transients), and from the fact that the liquid does not obey Stokes' flow conditions in general. Also, for e.g. very small capillary numbers it is possible that precursors (film flow) or the particular, peculiar pore structure play a role. We believe that several of these effects merit separate studies, particularly in connection to their experimental effects on the roughness. The statistical physics viewpoint would be that such microscopic phenomena give rise to yet another length-scale: beyond this the effect of liquid conservation should dominate as usual. Now the question is to understand the dependence on time and on quantifiable measures of microscopic structure, of such scales.

The *coarse-grained* description of these effects can also be improved; the phase field models described earlier do not do yet a very good job on the actual fluid dynamics level. Generalisations to account for this are of course possible. The scaling away from the micro-scale towards an effective large-scale description presents in the context of imbibition several challenges. At least three can be listed. In spontaneous dynamics, the time-scales change continuously as the interface slows down (recall that even without an asymptotic equilibrium $\partial_t h \sim 1/h$). Second, as noted the dynamics on the pore level can be very slow (coming from surfactant diffusion or induced dissipation at the contact line) or very fast (Bosanquet-flow). Third, the correlations in the pore structure and their size distribution can resist attempts to average, without even mentioning time-dependent structural changes. In particular, also in relation to the actual kinetic roughening properties, it is challenging to describe the dynamics of imbibition when the interface advancement becomes slow, and stick-slip motion typical of general depinning/pinning transitions takes place. In the experimental Section and in the Introduction we pointed out evidences for deviations from Washburn-like approaches to a pinning height at late stages. These can in some cases arise from a change in the morphology of the interface from a compact (but rough) front, perhaps, and indeed involve further scales. Likewise, one should note that it should be evidently possible to construct phase-field-style theories that would allow to handle the smoothening and dispersion of the front e.g. in the presence of initial wetting fluid saturations.

Complete stochastic description: another promising avenue for future work is to concentrate on issues other than those dealing with traditional "scaling exponents". The dynamics of an interface in the presence

of external (thermal) and quenched noise is of course a stochastic process and can be characterised in many ways. In the statistical physics community, much attention has been recently paid to concepts like persistence, or equivalently, first-return properties [146, 165, 208, 209, 210, 229]. For example, the local interface height $h(x, t)$ (after subtracting the average) and the local velocity of the interface $v(x, t)$ are both stochastic variables. As in the simple cases of Brownian motion or ordinary random walks, it is then possible to explore the time-series of h , or e.g. return-to-origin statistics. In usual kinetic roughening models, which are most often in the steady-state, it follows that this defines a *persistence* exponent, simply related to the exponent β of the two-point temporal correlation function if the dynamics is Markovian. The probability distributions or *scaling functions* of various statistical and fluctuating quantities, such as the velocity distribution $P(v, L)$ (see Fig. 26) or the roughness distribution in depinning problems of the QEW type $P(w, F)$ [287] can be also similar alternatives descriptions. There has also been some recent interest in distributions such as “ $P(v)$ ” as general signatures of non-equilibrium behaviour and the possible universality therein [37].

It has to be stressed however that the non-local dynamics of imbibition does not necessarily maintain local scale-invariance, and thus many of these questions have to be re-evaluated. Also, one probably cannot expect analytical solutions as in the case of KPZ interfaces with their deep connections to random matrices [267].

The scaling exponents of ordinary local interface equations are also manifest in many other properties. Examples are found in non-equilibrium steady states, as in the SOC ensemble [3], and in case the system is driven, e.g., in an oscillatory manner. In this case, one runs into concepts such as hysteresis, aging, and the general effect of “AC” driving fields [107, 250]. In the context of imbibition it is clear that analogous scenarios are easy to set up in experiments by, e.g., varying the injection rate in a forced fluid flow test.

C. Experimental and practical implications

To finish the discussion on possible directions for further work we outline some suggestions for experimentalists. Kinetic roughening and related questions should be studied in systems, where the micro-structure is under control — which is certainly not the case for the “classical” imbibition of water into paper. The often-used micro-channel networks are perhaps too idealised for such purposes. First of all, the average flow and its influence on the lateral length scale ξ_x should be addressed. Roughness exponents should be measured very carefully, not by a mere *bona fide* fit to various moments of height differences $\langle |h(x + \xi, t) - h(x, t)|^q \rangle^{1/q}$, but also by analysing the structure factor and the probability distribution functions of these quantities.

The predictions of the phase field model can be applied

directly also to the length-scales. For the ξ_x , Eq. (32) implies that a knowledge of the most important fluid parameters and a characterisation of the porous medium can be used to estimate its range and effects on scaling. Consider e.g. a Hele-Shaw cell, analogous to [121]. Using water and beads of size 0.4 mm, and varying the flow velocity between 10^{-6} to 10^{-3} m/s yields capillary numbers in the range 10^{-5} to 10^{-2} . Assuming now that the typical pore size is of the same order of magnitude as the beads, this yields (with a surface tension of ~ 72.5 mJ/m²) ξ_x -values of about 1.5 mm for $C_a = 10^{-2}$. In other words, a rather small length-scale if compared to typical kinetic roughening experiments. For ordinary paper the pores are smaller by only one order of magnitude. This shows that the roughness often seen in paper-based imbibition experiments may directly be due to the structural disorder which is *discrete* on the sub-millimetre scales (recall that a typical fibre length is up to 2 to 4 mm) and does not follow any real “continuum description”.

A central question for the dynamics is interface propagation by avalanches close to pinning. The complicated behaviour of simultaneous avalanches, in a system with non-local dynamics, is not understood well theoretically as already Fig. 26 above indicates. Possibly it may eventually become feasible to explore the details of fluid dynamical fluctuations (pressure), as e.g. Ref. [331] hints. The question of pore-scale physics in this context and its relation to interface dynamics would seem to merit attention [185].

Last we recall that quantitatively by far the largest amount of work has been done in detailed studies of phenomena relevant to all kinds of applications. Our understanding is that this will remain so, since many of the phenomena listed in the experimental Section III can be examined more thoroughly: Pre-wetting layers along and inside pores, the influence of surfactants and solubles, partial saturation, the flow and transport in the bulk, and in particular behaviour with non-Newtonian liquids. Advances in various experimental techniques (X-ray tomography for pore structure determination, NMR with high enough temporal resolution for dynamical measurements) should also provide with new results. As mentioned in the Introduction, such methods are very close to getting to the level of imagining imbibition fronts with sufficient accuracy, and comparisons can then be made to the local pore structure including cross-correlations.

D. Last outlook

In this Review we have collected experimental and theoretical studies of imbibition and tried to place them in a common framework of understanding the phenomenon. This can not be gained without including the lateral length-scale ξ_x appearing in the interface fluctuations, which is a central point in our theory Section. Also the scaling behaviour of interface fluctuations has to be studied carefully. Different methods have to be compared

for consistency, in particular most valuable information can be obtained from the structure factor $S(k, t)$ and the probability distribution of height and velocity fluctuations.

To finish this work we mention a few directions that should be interesting to follow or which may very well become more important in the future than what one might conclude from our exposition of the field here. First of all, we hope that ideas about the nature of systems where disorder and global conservation laws combine can benefit from the phase field lessons. One particular example could be the description of vortex phases in superconductors and the coarse-grained theories thereof [103, 138, 233, 240, 345, 346].

Second, we have not discussed the complications that ensue in the presence of more than two phases (three phase imbibition) except briefly in the context of surfactants. These systems are of obvious interest in some oil recovery scenarios, but have so far been analysed mainly numerically in the literature [76, 77, 96, 119, 182, 211]. Here the pore-scale complications get even more manifold, and it is obvious that coarse-graining these into any kind of continuum theory is a challenge. Similar scenarios exist if non-Newtonian fluids are involved [155, 327]: the rate-dependence of the liquid(s) will make itself manifest already inside single pores, and if one for instance considers the slow-down in spontaneous penetration, it is evident that the *average* flow of the wetting liquid is hard to quantify. This area is however apt for much future development given the natural role of surfactants in many practical applications, and the fact that e.g. in petroleum industry -related scenarios even the basic constituents - like crude - have very non-ideal properties [241].

Another aspect not mentioned is the presence of simultaneous transport processes (e.g. heat) during imbibition (see [226] for the effect of thermal gradients). This can be complicated further, if some of the phases

involved undergo chemical reactions (see [73] and references therein). The fingering properties of such processes have been investigated in Hele-Shaw cells, but imbibition-related conditions have not been considered in general. One may for instance consider a porous medium, where a more viscous fluid displaces another, while at the front chemical reactions take place. These may involve or even produce a surfactant, giving rise to a coupling to the contact angle.

Third, we believe also that a sufficient understanding of imbibition will prove to be of interest in a variety of technological applications. Micro- and nano-machinery and chemically structured surfaces should provide ample examples of situations of practical and industrial interest [105, 275], as imbibition into carbon nanotubes [318]. In such contexts the continuum description may fail due to the small scales that necessitate an atomistic treatment; consider for instance the physics of contact lines for a start. It should on the other hand be of interest to be able control imbibition properties (including dynamics) together with the permeability as hinted many times earlier, here.

Acknowledgements:

MJA would like to thank the Centre of Excellence program of the Academy of Finland for support and the SMC centre at La Sapienza, Rome, for hospitality. MD would like to thank the Canada Research Chair on Value Added Paper and Joe Aspler, Francois Drolet and Lyne Cormier for interesting discussions. MR was supported by SFB 611 (*Singuläre Phänomene in mathematischen Modellen*) of Deutsche Forschungsgemeinschaft and thanks Helsinki University of Technology for its hospitality. All authors wish to thank Ken R. Elder, Sami Majaniemi, and Tapio Ala-Nissilä for collaboration on several works on imbibition theory. Also Janoinen Lohi is gratefully acknowledged for a long-standing and very fruitful collaboration.

-
- [1] R. Acevedo, A. Cuadrado, C. De la Torre, and S.M.D. de la Espina, *Eur. J. Histochem.* **46**, 143 (2002)
- [2] S. Akin, J.M. Schembre, S.K. Bhat, and A.R. Kovacek, *J. Pet. Sci. Eng.* **25**, 149 (2000).
- [3] M.J. Alava, *J. Phys. Cond. Mat.* **14**, 2353 (2002).
- [4] M. Alava and K. B. Lauritsen, *Europhys. Lett.* **53**, 563 (2001).
- [5] M.J. Alava, to appear in *Advances in Condensed Matter and Statistical Mechanics*, Eds. E. Korutcheva and R. Cuerno, (Nova Science Publishers); cond-mat/0307668.
- [6] R. Albert, A.-L. Barabási, N. Carle, and A. Dougherty, *Phys. Rev. Lett.* **81**, 2926 (1998).
- [7] L.A.N. Amaral, A.-L. Barabási, S.V. Buldyrev, S. Havlin, and H.E. Stanley, *Phys. Rev. Lett.* **72**, 641 (1994).
- [8] D. Ambrosi and L. Preziosi, *SIAM J. App. Math.* **61**, 22 (2000).
- [9] D. Antonelli and A. Farina, *Composites* **A30**, 1367 (1999).
- [10] J.-Y. Arns, C.H. Arns, A.P. Sheppard, R.M. Sok, M.A. Knackstedt, and W.V. Pinczewski, *J. Pet. Sci. Eng.* **39**, 247 (2003).
- [11] J. Asikainen, S. Majaniemi, M. Dube, and T. Ala-Nissila, *Phys. Rev.* **E65**, 052104 (2002).
- [12] J.S. Aspler, S. Davis, and M.B. Lyne, *J. Pulp and Paper Sci.* **13**, J55 (1987).
- [13] J. Aspler, *Nordic Pulp Paper Res. J.* **1**, 68 (1993).
- [14] J.C. Bacri, M. Rosen, and D. Salin, *Europhys. Lett.* **11**, 127 (1990).
- [15] P. Bak, C. Tang and K. Wiesenfeld, *Phys. Rev. Lett.* **59**, 381 (1987).
- [16] A.S. Balankin, A. Bravo-Ortega, and D. M. Matamoros, *Phil. Mag. Lett.* **80**, 503 (2000).
- [17] A.S. Balankin, O. Susarrey, and J.M. Gonzales, *Phys. Rev. Lett.* **90**, 096101 (2003).
- [18] B.A. Baldwin and E.A. Spinler, *J. Pet. Sci. Eng.* **35**, 23 (2002).
- [19] A.-L. Barabási, S.V. Buldyrev, S. Havlin, G. Huber, H.E. Stanley, and T. Vicsek, in *Surface Disordering: Growth, Roughening and Phase Transitions*, Eds. R. Jullien, J.

- Kertész, P. Meakin and D.E. Wolf, Nova Science, Com-mack (1992).
- [20] A.-L. Barabási and H.E. Stanley, *Fractal Concepts in Surface Growth*, Cambridge University Press, Cambridge (1995).
- [21] H. Barkhausen, *Physik. Zeitschr.* **20**, 401 (1919).
- [22] J. Bear and Y. Bachmat, *Introduction to Modeling of Transport Phenomena in Porous Media*, Kluwer Academic Publishers (1990).
- [23] A.Y. Beliaev and S.M. Hassanizadeh, *Transp. Porous Media* **43**, 487 (2001).
- [24] B. Berkowitz and R.P. Ewing, *Surv. Geophys.* **19**, 23 (1998).
- [25] M.G. Bernadiner, *Transp. Porous Media* **30**, 251 (1998).
- [26] M.R. Bet, G. Goissis, S. Vargas, and H.S. Seliste-de-Araujo, *Biomaterials* **24**, 131 (2003).
- [27] J. Bico and D. Quéré, *Europhys. Lett.* **61**, 348 (2003).
- [28] J. Bico, C. Tordeux, and D. Quéré, *Europhys. Lett.* **55**, 214 (2001).
- [29] M. Blunt and P. King, *Phys. Rev. A* **42**, 4780 (1990).
- [30] M. Blunt, M.J. King, and H. Scher, *Phys. Rev. A* **46**, 7680 (1992).
- [31] M.J. Blunt and H. Scher, *Phys. Rev. E*, **52** 6387 (1995).
- [32] M.J. Blunt, *Curr. Opin. Colloid Interface Sci.* **6**, 197 (2001).
- [33] M.J. Blunt, M.D. Jackson, M. Piri, and P.H. Valvatne, *Adv. Water Resour.* **25**, 1069 (2002).
- [34] J. Boiffin, L. Bruckler, and C. Aubry, *Agronomie* **3**, 291-302 (1983).
- [35] D.T. Booth, *J. Arid Environments* **43**, 91 (1999).
- [36] C.H. Bosanquet, *Philos. Mag. ser. 6* **45**, 525 (1923).
- [37] S.T. Bramwell, P.C.W. Holdsworth, and J.F. Pinton, *Nature* **396**, 552 (1998).
- [38] A.J. Bray, *Adv. in Phys.* **43**, 357 (1994).
- [39] J.A. Bristow, *Svensk Papperstidning* **20**, 645 (1971).
- [40] L. Bruckler, *Agronomie* **3**, 213-222; *ibid.* 223-232 (1983).
- [41] R. Bruinsma and G. Aepli, *Phys. Rev. Lett.* **52**, 1547 (1984).
- [42] S. Bryant, P.R. King, and D.W. Mellow, *Transp. Porous Media* **11**, 53 (1993).
- [43] S.E. Buckley and M. Leverett, *Trans. AIME* **146**, 107 (1942).
- [44] Burgers, *The nonlinear diffusion equation* (1974).
- [45] S.V. Buldyrev, A.-L. Barabási, F. Caserta, S. Havlin, H.E. Stanley and T. Vicsek, *Phys. Rev. A* **45** R8313 (1992).
- [46] S.V. Buldyrev, A.-L. Barabási, S. Havlin, J. Kertész, H.E. Stanley, and H.S. Xenias, *Physica* **191 A**, 220 (1992).
- [47] M. Cachile, R. Chertcoff, A. Calvo, M. Rosen, J.P. Hulin, and A.M. Cazabat, *J. Colloid Interface Sci.* **182**, 483 (1996).
- [48] J.W. Cahn and J.E. Hilliard, *J. Chem. Phys.* **28**, 258 (1958).
- [49] J. Carmeliet, F. Descamps, and G. Houvenaghel, *Transp. Porous Media* **35**, 67 (1999).
- [50] J.S. Ceballos-Ruano, T. Kupka, D.W. Nicoll, J.W. Benson, M.A. Ioannidis, C. Hansson, and M.M. Pinter, *J. Appl. Phys.* **91**, 6588 (2002).
- [51] D.Y.C. Chan, B.D. Hughes, L. Paterson, and C. Sirakoff, *Phys. Rev.* **A38**, 4106 (1988).
- [52] D. Chang and M.A. Ioannidis, *J. Coll. Int. Sci.* **253**, 159 (2002).
- [53] P. Chauve, P. Le Doussal and K.J. Wiese, *Phys. Rev. Lett.* **86**, 1785 (2001).
- [54] K.S.A. Chen and L.E. Scriven, *Tappi Journal* **73**, 151 (1990).
- [55] Q. Chen, M.K. Gingras, and B.J. Balcom, *J. Chem. Phys.* **119**, 9609 (2003).
- [56] T. Chen, O. Chen, and P. Chen, *J. Can. Pet. Technol.* **40**, 29 2001
- [57] X. Chen, K.G. Kornev, Y.K. Kamath, and A.V. Neimark, *Text. Res. Journ.* **71**, 862 (2001).
- [58] E. Chibowski, and F. González-Caballero, *Langmuir* **9**, 330 (1993).
- [59] E. Chibowski, and L. Holysz, *J. Adhes. Sci. Technol.* **11**, 1289 (1997).
- [60] T.W. Chiu, R.J. Wakeman, P.R. Harris, and O.F.J. Meuric, *Chem. Engng. Res. & Design* **74**, 220 (1996).
- [61] M. Cil and J.C. Reis, *J. Pet. Sci. Eng.* **16**, 61 (1996).
- [62] A. Clarke, T.D. Blake, K. Carruthers, and A. Woodward, *Langmuir* **18**, 2080 (2002).
- [63] G.N. Constantinides and A.C. Payatakes, *Transp. Porous Media* **38**, 291 (2000)
- [64] R. Cuerno and M. Castro, *Phys. Rev. Lett.* **87**, 236103 (2001).
- [65] H. Dahle and M. Celia *Comput. Geosci.* **3**, 1 (1999).
- [66] E. Dana, and F. Skoczylas, *Int. J. Multip. Flow* **28**, 1965 (2002).
- [67] H.T. Davis, R.A. Novy, L.E. Scriven, and P.G. Toledo, *J. Phys. Cond. Mat.* **2**, SA457 (1990).
- [68] S.H. Davis and L.M. Hocking, *Phys. Fluids* **12**, 1646 2000.
- [69] P.G. De Gennes, In: *Physics of Disordered Materials*, eds. D. Adler et al. (Plenum, NY, 1985), p. 227.
- [70] P.G. de Gennes, *Rev. Mod. Phys.* **57**, 827 (1985)
- [71] T. Delker, D.B. Pengra, and P.-z. Wong, *Phys. Rev. Lett.* **76**, 2902 (1996).
- [72] M. De Meijer, B. Van de Velde, and H. Militz, *J. Coatings Tech.* **914**, 39 (2001).
- [73] A. De Wit, *Phys. Fluids* **15**, 163 (2004).
- [74] M.M. Dias and A.C. Payatakes, *J. Fluid Mech.* **164**, 305 (1988).
- [75] R. Dickman, M. A. Muñoz, A. Vespignani, and S. Zapperi, *Braz. J. Phys.* **30**, 27 (2000).
- [76] M.I.J. van Dijke and K.S. Sorbie, *J. Pet. Sci. Eng.* **39**, 201 (2003).
- [77] M.I.J. van Dijke and K.S. Sorbie, Paper SCA 2001-36, SCA Conference 2001, Edinburgh, September 2001.
- [78] F. Domínguez, M.C. González, and F.J. Cejudo, *Planta* **215** 727 (2002)
- [79] M.Z. Dong, F.A.L. Dullien, and J. Zhou, *Transp. Porous Media* **31**, 213 (1998).
- [80] T. Dopler, A. Modaressi, and V. Michaud, *Metall. Mat. Trans. B* **31**, 225 (2000).
- [81] A. Dougherty and N. Carle, *Phys. Rev. E* **58**, 2889 (1998).
- [82] M. Dubé, M. Rost, K.R. Elder, M. Alava, S. Majaniemi, and T. Ala-Nissila, *Phys. Rev. Lett.* **83**, 1628 (1999).
- [83] M. Dubé, M. Rost and M. Alava, *Eur. Phys. J. B* **15**, 691 (2000).
- [84] M. Dubé, M. Rost, K. R. Elder, M. Alava, S. Majaniemi and T. Ala-Nissila, *Eur. Phys. J. B* **15**, 701 (2000).
- [85] M. Dubé, S. Majaniemi, M. Rost, K. R. Elder, M. Alava, and T. Ala-Nissila, *Phys. Rev. E* **64**, 051605 (2001).
- [86] F.A.L. Dullien, *J. Porous Media* **1**, 29 (1998).
- [87] F.A.L. Dullien and M. Dong, *J. Porous Media* **5**, 1 (2002).
- [88] K. Deckelnick and G. Dziuk, *Interfaces and Free Boundaries* **2**, 341 (2000).

- [89] S.F. Edwards and D. Wilkinson, Proc. Roy. Soc. Lond. A (1982).
- [90] See, eg., D.E. Eklund, and P.J. Salminen, Tappi Journal **69** (9), 116 (1986).
- [91] K. R. Elder, M. Grant, N. Provatas, and J. M. Kosterlitz, Phys. Rev. E **64**, 21604 (2001).
- [92] A. Endruweit, T. Luthy, and P. Ermanni, Polym. Compos. **23**, 538 (2002).
- [93] B.J. Enquist, Plant, Cell & Environment **26**, 151 (2003).
- [94] R.P. Ewing and S.C. Gupta, Water Resour. Res. **29**, 3179 (1993).
- [95] F. Family, K.C.B. Chan, J.G. Amar, in *Surface Disorder: Growth, Roughening and Phase Transitions*, R. Jullien, J. Kertész, P. Meakin and D.E. Wolf, Nova Science, Commack (1992).
- [96] D.H. Fenwick and M.J. Blunt, Adv. Water Resour. **21**, 121 (1998).
- [97] J.M. Frey, P. Schmitz, J. Dufreche, and I.G. Pinheiro, Transp. Porous Media **37**, 25 (1999).
- [98] R.E. Gagnon, G.D. Parish and D.W. Bousfield, Tappi Journal **84**, 66 (2001).
- [99] V. Ganesan and H. Brenner, Phys. Rev. Lett. **81**, 578 (1998).
- [100] W.R. Garder and M.S. Mayhugh, Proc. Soil Sci. Soc. Amer. **22**, 187 (1958).
- [101] D. Geromichalos, F. Mugele, and S. Herminghaus, Phys. Rev. Lett. **89**, 104503 (2002).
- [102] D. Geromichalos, personal communication (2003).
- [103] T. Giamarchi and S. Bhattacharya, In "High Magnetic Fields: Applications in Condensed Matter Physics and Spectroscopy", p. 314, ed. C. Berthier et al., Springer-Verlag, 2002 (also cond-mat/0111052).
- [104] T. Gillespie, J. Coll. Science **13**, 32 (1958), and *ibid* **14**, 123 (1959).
- [105] N. Giordano and J.T. Cheng, J. Phys. Cond. Mat. **13**, R271 (2001).
- [106] M. Gladkikh and S. Bryant, Adv. Water Resour. **26**, 609 (2003).
- [107] A. Glatz, T. Nattermann, and V. Pokrovsky Phys. Rev. Lett. **90**, 047201 (2003).
- [108] W. Gray and S. Hassanizadeh, Water Resour. Res. **27**, 1855 (1991).
- [109] W.G. Gray and C.T. Miller, Phys. Rev. **E61**, 2150 (2000).
- [110] M.L.H. Gruwel, B. Chatson, X.S. Yin, S. Abrams, Int. J. Food Sci. Tech. **36**, 161 (2001).
- [111] M.L.H. Gruwel, X.S. Yin, M.J. Edney, S.W. Schroeder, A.W. MacGregor, S. Abrams, J. Agric. Food Chem. **50**, 667 (2002)
- [112] J. D. Gunton, M. San Miguel, and P. Sahní, in *Phase Transitions and Critical Phenomena*, edited by C. Domb and J. L. Lebowitz (Academic Press, London, 1983), vol 8, p. 267.
- [113] B.S. Gupta, Tappi Journal **71**, 147 (1988).
- [114] L. L. Handy, Trans. Am. Inst. Mech. Eng. **219**, 75 (1960).
- [115] B.I. Halperin and P.C. Hohenberg, Rev. Mod. Phys. **49**, 435 (1977).
- [116] T. Halpin-Healy and Y.-C. Zhang, Phys. Rep. **254**, 215 (1995).
- [117] A. Hamraoui and T. Nylander, J. Coll. Int. Sci. **250**, 415 (2002).
- [118] A. Hamraoui, K. Thureson, T. Nylander, and V. Yaminsky, J. Coll. Int. Sci. **226**, 199 (2000).
- [119] M. Hashemi, B. Dabir, and M. Sahimi, Aiche J. **45**, 1365 (1999).
- [120] J.A. Hayashi and A. Soria, Aiche J. **47** 1513, (2001).
- [121] S. He, G.L.M.K.S. Kahanda, and P.-z. Wong, Phys. Rev. Lett. **69**, 3731 (1992).
- [122] A. Hernández-Machado, J. Soriano, A.M. Lacasta, M.A. Rodriguez, L. Ramirez-Piscina, and J. Ortín, Europhys. Lett. **55**, 194 (2001).
- [123] R. Hilfer, Phys. Rev. E **55**, 5433 (1997).
- [124] R. Hilfer and H. Besserer, Physica B **279**, 125 (2000).
- [125] M. Hilpert, R. Glantz, and C.T. Miller, Transp. Porous Media **51**, 267 (2003).
- [126] L.M. Hirsch and A.H. Thompson, Phys. Rev. **E50**, 2069 (1994).
- [127] K.T. Hodgson and J. C. Berg, J. Colloid Interface Sci. **121**, 22 (1988).
- [128] V.K. Horváth, F. Family, and T. Vicsek, J. Phys. A **24**, L25 (1991).
- [129] V. K. Horváth, F. Family, and T. Vicsek, Phys. Rev. Lett. **67**, 3207 (1991).
- [130] V.K. Horváth and H.E. Stanley, Phys. Rev. E **52**, 5166 (1995).
- [131] J.Q. Hou, E.J. Kendall, G.M. Simpson, J. Exp. Bot. **48**, 683 (1997).
- [132] R.W. Hoyland, Trans. BPBIF Symp. Fiber-Water Interactions in Papermaking (Oxford), p. 557-579 (1976).
- [133] Y.L. Hshieh and B.L. Yu, Text. Res. Journ. **62**, 677 (1992).
- [134] Y.L. Hshieh, B.L. Yu, and M.M. Hartzell, Text. Res. Journ. **62**, 697 (1992).
- [135] G. Huber, M.H. Jensen, and K. Sneppen, Phys. Rev. **E52**, R2133 (1995).
- [136] R.G. Hughes and M.J. Blunt, Transp. Porous Media **40**, 295 (2000).
- [137] J.P. Hulin, Adv. Colloid Interface Sci. **49**, 47 (1994).
- [138] D.K. Jackson, M. Nicodemi, G. Perkins, N.A. Lindop, and H.J. Jensen, Europhys. Lett. **52**, 210 (2000).
- [139] P.I. Jansen and R.L. Ison, Seed Sci. Tech. **22**, 435 (1994)
- [140] D. Jasnow and J. Viñals, Phys. of Fluids **7**, 747 (1996).
- [141] G.R. Jerauld and S.J. Salter, Transp. Porous Media **5**, 103 (1990).
- [142] H. Ji, M.O. Robbins, Phys. Rev. A **44**, 2538 (1991).
- [143] J.F. Joanny and L. Léger, Rep. Prog. Phys. **55**, 431 (1992).
- [144] M. Jost and K.D. Usadel, Phys. Rev. B **54**, 9314 (1996).
- [145] M.A. Kader and S.C. Jutzi, J. Agronom. Crop Sci. **188**, 286 (2002)
- [146] H. Kallabis and J. Krug, Europhys. Lett. **45**, 20 (1999).
- [147] M. Kardar, G. Parisi, and Y.-C. Zhang, Phys. Rev. Lett. **56**, 889 (1986).
- [148] M. Kardar, Physics Reports **301**, 85 (1998).
- [149] K. Kawasaki and T. Ohta, Prog. Theo. Phys. **68**, 129 (1982).
- [150] P. Kechagia, Y.C. Yortsos, and P. Lichtner, Phys. Rev. **E64**, 016315 (2001).
- [151] D.A. Kessler, H. Levine, and Y.H. Tu, Phys. Rev. **A43**, 4551 (1991).
- [152] E. Kissa, Text. Res. Journ. **66**, 660 (1996).
- [153] M.A. Knackstedt, A.P. Sheppard, and M. Sahimi, Adv. in Water Res. **24**, 257 (2001).
- [154] B. Koiller, H. Ji, M.O. Robbins, Phys. Rev. B **45**, 7762 (1992).
- [155] L. Kondic, M. J. Shelley, and P. Palfy-Muhoray, Phys. Rev. Lett. **80**, 1433 (1998).

- [156] J. Koplik and T.J. Lasseter *SPE J.* **25**, 89 (1985).
- [157] J. Koplik and H. Levine, *Phys. Rev.* **B32**, 280 (1985).
- [158] A. Koponen, D. Kandhai, E. Hellén, M. Alava, A. Hoekstra, M. Kataja, K. Niskanen, P. Slood, and J. Timonen, *Phys. Rev. Lett.* **80**, 716 (1998).
- [159] K.G. Kornev and A.V. Neimark, *J. Coll. Int. Sci.* **235**, 101 (2001).
- [160] J. Krug and P. Meakin, *Phys. Rev. Lett.* **66**, 703 (1991).
- [161] J. Krug and H. Spohn, in *Solids Far From Equilibrium*, Ed. C. Godrèche, Cambridge University Press, Cambridge (1992).
- [162] J. Krug, *Phys. Rev. Lett.* **72**, 2907 (1994).
- [163] J. Krug and L.-H. Tang, *Phys. Rev.* **E50**, 104 (1994).
- [164] J. Krug, *Adv. Phys.* **46**, 139 (1997).
- [165] J. Krug, H. Kallabis, S.N. Majumdar, S.J. Cornell, A.J. Bray and C. Sire, *Phys. Rev. E* **56** 2702 (1997).
- [166] P.B.S. Kumar and D. Jana, *Physica A* **224**, 199 (1996).
- [167] M.C. Kuntz and J.P. Sethna, *Phys. Rev. E* **62** 11699 (2000).
- [168] M. Kuntz, J. Van Mier, and P. Lavallee, *Transp. Porous Media* **43**, 289 (2001).
- [169] M. Kuntz and P. Lavallee, *J. Phys D: Appl. Phys.* **34**, 2547 (2001).
- [170] T.H. Kwon, A.E. Hopkins, and S.E. O'Donnell, *Phys. Rev. E* **54**, 685 (1996).
- [171] L. Labajos-Broncano, M.L. González-Martín, and J.M. Bruque, *J. Adhes. Sci. Technol.* **16**, 1515 (2002).
- [172] L. Labajos-Broncano, M.L. González-Martín, J.M. Bruque, and C.M. González-García, *J. Coll. Int. Sci.* **233**, 356 (2001).
- [173] L. Labajos-Broncano, M.L. González-Martín, J.M. Bruque, C.M. González-García, and B. Janczuk, *J. Coll. Int. Sci.* **219**, 275 (1999).
- [174] L. Labajos-Broncano, M.L. González-Martín, B. Janczuk, J.M. Bruque, and C.M. González-García, *J. Coll. Int. Sci.* **211**, 175 (1999).
- [175] F. Lacombe, S. Zapperi and H. J. Herrmann, *Phys. Rev.* **B63**, 104104 (2001).
- [176] M. Lago and M. Araujo, *J. Coll. Int. Sci.* **234**, 35 (2001).
- [177] M. Lago and M. Araujo, *Physica A* **289**, 17 (2001).
- [178] C.-H. Lam and V.K. Horváth, *Phys. Rev. Lett.* **85**, 1238 (2000).
- [179] L.D. Landau and E.M. Lifshits, *Gidrodinamika* (Hydrodynamics) 3rd. edition, Nauka, Moscow, (1986).
- [180] J.S. Langer and L.A. Turski, *Acta Metall.* **25**, 1113 (1977).
- [181] J.S. Langer, in *Solids Far From Equilibrium*, Ed. C. Godrèche, Cambridge University Press, Cambridge (1992).
- [182] C. Laroche C, O. Vizika, and F. Kalaydjian, *J. Pet. Sci. Eng.* **24**, 155 (1999).
- [183] K. B. Lauritsen, P. Fröjdh, and M. Howard, *Phys. Rev. Lett.* **81**, 2104 (1998).
- [184] P. Le Doussal, K.J. Wiese and P. Chauve, *Phys. Rev. B* **66**, 174201 (2002).
- [185] R. Lenormand and C. Zarcone, *Soc. of Petroleum Engineers No. 13264*, in: *Proceedings of the 59th Ann. Tech. Conf. SPE* (SPE, Richardson, TX, 1984).
- [186] R. Lenormand, E. Touboul, and C. Zarcone, *J. Fluid. Mech.* **189**, 165 (1988).
- [187] R. Lenormand, *J. Phys. Cond. Mat.* **2**, SA79 (1990).
- [188] H. Leschhorn, *Physica A* **195**, 324 (1993).
- [189] H. Leschhorn and L.-H. Tang, *Phys. Rev. Lett.* **70**, 2973 (1993).
- [190] H. Leschhorn and L.H. Tang, *Phys. Rev. E* **49**, 1238 (1994).
- [191] H. Leschhorn, *Phys. Rev. E* **54**, 1313 (1996).
- [192] H. Leschhorn, T. Nattermann, S. Stepanow, and L.-H. Tang, *Ann. Physik* **6**, 1 (1997).
- [193] S. Letelier, H.J. Leutheusser, and Z. Rosas, *J. Coll. Int. Sci.* **72**, 465 (1979).
- [194] G. Leubner-Metzger, *Planta* **215**, 959 (2002) effects on tobacco testa rupture and dormancy release
- [195] A. Leventis, D.A. Verganelakis, M.R. Halse, J.B. Webber and J.H. Strange, *Transp. Porous Media* **39**, 143 (2000)
- [196] Y. Li, N.R. Morrow, and D. Ruth, *J. Pet. Sci. Eng.* **39**, 309 (2003).
- [197] D.A. Lockington and J.Y. Parlange, *J. Phys D: Appl. Phys.* **36**, 760 (2003).
- [198] J.M. López, M.A. Rodríguez, and R. Cuerno, *Phys. Rev. E* **56**, 3993 (1997).
- [199] J.M. López, *Phys. Rev. Lett.* **83**, 4594 (1999).
- [200] P.J. Love, J.-B. Maillet, and P.V. Coveney, *Phys. Rev. E* **64**, 061302 (2001).
- [201] T.X. Lu, J.W. Biggar, and D.R. Nielsen, *Water Resour. Res.* **30**, 3275 (1994).
- [202] T.X. Lu, J.W. Biggar, and D.R. Nielsen, *Water Resour. Res.* **30**, 3283 (1994).
- [203] T.X. Lu, D.R. Nielsen, and J.W. Biggar, *Water Resour. Res.* **31**, 11 (1995).
- [204] P.E. Luner and D. Van Der Kamp, *J. Pharmac. Sci.* **90**, 348 (2001).
- [205] B.B. Luukkala, S. Garoff, R.D. Tilton, and R.M. Suter, *Langmuir* **17**, 5917 (2001).
- [206] S.X. Ma, N.R. Morrow, and X.Y. Zhang, *J. Pet. Sci. Eng.* **18**, 165 (1997).
- [207] J.-B. Maillet and P.V. Coveney, *Phys. Rev. E* **62**, 2898 (2000).
- [208] S.N. Majumdar, *Curr. Sci. (India)*, **77**, 370 (1999).
- [209] S.N. Majumdar and A.J. Bray, *Phys. Rev. Lett.* **86**, 3700 (2001).
- [210] S.N. Majumdar and A.J. Bray, *Phys. Rev. Lett.* **91**, 030602 (2003).
- [211] V. Mani and K.K. Mohanty, *SPE J.* **3**, 238 (1998).
- [212] V. Mani and K.K. Mohanty, *J. Pet. Sci. Eng.* **23**, 173 (1999).
- [213] J.A. Mann, L. Romero, R.R. Rye, and F.G. Yost, *Phys. Rev. E* **52**, 3967 (1995).
- [214] P. Manneville and H. Chaté, *Physica D* **96**, 30 (1996).
- [215] A. Marmur and R.D. Cohen, *J. Coll. Int. Sci.* **189**, 299 (1997).
- [216] J. Marro and R. Dickman *Nonequilibrium Phase Transitions in Lattice Models* (Cambridge University Press, Cambridge, 1999).
- [217] J.A. Marsh, S. Garoff, and E.B. Dussan, *Phys. Rev. Lett.* **70**, 2778 (1993).
- [218] M. Marsili, A. Maritan, F. Toigo, and J.R. Banavar, *Rev. Mod. Phys.* **68**, 963 (1996).
- [219] G. Martic, F. Gentner, D. Seveno, D. Coulon, J. De Coninck, and T.D. Blake, *Langmuir* **18**, 7971 (2002).
- [220] N. Martys, M. Cieplak and M. O. Robbins, *Phys. Rev. Lett.* **69**, 3193 (1991).
- [221] A. Maximenko and V.V. Kadet, *J. Pet. Sci. Eng.* **28**, 145 (2000).
- [222] M.B. McDonald, J. Sullivan, M.J. Lauer, *Seed Sci. Tech.* **22**, 79 (1994).
- [223] E. McEntyre, R. Ruan, R.G. Fulcher, *Cereal Chem.* **75**,

- 792 (1998)
- [224] P. Meakin, *Fractals, scaling and growth far from equilibrium*, Cambridge University Press, Cambridge, UK (1998).
- [225] A. Medina, C. Pérez-Rosales, A. Pineda, F.J. Higuera, *Rev. Mex. Fis.* **47**, 537 (2001).
- [226] A. Medina, A. Pineda, and C. Trevino, *J. Phys. Soc. Jpn.* **72**, 979 (2003).
- [227] Y. Meléan, D. Broseta, and R. Blossey, *J. Pet. Sci. Eng.* **39**, 327 (2003).
- [228] Y. Mélean, D. Broseta, A. Hasmy, and R. Blossey, *Europhys. Lett.* **62**, 505 (2003).
- [229] J. Merikoski, J. Maunuksela, M. Myllys, J. Timonen, and M. Alava, *Phys. Rev. Lett.* **90** 024501 (2003)
- [230] V. Michaud and A. Mortensen, *Compos. Pt. A-Appl. Sci. Manuf.* **32**, 981 (2001)
- [231] V. Michaud and J.A.E. Manson, *J. Compos. Mater.* **35**, 1150 (2001).
- [232] V. Michaud, R. Tornqvist, and J.A.E. Manson, *J. Compos. Mater.* **35**, 1174 (2001).
- [233] M.-Carmen Miguel, J.S. Andrade Jr., and S. Zapperi, cond-mat/0304555; submitted to a special issue in the Brazilian Journal of Physics.
- [234] C.T. Miller, G. Christakos, P.T. Imhoff, J.F. McBride, J.A. Pedit, and J.A. Trangenstein, *Adv. Water Resour.* **21**, 77 (1998).
- [235] S.J. Mitchell, cond-mat/0210239.
- [236] I. Mitkov, D.M. Tartakovsky, and C.L. Winter, *Phys. Rev.* **E58** R5245, (1998).
- [237] I. Mitkov, D.M. Tartakovsky, and C.L. Winter, *Phys. Rev.* **E61**, 2152 (2000).
- [238] K. Mogensen and E.H. Stenby, *Transp. Porous Media* **32**, 299 (1998).
- [239] K.K. Mohanty, T. Davis, and L.E. Scriven, *Soc. Pet. Eng. Reservoir Eng.* **1**, 113 (1987).
- [240] A. A. Moreira and J. S. Andrade Jr., Mendes Filho J. and S. Zapperi, *Phys. Rev. B* **66**, 174507 (2002).
- [241] N.R. Morrow and G. Mason, *Curr. Op. Coll. Int. Sci.* **6**, 321 (2001).
- [242] T.E. Mumley, C.J. Radke, and M.C. Williams, *J. Colloid Interface Sci.* **109**, 398 (1986), and *ibid* **109**, 413 (1986).
- [243] S. Mukherji and S.M. Bhattacharjee, *Phys. Rev. Lett.* **79**, 2502 (1997).
- [244] W.W. Mullins and R.F. Sekerka, *J. Appl. Phys.* **35**, 444 (1964).
- [245] M. Myllys, J. Maunuksela, M. Alava, T. Ala-Nissilä, J. Merikoski and J. Timonen, *Phys. Rev. E* **64**, 036101 (2001).
- [246] T. Nagamine and S. Miyazima, *Fractals* **4**, 293 (1996).
- [247] O. Narayan and D. S. Fisher, *Phys. Rev.* **B48**, 7030 (1993).
- [248] O. Narayan, *Phys. Rev. E* **62**, R7563 (2000).
- [249] T. Nattermann, S. Stepanow, L.-H. Tang, and H. Leschhorn, *J. Phys. (France) II* **2**, 1483 (1992).
- [250] T. Nattermann, V. Pokrovsky, and V.M. Vinokur *Phys. Rev. Lett.* **87**, 197005 (2001).
- [251] C.J. Nederveen, *Tappi Journal* **77**, 174 (1994).
- [252] M. Nicodemi and H.J. Jensen, *J. Phys. A* **34**, L11 (2001).
- [253] K.J. Niskanen (ed.), *Paper Physics*, Fapet, Helsinki (1998).
- [254] K.J. Niskanen and M.J. Alava, *Phys. Rev. Lett.* **73**, 3475 (1994).
- [255] H.F. Nordhaug, M. Celia, and H.K. Dahle, *Adv. Water Resour.* **26**, 1061 (2003).
- [256] Z. Olami, I. Procaccia and R. Zeitak, *Phys. Rev. E* **49**, 1232 (1994).
- [257] P.E. Oren, S. Bakke, and O.J. Arntzen, *SPE J.* **3**, 324 (1998).
- [258] P.E. Oren and S. Bakke, *J. Pet. Sci. Eng.* **39**, 177 (2003).
- [259] X.R. Ouyang, T. van Voorthuysen, P.E. Toorop, H.W.M. Hilhorst, *Int. Jour. Plant Sci.* **163**, 107 (2002).
- [260] M. Paczusi, S. Maslov and P. Bak, *Phys. Rev. E* **53**, 414 (1996).
- [261] E. Pauné and J. Casademunt, *Phys. Rev. Lett.* **90**, 144504 (2003)
- [262] J.R.A. Pearson and P.M.J. Tardy, *J. Non-Newt. Fluid Mech.* **102**, 447 (2002).
- [263] I. Pézron, G. Bourgain, and D. Quéré, *J. Colloid Interface Sci.* **173**, 319 (1995).
- [264] L.N. Pietrzak, J. Fregeau-Reid, B. Chatson, and B. Blackwell, *Can. J. Plant Sci.* **82**, 512 (2002).
- [265] E.J. Pinthus and I.S. Saguy, *J. Food Sci.* **59**, 804 (1994).
- [266] N. Poulin, P. Tanguy, J. Aspler, and L. Larrondo, *Can. J. Chem. Eng.* **75** 949 (1997).
- [267] M. Prähofer and H. Spohn, *Phys. Rev. Lett.* **84**, 4882 (2000).
- [268] L. Preziosi, D.D. Joseph, and G.S. Beavers, *Int. J. Multiphase Flow* **22**, 1205 (1996).
- [269] N. Provatas, M.J. Alava, and T. Ala-Nissilä, *Phys. Rev.* **E54**, R336 (1996).
- [270] D. Quéré, *Europhys. Lett.* **39**, 533 (1997).
- [271] D. Quéré, E. Raphaël, and J.Y. Ollitrault, *Langmuir* **15**, 3679 (1999).
- [272] D. Rajagopalan, A.P. Aneja, and J.-M. Marchal, *Text. Res. Journ.* **71**, 813 (2001).
- [273] E. Rame, *J. Fluid Mech.* **440**, 205 (2001).
- [274] E.R. Rangel-German and A.R. Kovscek, *J. Pet. Sci. Eng.* **36**, 45 (2002).
- [275] M. Rauscher and S. Dietrich, cond-mat/0303639
- [276] P. Reeves and M. Celia, *Water Resour. Res.* **32**, 2345 (1996).
- [277] L.A. Richard, *Physics (N.Y.)* **1**, 318 (1931).
- [278] E.K. Rideal, *Philos. Mag.* **44**, 1152 (1922).
- [279] C.J. Ridgway and P.A.C. Gane, *Colloid Surf. A* **206**, 217 (2002).
- [280] C.J. Ridgway and P.A.C. Gane, *Nordic Pulp Paper Res. J.* **17**, 119 (2002).
- [281] C.J. Ridgway, P.A.C. Gane, and J. Schoelkopf, *J. Coll. Int. Sci.* **252**, 373 (2002).
- [282] R.F. Rodriguez, E. Salinas-Rodriguez, J. A. Hayashi, A. Soria, and J.M. Zamora, *Aiche J.* **47**, 1721 (2001).
- [283] S. Roels, J. Carmeliet, and H. Hens, *Transp. Porous Media* **52**, 351 (2003).
- [284] J.G. Roof, *Soc. Pet. Eng. J.* **10**, 85 (1970).
- [285] J. Rosinski, *Am. Ink Maker* **71**, 40 (1993).
- [286] A. Rosso and W. Krauth, *Phys. Rev. Lett.* **87** (2001) 187002.
- [287] A. Rosso, W. Krauth, P. Le Doussal, J. Vannimenus and K.J. Wiese, cond-mat/0301464 (2003).
- [288] M.A. Rubio, C. Edwards, A. Dougherty, and J.P. Golub, *Phys. Rev. Lett.* **63**, 1685 (1989).
- [289] R.R. Rye, J.A. Mann, and F.G. Yost, *Langmuir* **12**, 555 (1996).
- [290] M. Sacande, E.A. Golovina, A.C. van Aelst, F.A. Hoekstra, *J. Exp. Bot.* **52**, 919 (2001).
- [291] P.G. Saffman and G.I. Taylor, *Proc. Roy. Soc. London*

- A **245**, 312 (1958).
- [292] M. Sahimi, *Rev. Mod. Phys.* **65**, 1393 (1993).
- [293] E. J. Samuelsen, O.W. Gregersen, P.J. Houen, T. Helle, C. Raven, and A. Snigirev, *J. Pulp Pap. Sci.* **27**, 50 (2001).
- [294] K. Saripalli, H. Kim, P. Rao, and M. Annable, *Environ. Sci. Technol.* **31**, 932 (1997).
- [295] A. E. Scheidegger, *The Physics of Flow through Porous Media*, 3rd Ed., University of Toronto Press, Toronto (1974).
- [296] J.M. Schembre and A.R. Kovscek, *J. Pet. Sci. Eng.* **39**, 159 (2003).
- [297] J. Schmittbuhl, J. Vilotte, and S. Roux, *Phys. Rev. E* **51**, 131 (1995).
- [298] J. Schoelkopf, P.A.C. Gane, C.J. Ridgway, and G.P. Matthews, *Colloid Surf. A* **206**, 445 (2002)
- [299] J. Schoelkopf, P.A.C. Gane, C.J. Ridgway, and G.P. Matthews, *Nordic Pulp Paper Res. J.* **15**, 422 (2000).
- [300] J. Schoelkopf, C.J. Ridgway, P.A.C. Gane, G.P. Matthews, and D.C.J. Spielmann, *J. Coll. Int. Sci.* **227**, 119 (2000).
- [301] D.R. Schuchardt and J.C. Berg, *Wood Fib. Sci.* **23**, 342 (1991).
- [302] T.J. Senden, M.A. Knackstedt, and M.B. Lyne, *Nordic Pulp Paper Res. J.* **15**, 554 (2000).
- [303] E.T. Seppälä, V. Petäjä, and M.J. Alava, *Phys. Rev. E* **58**, R5217 (1998).
- [304] A. Siebold, M. Nardin, J. Schultz, and A. Walliser, *Colloid Surf. A* **161**, 81 (2000)
- [305] D.E. Smiles, *Chem. Eng. Sci.* **53**, 2211 (1998).
- [306] K. Sneppen, *Phys. Rev. Lett.* **69**, 3539 (1992).
- [307] K. Sneppen and M.H. Jensen, *Phys. Rev. Lett.* **71**, 101 (1993).
- [308] R.M. Sok, M.A. Knackstedt, A.P. Sheppard, W.V. Pinczewski, W.B. Lindquist, A. Venkatarangan, and L. Paterson, *Transp. Porous Media* **46**, 345 (2002).
- [309] J.L. Sommer and A. Mortensen, *J. Fluid. Mech.* **311**, 193 (1996).
- [310] K.S. Sorbie, Y.Z. Wu, and S.R. McDougall, *J. Coll. Int. Sci.* **174**, 289 (1995).
- [311] J. Soriano, J.J. Ramasco, M.A. Rodríguez, A. Hernández-Machado and J. Ortín, *Phys. Rev. Lett.* **89**, 026102 (2002).
- [312] J. Soriano, J. Ortín and A. Hernández-Machado, *Phys. Rev. E* **66** 031603 (2002).
- [313] J. Soriano, J. Ortín and A. Hernández-Machado, *cond-mat/0208432*.
- [314] D. Sornette, *Critical Phenomena in Natural Sciences* (Springer, Berlin, 2000).
- [315] K. Stoev, E. Rame, T. Leonhardt, and S. Garoff, *Phys. Fluids* **10**, 1793 (1998).
- [316] K. Stoev, E. Rame, and S. Garoff, *Phys. Fluids* **11**, 3209 (1999).
- [317] J.P. Stokes, D.A. Weitz, J.P. Gollub, A. Dougherty, M.O. Robbins, P.M. Chaikin, and H.M. Lindsay, *Phys. Rev. Lett.* **57**, 1718 (1986).
- [318] S. Supple and N. Quirke, *Phys. Rev. Lett.* **90**, 214501 (2003).
- [319] J. Székely, A.W. Neumann, and Y.K. Chuang, *J. Colloid Interface Sci.* **35**, 273 (1971).
- [320] A. Takahashi, M. Häggkvist, and T.Q. Li, *Phys. Rev. E* **56**, 2035 (1997).
- [321] L.-H. Tang, M. Kardar, and D. Dhar, *Phys. Rev. Lett.* **74**, 920 (1995).
- [322] A. Tanguy, M. Gounelle, and S. Roux, *Phys. Rev. E* **58**, 1577 (1999).
- [323] K. E. Thompson, *Aiche J.* **48** 1369, 2002.
- [324] C. Thorenz, G. Kosakowski, O. Kolditz, and B. Berkowitz, *Water Resour. Res.* **38**, 1069 (2002).
- [325] F. Tiberg, B. Zhmud, K. Hallstensson, and M. von Bahr, *Phys. Chem. Chem. Phys.* **2**, 5189 (2000).
- [326] C.D. Tsakiroglou and A.C. Payatakes, *Adv. Water Resour.* **23**, 773 (2000).
- [327] C.D. Tsakiroglou, M. Theodoropoulou, V. Karoutsos, D. Pananicolaou, and V. Sygouni, *J. Colloid Interface Sci.* **267**, 217 (2003).
- [328] G. C. Tzimas, T. Matsuura, D.G. Avraam, W. Van der Bruggen, G.N. Constantinides, and A.C. Payatakes, *J. Colloid Interface Sci.* **189**, 27 (1997).
- [329] G.C. Tzimas, T. Matsuura, D.G. Avraam, W. Van Der Bruggen, G.N. Constantinides, A.C. Payatakes, *J. Coll. Int. Sci.* **189**, 27 (1997).
- [330] O. van Genabeek and D.H. Rothman, *Annu. Rev. Earth Planet. Sci.* **24**, 63 (1996).
- [331] S. C. van der Marck and J. Glas, *Eur. J. Mech. B-Fluids* **16**, 681 (1997).
- [332] W. van Saarloos, *Phys. Rep.* **301**, 9 (1998).
- [333] A. Vernhet, M.N. Bellon Fontaine, J.M. Brillouet, E. Roesink, and M. Moutounet, *J. Membr. Sci.* **128**, 163 (1997).
- [334] A.M. Vidales, J.L. Riccardo, and G. Zgrablich, *J. Phys. D Appl. Phys.* **31**, 2861 (1998).
- [335] O. Vizika, D.G. Avraam, and A.C. Payatakes, *J. Colloid Interface Sci.* **165**, 386 (1994).
- [336] H.J. Vogel and K. Roth, *J. Hydrology* **272**, 95 (2003)
- [337] M.E.P. Walinder and D.J. Gardner, *J. Adh. Sci. Tech.* **13**, 1363 (1999).
- [338] N.C. Wardlaw and Li Yu *Transp. Porous Media* **3**, 17 (1988)
- [339] E.W. Washburn, *Phys. Rev.* **17**, 273 (1921).
- [340] G.J. Weir and S.P. White, *Transp. Porous Media* **25**, 79 (1996).
- [341] D. Wildenschild, J.W. Hopmans, C.M.P. Vaz, M.L. Rivers, D. Rikard, and B.S.B. Christensen, *J. Hydrology* **267**, 285 (2002)
- [342] D. Wilkinson, *Phys. Rev. A* **34**, 1380 (1986).
- [343] Y.S. Wu, K. Pruess, and P.A. Witherspoon, *Transp. Porous Media* **6**, 115 (1991).
- [344] E.F. Wuebker, R.E. Mullen, and K. Koehler, *Crop Science* **41**, 1857 (2001).
- [345] S. Zapperi, A. A. Moreira and J. S. Andrade Jr., *Phys. Rev. Lett.* **86**, 3622 (2001).
- [346] S. Zapperi, J. S. Andrade Jr., and A.A. Moreira, *cond-mat/0311034*.
- [347] X.Y. Zhang, N.R. Morrow, and S.X. Ma, *SPE Reserv. Engng.* **11**, 280 (1996)
- [348] D.X. Zhang, R.Y. Zhang, S.Y. Chen, and V.E. Soll, *Geophys. Res. Lett.* **27**, 1195 (2000).
- [349] D. Zhou, L. Jia, J. Kamath, and A.R. Kovscek, *J. Pet. Sci. Eng.* **33**, 61 (2002).
- [350] O. Zik, E. Moses, Z. Olami, and I. Webman, *Europhys. Lett.* **38**, 509 (1997).
- [351] O. Zik, T. Kustanovich, E. Moses, and Z. Olami, *Phys. Rev. E* **58**, 689 (1998).